DESIGN OPTIMIZATION OF STRUCTURES UNDER FATIGUE LOADING

by

Ahmet Hanifi Ertaş

B.S., Mechanical Engineering, Atatürk University, 1997

M.S., Mechanical Engineering, Boğaziçi University, 2004

Submitted to the Institute for Graduate Studies in
Science and Engineering in partial fulfillment of
the requirements for the degree of
Doctor of Philosophy

Graduate Program in Mechanical Engineering

Boğaziçi University

2009

DESIGN OPTIMIZATION OF STRUCTURES UNDER FATIGUE LOADING

APPROVED BY:

Assoc. Prof. Fazıl Önder Sönmez (Thesis Supervisor)	……
Assist. Prof. Nuri Ersoy	……
Prof. Öktem Vardar	……
Assoc. Prof. Cem Yalçın	……
Assist. Prof. Çetin Yılmaz	……

DATA OF APPROVAL: …./…./….

ACKNOWLEDGEMENTS

I am particularly grateful to my thesis supervisor, Assoc. Prof. Fazıl Önder Sönmez, for his technical support, leadership and guidance as well as his encouragement and mentoring during my study and research. I especially appreciate his patience and understanding.

My special thanks go to Prof. Öktem Vardar for generously sharing his time and knowledge. He stimulated my fascination for the discipline of solid mechanics. I am also profoundly grateful to my thesis committee member of Assist. Prof. Nuri Ersoy for his invaluable support and advices throughout the study. I would also like to express my gratitude to Assist. Prof. Çetin Yılmaz and Assoc. Prof. Cem Yalçın, who served as my committee members, for their valuable time used in reviewing and commenting on my dissertation.

I would like to thank my parents and brothers for their patience and unceasing warm supports and my wife, who has always been an inspiration and motivation for me with his wisdom and intellect.

I would also like to acknowledge the support by the Scientific Research Project of TUBITAK with the code number 106M301 in the duration of this thesis.

to my wife, Nil, and my daughter, Kübra

ABSTRACT

DESIGN OPTIMIZATION OF STRUCTURES UNDER FATIGUE LOADING

Many of the engineering failures are caused by fatigue. Fatigue failure can be defined as the tendency of a material to fracture by means of progressive brittle cracking under cyclic stresses. Because mechanical components usually experience cyclic loading during their operation, fatigue failure prevention is the foremost design requirement. Fatigue strength, thus structural performance, can greatly be increased through design optimization. Hence in this study, the general objective is to maximize the fatigue life of structures.

Firstly, high cycle fatigue assessment models for homogeneous materials were investigated. Then, they were applied to predict fatigue lives of spot welded specimens. Reliability of these models depends on accurate calculation of the cyclic stress and strain states within the structure. For this purpose, a nonlinear finite element analysis was carried out taking into account plastic deformations, residual stresses developed after unloading, and contacting surfaces. Among the general purpose fatigue models, Coffin - Manson and Morrow's mean stress models were found to correlate best with the experimental data. After that, a parametric study on fatigue strength of spot weld joints was conducted. The design variables considered in this study that were known to affect the strength of spot weld joints were sheet thickness, spot weld nugget diameter, number of spot welds, and the joint type as exemplified in tensile shear (TS), modified tensile shear (MTS), coach peel (CP), and modified coach peel (MCP) specimens. The results provide designers with some guidelines to foresee the impact of design changes on fatigue strength of spot weld joints.

Secondly, a methodology was proposed to find the optimum locations of spot welds and the optimum overlapping length of the joined plates for maximum fatigue life. Minimum weld-to-weld and weld-to-edge distances recommended by the industry were

considered as side constraints. The total strain life equation was used to predict the fatigue life. In order to use this model, the strain state in the structure developed under cyclic loading was calculated. Nelder-Mead (Sequential Simplex) was employed as the search algorithm in the optimization procedure. A number of problems were solved to demonstrate the effectiveness of the proposed method.

Finally, a methodology was developed to optimize composite laminates subject to in-plane loads for maximum fatigue life. For this purpose, a parametric fatigue life prediction model, proposed by Fawaz and Ellyin, was coupled with a global optimization technique called Direct Simulated Annealing (DSA). Fiber orientation angles were chosen as design variables. A computer code was developed in ANSYS parametric language and results were obtained for different configurations and loading conditions.

ÖZET

YORULMA YÜKLEMESİNE MARUZ KALAN YAPILARIN TASARIM ENİYİLEMESİ

Yorulma mühendislik arızalarının en önemli nedenlerinden biridir. Yorulma, tekrarlı yüklere maruz kalan malzemelerde zamanla çatlakların ve daha sonrada kırılmaların oluşması olarak tanımlanabilir. Makina parçalarının çalışmaları esnasında genel olarak tekrarlı yüklere maruz kalmalarından dolayı, yorulmanın önlenmesi en önemli tasarım gereğidir. Yorulma dayanımı ve dolayısıyla yapısal performans, tasarım eniyilemesi yardımı ile büyük ölçüde artırılabilir. Sonuç olarak bu çalışmada temel amaç, yapıların yorulma ömrünü azamiye çıkarmaktır.

İlk olarak, homojen malzemeler için, yüksek tekrarlı yorulma modelleri incelenmiştir. Daha sonra, bu modeller punta kaynaklı numunelerin yorulma ömürlerinin hesabında kullanılmıştır. Sözkonusu modellerin güvenilirlikleri, yapının içerisinde oluşan yorulma gerilmesi ve deformasyonların doğru hesaplanmasına bağlıdır. Bu nedenle; plastik deformasyonların, yüklemenin kaldırılması ile ortaya çıkan artık gerilmelerin ve temas yüzeylerinin etkilerinin de dikkate alındığı doğrusal olmayan sonlu elemanlar analizi yapılmıştır. Genel amaçlı modeller içerisinde, Coffin-Manson ve Morrow'un ortalama gerilme modellerinin deneysel sonuçlar ile benzerlik gösterdikleri bulunmuştur. Daha sonra, punta kaynaklı numunelerin yorulma davranışlarının incelenmesi üzerine bir parametrik çalışma yapılmıştır. Bu çalışmada, punta kaynaklı numunelerin dayanımına etkisinin olduğu düşünülen metal kalınlığı, punta kaynağının çapı, punta kaynağı sayısı ve geometri (ele alınan numune geometrileri TS, MTS, CP ve MCP olarak adlandırılıyorlar) tasarım değişkenleri olarak dikkate alınmıştır. Sonuçlar, tasarımcılara tasarım değişkenlerinin punta kaynaklı numunelerin yorulma dayanımlarına etkisi üzerine bilgiler sunmaktadır.

İkinci olarak, yorulma ömrünü azamiye çıkarmak amacıyla punta kaynaklı palakalarda punta kaynaklarının optimum yerleşimlerini ve plakalardaki temas uzunluğunu bulan bir metodoloji tasarlanmıştır. Sanayi tarafından önerilen punta kaynakları arasında ve punta kaynağı ile metal plakanın kenarları arasında olması gereken minimum mesafe değerleri kısıtlamalar olarak dikkate alınmıştır. Yorulma ömrü tayini için toplam plastik gerinim denklemi kullanılmıştır. Sözkonusu bu denklemi (modeli) kullanabilmek için, tekrarlı yada yorulma yüklemesine maruz kalan bir numunedeki gerinim durumu hesaplanmıştır. Eniyileme yönteminde, arama algoritması olarak Nelder-Mead (Sequential Simplex) kullanılmıştır. Önerilen yöntemin etkinliğini göstermak amacıyla farklı problemler incelenmiştir.

Son olarak, yine yorulma ömrünü azamiye çıkarmak amacıyla düzlem yüklere maruz kompozit plakaların eniyilemesi için bir metodoloji geliştirilmiştir. Bu amaçla, parametrik yorulma ömrü öngörü modeli olan Fawaz & Ellyin modeli genel bir eniyileme yöntemlerinden biri olan Direct Simulated Annealing (DSA) ile birleştirilmiştir. Tasarım değişkeni olarak elyaf yönlenme açıları seçilmiştir. Bu maksatla ANSYS'in parametrik dili kullanılarak bir bilgisayar kodu geliştirilmiştir ve farklı yapılandırma ve yükleme durumları için sonuçlar elde edilmiştir.

TABLE OF CONTENTS

ACKNOWLEDGEMENTS iii
ABSTRACT v
ÖZET vii
LIST OF FIGURES xii
LIST OF TABLES xx
LIST OF SYMBOLS/ABBREVIATIONS xxii
1. FATIGUE OF MONOLITHIC MATERIALS: FATIGUE OF SPOT WELD JOINTS . 1
1.1. Introduction 1
1.2. Models for Fatigue Life Prediction 4
1.2.1. Stress-Based Approaches 4
1.2.2. Strain-Based Approaches 5
1.3. Geometry of the Spot Weld Joints 8
1.4. Material Properties 11
1.5. Fatigue Lives 13
1.6. Statistical Analysis of the Experimental Data 14
1.7. Finite Element Model 18
1.8. Boundary Conditions 24
1.9. Resulting Stress States 26
1.10. Estimated Fatigue Lives 35
1.10.1. Calculation of Fatigue Lives 35
1.10.2. Comparison of the Predicted and Measured Fatigue Lives 35
1.10.3. Results and Discussion 41
2. OPTIMIZATION OF MONOLITHIC MATERIALS: DESIGN OPTIMIZATION OF SPOT WELDED PLATES FOR MAXIMUM FATIGUE LIFE 46
2.1. Introduction 46
2.2. Literature Survey 47
2.3. Problem Statement 48
2.4. Methodology 49
2.4.1. Objective Function 49
2.4.2. Optimization Algorithm 50

2.4.3. Finite Element Analysis....51
2.5. Results and Discussions....54
2.5.1. Optimization of a Joint with Two Spots under Cyclic Axial Loading....54
2.5.2. Optimization of a Joint with Two Spots under Cyclic Axial and Transverse Loading....60
2.5.3. Optimization of a Joint with Three Spots under Cyclic Axial Loading....63
2.5.4. Optimization of a Joint with Three Spots under Cyclic Axial and Transverse Loading....65
3. OPTIMIZATION OF COMPOSITE MATERIALS: DESIGN OPTIMIZATION OF FIBER REINFORCED LAMINATES FOR MAXIMUM FATIGUE LIFE....67
3.1. Introduction....67
3.2. Problem Statement....71
3.3. Fatigue Life Assessment Models for Composite Materials....71
3.4. Fawaz & Ellyin's Parametric Fatigue Life Prediction Model....75
3.4.1. Unidirectional Laminae....78
3.4.2. Bidirectional Laminae....80
3.4.3. Experimental Correlation of the Model....82
3.5. Structural Optimization using Simulated Annealing....83
3.5.1. The SA Algorithm....84
3.6. Optimization Methodology....89
3.6.1. Formulation of the Objective Function....90
3.6.2. Optimization Algorithm....90
3.6.3. Validity of the Optimization Algorithm....93
3.6.4. Finite Element Model....95
3.6.5. Geometry....96
3.7. Analysis of a Laminated Composite Plate....97
3.8. Numerical Results and Discussions....98
4. CONCLUSIONS....103
APPENDIX A: THE SIMPLEX METHOD....106
APPENDIX B: DIRECT SIMULATED ANNEALING....109
APPENDIX C: FATIGUE LIFE PREDICTION MODELS FOR COMPOSITE MATERIALS....116
C.1. Fatigue Degradation Approach....116

C.2. Residual Strength Degradation Approach 117
C.3. Fracture Mechanics Approach 119
C.4. Damage Accumulation Approach 120
C.5. A Finite Element Model Approach 121
C.6. A Matrix Damage Model (Secant Modulus) Approach 123
C.7. Statistical Distribution Model Approach 125
APPENDIX D: FATIGUE LIFE PREDICTION MODELS FOR MONOLITHIC MATERIALS: SPOT WELD JOINTS 130
D.1. Local Strain-Based Approach 130
D.2. Linear Fracture Mechanics Approach 132
D.3. Nugget Deformation Approach 137
D4. Combined Initiation and Propagation Method 139
D5. Structural Stress Method 141
D.5.1. Sheppard's Structural Stress Method 142
D.5.2. Radaj's Structural Stress Method 145
D.5.3. Rupp's Structural Stress Method 147
D.5.4. Henrysson's Structural Stress Method 148
REFERENCES 149

LIST OF FIGURES

Figure 1.1.	The resistance spot welding process……..	1
Figure 1.2.	Geometry of the tensile shear (TS) specimens (bottom and side views)…….	8
Figure 1.3.	Geometry of the modified tensile shear (MTS) specimens (bottom and side views)…….	9
Figure 1.4.	Geometry of the coach peel (CP) specimens (side and top views)…..	10
Figure 1.5.	Geometry of the modified coach peel (MCP) specimens (side and top views)……...	11
Figure 1.6.	Engineering stress-strain curve…….....	12
Figure 1.7.	The resulting curve of the regression analysis for both the manual-type and the automated-type spot welds……..	17
Figure 1.8.	General geometry of SOLID 92 element…….	20
Figure 1.9.	General geometry of BEAM 188 element……...	20
Figure 1.10.	General geometry of TARGE170 element……..	21
Figure 1.11.	General geometry of CONTA175 element……..	21
Figure 1.12.	Convergence in terms of element size…….	22
Figure 1.13.	Finite element model for the MTS specimen……...	22

Figure 1.14. A detail of the mesh at and around the right spot weld of the specimen…….. 23

Figure 1.15. Convergence in terms of substeps…… 23

Figure 1.16. Boundary conditions of the finite element model of TS…….. 24

Figure 1.17. Boundary conditions of the finite element model of TS…….. 25

Figure 1.18. Boundary conditions of the finite element model of CP…….. 25

Figure 1.19. Boundary conditions of the finite element model of MCP…….. 26

Figure 1.20. Distribution of σ_{xx} component of true stress (in MPa) on the inner and outer surfaces of the central plate of a TS specimen developed due to the maximum load. (t = 1 mm, d = 4 mm, number of spots = 2)……. 27

Figure 1.21. Distribution of σ_{xx} component of true stress (in MPa) on the inner and outer surfaces of the central plate of a TS specimen developed due to the minimum load. (t = 1 mm, d = 4 mm, number of spots = 2)……. 28

Figure 1.22. Distribution of σ_{xx} component of true stress (in MPa) on the inner and outer surfaces of the central plate of a MTS specimen developed due to the maximum load. (t = 1 mm, d = 4 mm, number of spots = 2)……. 29

Figure 1.23. Distribution of σ_{xx} component of true stress (in MPa) on the inner and outer surfaces of the central plate of a MTS specimen developed due to the minimum load (t = 1 mm, d = 4 mm, number of spots = 2)…….. 30

Figure 1.24. Distribution of σ_{xx} component of true stress (in MPa) on the inner surface of the central plate of a TS specimen developed due to the maximum load. (t = 1 mm, d = 2 mm, number of spots = 2)……... 31

Figure 1.25. Distribution of σ_{xx} component of true stress (in MPa) on the inner surface of the central plate of a TS specimen developed due to the maximum load. (t = 1 mm, d = 6 mm, number of spots = 2)……... 31

Figure 1.26. Distribution of σ_{xx} component of true stress (in MPa) on the inner surface of the central plate of a TS specimen developed due to the maximum load. (t = 2 mm, d = 4 mm, number of spots = 2)……... 32

Figure 1.27. Distribution of σ_{xx} component of true stress (in MPa) on the inner surface of the central plate of TS specimen developed due to the minimum load. (t = 4 mm, d = 4 mm, number of spots = 2)……... 33

Figure 1.28. Distribution of σ_{xx} component of true stress (in MPa) on the inner surface of the central plate of TS specimen developed due to the maximum and minimum load. (t = 1 mm, d = 2 mm, number of spots = 8)…….. 34

Figure 1.29. Comparison of the fatigue lives predicted using stress-based approaches and experimental results……... 36

Figure 1.30. Comparison of the fatigue lives predicted using strain-based approaches and the experimental results…….. 37

Figure 1.31. Comparison of the fatigue lives predicted using Morrow's mean stress model with different equivalent strain approaches…….. 38

Figure 1.32. Comparison of the fatigue lives predicted for different gap values using Morrow's mean stress approach and experimental results……. 39

Figure 1.33. Comparison of predicted fatigue lives with experimental results obtained by Pan (for DQSK MCP specimens)……..... 40

Figure 1.34. Comparison of predicted fatigue lives with experimental results obtained by Pan (for DQSK MTS specimens)……. 40

Figure 1.35. Comparison of predicted fatigue lives with experimental results obtained by Ertas *et al.* (for DIN 1623 MTS specimens)……..... 41

Figure 1.36. Fatigue lives predicted using Modified Coffin-Manson approach for TS specimens with 1-mm thickness and different spot weld diameters. 42

Figure 1.37. Fatigue lives predicted using Modified Coffin-Manson approach for TS specimens with 4-mm spot diameter and different metal sheet thicknesses……... 42

Figure 1.38. Comparison of fatigue lives predicted using Modified Coffin-Manson approach for MTS and TS specimens with 4-mm spot diameter and different metal sheet thicknesses……. 43

Figure 1.39. Comparison of fatigue lives predicted using Modified Coffin-Manson approach for MTS and TS specimens with 1-mm thickness and different spot-weld diameters…….. 44

Figure 2.1. Geometry of the joint with three spot welds (top and side views)….. 48

Figure 2.2. The optimization procedure……. 51

Figure 2.3. Finite element model for two spot-welded TS joint……..... 52

Figure 2.4. Boundary conditions of the finite element model for the axial loading case……... 53

Figure 2.5. Boundary conditions of the finite element model for the axial and transverse loading case……... 53

Figure 2.6. Distribution of σ_{xx} component of stress (in MPa) on the inner surface of one plate with two spot welds subject to the maximum axial load (upper figure) and the minimum axial load (lower figure) for the initial design……... 55

Figure 2.7. Distribution of the stress components σ_{xx}, σ_{yy}, and τ_{xy} along the line L-N shown in Figure 2.6, which passes through one of the spot welds, for the maximum axial loading condition and for the initial design..... 56

Figure 2.8. Distribution of the stress components σ_{xx}, σ_{yy}, and τ_{xy} (in MPa) through the thickness along a line passing through the point P in Figure 2.6 for the maximum axial loading condition for the initial design……... 56

Figure 2.9. Fatigue life of the best current configuration generated during the optimization process……..... 57

Figure 2.10. Distribution of σ_{xx} component of stress (in MPa) on the inner surface of one plate with two spot welds subject to the maximum axial load (upper figure) and the minimum axial load (lower figure) for the optimized design…….. 58

Figure 2.11. Distribution of the stress components σ_{xx}, σ_{yy}, and τ_{xy} along the line L-N shown in Figure 2.10, which passes through one of the spot welds, for the maximum axial loading condition and for the optimized design……... 59

Figure 2.12. Distribution of the stress components σ_{xx}, σ_{yy}, and τ_{xy} (in MPa) through the thickness along a line passing through the point P in Figure 2.10 for the maximum axial loading condition for the optimized design……... 59

Figure 2.13. Distribution of σ_{xx} component of stress (in MPa) on the inner surface of one plate with two spot welds subject to the maximum axial and transverse loads (upper figure) and the minimum axial and transverse loads (lower figure) for the initial design……..... 61

Figure 2.14. Fatigue life of the best current configuration generated during the optimization process……..... 62

Figure 2.15. Distribution of σ_{xx} component of stress (in MPa) on the inner surface of one plate with two spot welds subject to the maximum axial and transverse loads (upper figure) and the minimum axial and transverse loads (lower figure) for the optimized design…….. 62

Figure 2.16. Distribution of σ_{xx} component of stress (in MPa) on the inner surface of one plate with three spot welds subject to the maximum axial load (upper figure) and the minimum axial load (lower figure) for the initial design……..... 63

Figure 2.17. Fatigue life of the best current configuration generated during the optimization process……..... 64

Figure 2.18. Distribution of σ_{xx} component of stress (in MPa) on the inner surface of one plate with three spot welds subject to the maximum axial load (upper figure) and the minimum axial load (lower figure) for the optimized design…….. 64

Figure 2.19. Distribution of σ_{xx} component of stress (in MPa) on the inner surface of one plate with three spot welds subject to the maximum axial and transverse loads (upper figure) and the minimum axial and transverse loads (lower figure) for the initial design……..... 65

Figure 2.20. Fatigue life of the best current configuration generated during the optimization process……..... 66

Figure 2.21. Distribution of σ_{xx} component of stress (in MPa) on the inner surface of one plate with three spot welds subject to the maximum axial and transverse loads (upper figure) and the minimum axial and transverse loads (lower figure) for the optimized design…….. 66

Figure 3.1. A representative geometry of a laminae showing stresses and fiber orientation angle……... 77

Figure 3.2. Comparison of the Fawaz & Ellyin's model with the results of Hashin and Rotem on unidirectional Glass/Epoxy for different orientation angles……... 82

Figure 3.3. Comparison of the Fawaz & Ellyin's model with the results of Smith on biaxial Glass/Epoxy for $\theta = 45^0$ and different stress ratios..... 83

Figure 3.4. The optimization procedure……. 92

Figure 3.5. Layer Stacking of the composite structure under distributed in plane load, N_{xx}…….. 94

Figure 3.6. General geometry of SOLID 46 element…… 95

Figure 3.7. Finite element model of the laminate…….. 96

Figure 3.8. A symmetric laminate under distributed in plane loads, N_{xx} and N_{yy}. 97

Figure 3.9. Deformation in the optimum laminate……. 99

Figure 3.10. Equivalent stress distribution in the optimal laminate……. 99

Figure 3.11. Tensile stress distribution, S_{xx}, in the optimal laminate……. 100

Figure 3.12. Tensile stress distribution, S_{yy}, in the optimal laminate……..... 100

Figure 3.13. Optimized layer stacking of the composite structure under distributed in plane load, N_{xx} and N_{yy}, and for the possible fiber orientation angles of 0°, 30°, 60°, 90°…….. 101

Figure C.1. Fatigue Life Curve……. 126

Figure D.1. Side view of a spot-weld connection under tensile-shear loading…. 138

LIST OF TABLES

Table 1.1. Mechanical properties of St 1203 (DIN 1623) steel……. 12

Table 1.2. Average (or mean) fatigue lives of the specimens and the number of samples tested, *n* …….. 14

Table 1.3. Mean, standard deviation, and COV values for the automated-type spot welds……... 15

Table 1.4. Mean, standard deviation, and COV values for the manual-type spot welds……... 15

Table 1.5. The 95% confidence interval of the mean for automated-type spot welded specimens using the values of Student's t-distribution…….. 16

Table 1.6. The 95% confidence interval of the mean for manual-type spot welded specimens using the values of Student's t-distribution…….. 17

Table 1.7. The confidence interval of the mean for automated-type spot welded specimens……... 18

Table 1.8. The confidence interval of the mean for manual-type spot welded specimens……... 18

Table 1.9. Fatigue data of the material used in the fatigue assessment models…. 35

Table 1.10. Comparison of the fatigue lives (number of cycles to failure) of different joint types (t = 1 mm and d = 4 mm)……..... 44

Table 1.11. Fatigue lives of TS specimens with different numbers and diameters of spots (t = 1 mm and d = 4 mm)…….. 45

Table 1.12. Fatigue lives of TS specimens with different numbers and diameters of spots (t = 1 mm and d = 5.66 mm)…… 45

Table 2.1 Results of maximum fatigue life optimization of the joint with two spots under cyclic axial loading……..... 60

Table 3.1. The comparison of the optimal designs data obtained with the Tsai-Wu failure criteria for the loading N_{xx} = 100 MPa m, $N_{yy} = N_{xy}$ = 0 MPa·m, and for two distinct fiber angles ($0 \le j \le 51$)……... 94

Table 3.2. The optimum lay-ups and corresponding fatigue life values for the distributed in plane loading, N_{xx} and N_{yy}, for 4 different number of distinct fiber angles and for different possible fiber orientation angles…….. 102

Table 3.3. The optimum lay-ups and corresponding fatigue life values for the distributed in plane loading, N_{xx} and N_{yy}, for 2 different number of distinct fiber angles and for different possible fiber orientation angles…….. 102

LIST OF SYMBOLS/ABBREVIATIONS

a_1	First biaxial ratio
a_2	Second biaxial ratio
b	Fatigue strength exponent
c	Fatigue ductility exponent
c_i	Coefficients used in objective functions
d	Spot weld nugget diameter
f	Cost value in DSA
f_h	Highest cost in the current set in DSA
f_l	Lowest cost in the current set in DSA
$f(x)$	A nondimensional entity named as static strength correlation factor
$g(x)$	A nondimensional entity named as stress ratio correlation factor
l	Length of the contacting surface between the joined metal sheets
m	A parameter whose values depend on material properties
n	A parameter whose values depend on material properties
n_k	Number of plies
r_i	Randomly chosen real number in DSA
s_{ij}	Distance between spot welds i and j
x	Current solution state in DSA
x_0	Initial solution state in DSA
x'	Randomly perturbed state in DSA
x_i	The variable of the design optimization process
y_i	The variable of the design optimization process
t	Sheet thickness
t_0	Thickness of an individual ply
w	Sheet width
A_t	Acceptability of a newly generated trial configuration in DSA

C_{last}	Cost associated with the last accepted state in DSA
$C(x)$	Cost function
E	Modulus of elasticity
N_{dof}	Number of degrees of freedom of the system in DSA
N_f	Number of cycles to fatigue failure
N_{in}	Number of acceptance-rejection loop iteration in DSA
N_{out}	Number of outer loop iterations in DSA
N_r	Reference life used to normalize the fatigue life
N_{xx}	Uniformly distributed in plane load on x
N_{yy}	Uniformly distributed in plane load on y
N_{xy}	Uniformly distributed in plane load on xy
P_i	Penalty values
$P_{\max}$	Applied maximum load
$P_{\min}$	Applied minimum load
P_r	A randomly generated number used in DSA
$P(\delta C)$	Probability of change in cost or objective function in DSA
R	Stress of Force ratio
R^2	Coefficient of determination
S	Out-of-plane shear strength
S_a	Alternating stress
S_f	Fully reversed fatigue strength
S_m	Mean stress
S_{ut}	Ultimate tensile strength
S_y	Yield strength
T	Current temperature in DSA
T_f	Final temperature in DSA
T_j	Temperature (or control) parameter in DSA

T_{last}	Temperature associated with the last accepted state in DSA
T_o	Initial temperature in DSA
X_c	In-plane normal strength in compression
X_r	Static strength along the x direction
X_t	In-plane normal strength in tension
Y_c	In-plane transverse strength in compression
Y_t	In-plane transverse strength in tension
Z_c	In-plane shear strength in compression
Z_t	In-plane shear strength in tension

δC	Change in cost or objective function in DSA
$\Delta\varepsilon$	Total strain
$\Delta\varepsilon_e$	Alternating true elastic strain
$\Delta\varepsilon_p$	Alternating true plastic strain
$\Delta\theta_{\max}$	Maximum variation of fiber orientation
ε_a	Alternating strain
ε_{a1}	First principal alternating strain
ε_{a2}	Second principal alternating strain
ε_{a3}	Third principal alternating strain
ε_e	Elastic component of the cyclic strain amplitude
ε_f	True fracture strain
ε_f'	Fatigue ductility coefficient
ε_p	Plastic component of the cyclic strain amplitude
ε_{qa}	Equivalent alternating strain
ρ	Random number in DSA
ν	Poisson's ratio

θ	Fiber orientation angle
θ_k	Fiber orientation angle in the kth layer in DSA
θ_k'	Fiber orientation angle of newly generated configuration in DSA
σ_1	First principal stress
σ_2	Second principal stress
σ_3	Third principal stress
σ_a	Stress amplitude
σ_f	True fracture strength
σ_f'	Fatigue strength coefficient
σ_m	Mean stress
$\sigma_{\max}$	Maximum stress
$\sigma_{\min}$	Minimum stress
σ_x	Static failure stress along the x direction
σ_{xx}	Stress component in x direction
σ_{yy}	Stress component in y direction
τ_{xy}	Stress component in xy direction

ANSI	American National Standards Institute
AWS	American Welding Society
CFRP	Carbon Fiber Reinforced Plastics
CLT	Classical Lamination Theory
COV	Coefficient of Variation
CP	Coach Peel specimen
DSA	Direct Simulated Annealing
FEA	Finite Element Analysis
FRM	Fiber Reinforced Materials
GFRP	Graphite Fiber Reinforced Plastics

HAZ	Heat Affected Zone
HB	Brinell Hardness
MCP	Modified Coach Peel specimen
MTS	Modified Tensile Shear specimen
PMA	Precision Metalforming Association
SA	Simulated Annealing
SAE	Society of Automotive Engineering
SLCD	Statistical Linear Cumulative Damage
TS	Tensile Shear specimen

1. FATIGUE OF MONOLITHIC MATERIALS: FATIGUE OF SPOT WELD JOINTS

1.1. Introduction

Automotive bodies, like many other structures, are composed of metal sheets joined by spot welds. A spot weld is materialized by clamping the sheets with two pincers while applying force and transmitting current as depicted in Figure 1.1 The electrical resistance of the contacting sheets generates sufficient heat at the faying surface to melt the metal; eventually a nugget develops and the interface locally disappears.

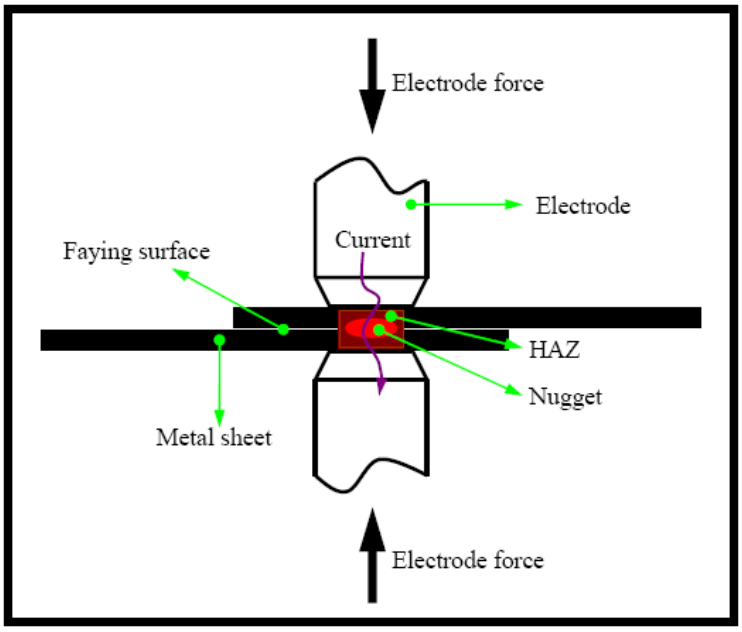

Figure 1.1. The resistance spot welding process

Despite the availability of other joining methods such as laser beam welding and adhesive bonding, resistance spot welding remains the primary method for joining panels and bodies especially in automobile, railroad, and airplane structures. The economical advantages of spot welding were realized many years ago in the aerospace industry [1]. About 90 percent of the welds used in an automotive body assembly are resistance spot

welds [2]. A typical vehicle contains more than 3000 spot welds [3-9]. This number may reach 5000 and sometimes 8000 in bus and coach bodies. The advantages of using spot welds are that the joining process is faster than the other type of joining techniques life bolted joints, bonded joints and riveted joints, no filler material is required, and dimensional accuracy is better preserved during welding with local heating [3-6, 9-11].

In service, mechanical components usually experience cyclic loading. This makes fatigue failure prevention the foremost design requirement. Considering that spot welds provide localized connection, thus creating inherent circumferential notches, they lead to stress concentrations and consequently make the structure more likely to fail due to fatigue. For instance, approximately 80 percent of all cases of fatigue failure in automotive components occur around a spot weld; 15 percent of them at a low-quality-cut edge, and only in 5 percent fatigue cracks initiate in sheet metal [12]. Accordingly, one may assume that under normal service conditions, fatigue strength of spot weld joints dominate the overall structural durability. Hence, a better understanding of spot-weld fatigue behavior and use of reliable fatigue assessment models should be considered as the requirements for reliable designs. For this reason, many researchers [2-4, 11-26] have focused on this subject.

A deeper understanding of the fatigue behavior can be attained through further experiments and observations. Basic fatigue characterization tests were commonly conducted using tensile-shear specimens (TS) [2, 3, 5, 9, 11, 14, 15, 19, 23, 27], which contain two or three plates joined by one or two spot welds loaded in shear. On the other hand, modified tensile shear specimens (MTS), which contain plates bent at their longitudinal edges, were rarely studied. MTS specimens have higher flexural stiffness and thus have higher resistance to bending and buckling. For this reason, this type of geometry is more commonly used in industrial applications. Although TS and MTS specimens are loaded uniaxially in fatigue tests, plates are subject to bending moment due to eccentricity. Higher flexural stiffness of MTS will therefore have an impact on fatigue life. However, there are a few experimental data [18] available on fatigue behavior of MTS. In the previous study [22], fatigue failure tests were conducted on MTS specimens to understand their fatigue failure behavior as in reference [18]; but a different material, geometry and R-ratio were used.

There are basically two types of spot welds, namely automated (or standard) and manual. An automated-type spot weld is produced by holding the plates from both faces with two pincers while applying force and transmitting current. A manual spot weld is materialized by touching the electrode on one surface of the specimen without applying force. This type of spot weld may be preferred in some industrial applications if the sheets cannot be gripped at both sides. The studies on fatigue strength of spot-welded joints focused on automated-type spot welds. In the previous study [22], automated-type as well as manual-type spot welds were investigated experimentally and the range of difference in their life spans was compared.

Even if plates joined by spot welds are subject to uniaxial in-plane loads, multiaxial stresses develop around the spot welds. Due to the high stress concentration, plastic deformation is likely to occur around the welds. These stresses control the useful life of the joint and thus the specimen. For a reliable fatigue life assessment, one is required to determine, first of all, the stress field around the spot weld accurately. In this study, a nonlinear finite element analysis was carried out using nonlinear material properties and contact elements on the inner surfaces of the plates to find the stress and strain states. Plastic deformation and residual stresses developed after unloading were determined and accounted for in calculating the range of stress and strain fluctuation.

Another requirement for accurate fatigue life predictions is to use a reliable fatigue failure model. Different approaches are available for fatigue life assessment such as the nominal stress approach, the structural or hot-spot stress approach [18], the notch stress approach considering stress concentration effects and notch intensity [16, 18, 19, 22, 28, 29], the notch strain approach [19, 22, 28, 30-32], volumetric fatigue approach [19, 26] and finally the crack propagation or fracture mechanics approach [11, 19, 22, 29, 33-35]. In this study, instead of using a fatigue model specifically developed for spot welds as in the previous studies, applicability of general fatigue models was investigated. It is more desirable for a designer to use a single model generally applicable to all types of connections rather than using a separate model for each one of them. For this purpose, a number of general purpose fatigue models were utilized to decide on which one of them would provide the best predictions for a spot weld joint.

In this study, taking into account the requirements for accurate fatigue life predictions, the fatigue failure behavior of tensile shear, modified tensile shear, coach peel, and modified coach peel specimens were investigated numerically. Using experimental data [18, 22], numerical and experimental results were compared.

1.2. Models for Fatigue Life Prediction

Fatigue is the main failure mechanism for structures under cyclic loading. Hence considerable research has been carried out for especially monolithic materials like metals. As a result of these studies, progresses have been made in developing fatigue life prediction methodologies. A large number of models for fatigue life assessment have been proposed in the literature. They are classified either as stress-based or strain-based approaches in general.

1.2.1. Stress-Based Approaches

These are based on the assumption that the range of values for stress controls the fatigue behavior of a component. They involve empirical relations between uniaxial fully reversed stress and fatigue life (S-N curves). However, mechanical components are usually subject to stresses oscillating about an average stress level. For these cases, a number of models were proposed.

$$\frac{S_a}{S_f}+\frac{S_m}{S_{ut}}=1 \text{ (Modified Goodman, England-1899)} \tag{1}$$

$$\frac{S_a}{S_f}+\left(\frac{S_m}{S_{ut}}\right)^2=1 \text{ (Gerber, Germany-1874)} \tag{2}$$

$$\frac{S_a}{S_f}+\frac{S_m}{S_y}=1 \text{ (Soderberg, USA-1930)} \tag{3}$$

$$\frac{S_a}{S_f}+\frac{S_m}{\sigma_f}=1 \text{ (Morrow, USA-1960s)} \quad (4)$$

where S_a is the alternating stress, S_m is the mean stress, S_f is the fully reversed fatigue strength of the material, S_{ut} is the ultimate tensile strength, S_y is the yield strength , σ_f is the true fracture strength, i.e. the true stress at final fracture. If a structure is subject to multiaxial stress state, equivalent uniaxial alternating and mean stresses can be used in fatigue calculations for proportional loading cases. The loading case considered in this study was assumed be proportional. Otherwise, more sophisticated models like critical plane approaches should be adopted.

1.2.2. Strain-Based Approaches

According to these models, the range of values for strain controls the fatigue life. They also take into account the effect of plastic strain. They are, therefore, especially suitable for cases where plastic effects dominate the fatigue behavior. Although most engineering structures and components are designed such that nominal stresses remain elastic, stress concentrations often cause plastic strains to develop in the vicinity of notches, e.g., spot welds in our case. Fatigue cracks usually nucleate due to plastic straining at the notches. The total strain amplitude can be resolved into elastic and plastic strain components, each of which has been shown to be correlated with fatigue life via power-law relationships for most metals [36]. The total strain life equation (or modified Coffin-Manson relationship) relates alternating true elastic and plastic strains, $\Delta\varepsilon_e$ and $\Delta\varepsilon_p$, to fatigue life, that is the number of cycles to failure (N_f), as follows [36, 37].

$$\frac{\Delta\varepsilon}{2}=\frac{\Delta\varepsilon_e}{2}+\frac{\Delta\varepsilon_p}{2}=\frac{\sigma'_f}{E}\left(2N_f\right)^b+\varepsilon'_f\left(2N_f\right)^c \quad (5)$$

where σ'_f is the fatigue strength coefficient, ε'_f is the fatigue ductility coefficient, and *b* and *c* are exponents determined by experiments.

In order to include the mean stress effect on fatigue life, several models were proposed in the literature. One method, often referred to as Morrow's mean stress method, replaces σ'_f by $\sigma'_f - \sigma_m$ in Equation (5), where σ_m is the mean stress [19, 36, 37]:

$$\frac{\Delta\varepsilon}{2} = \varepsilon_a = \frac{\Delta\varepsilon_e}{2} + \frac{\Delta\varepsilon_p}{2} = \frac{\sigma'_f - \sigma_m}{E}\left(2N_f\right)^b + \varepsilon'_f\left(2N_f\right)^c \tag{6}$$

An alternative version of this model where both the elastic and plastic terms are affected by the mean stress is given by [36, 38]

$$\frac{\Delta\varepsilon}{2} = \varepsilon_a = \frac{\Delta\varepsilon_e}{2} + \frac{\Delta\varepsilon_p}{2} = \frac{\sigma'_f - \sigma_m}{E}\left(2N_f\right)^b + \varepsilon'_f\left(\frac{\sigma'_f - \sigma_m}{\sigma'_f}\right)^{c/b}\left(2N_f\right)^c \tag{7}$$

In the case of multiaxial stress and strain states, the equivalent alternating strain can be used [36, 37, 39] in Equation (7) assuming proportional loading using either the maximum principal strain,

$$\varepsilon_{qa} = \varepsilon_{a1} \tag{8}$$

the maximum shear strain

$$\varepsilon_{qa} = \frac{\varepsilon_{a1} - \varepsilon_{a3}}{1+\nu} \tag{9}$$

or the octahedral shear strain,

$$\varepsilon_{qa} = \frac{\sqrt{\left(\varepsilon_{a1} - \varepsilon_{a2}\right)^2 + \left(\varepsilon_{a2} - \varepsilon_{a3}\right)^2 + \left(\varepsilon_{a3} - \varepsilon_{a1}\right)^2}}{\sqrt{2}\left(1+\nu\right)} \tag{10}$$

where ε_{a1}, ε_{a2}, and ε_{a3} are principal alternating strains with $\varepsilon_{a1} \rangle \varepsilon_{a2} \rangle \varepsilon_{a3}$ and ν is Poisson's ratio.

Another equation suggested by Smith, Watson, and Topper (often called the "SWT parameter") is given by [31, 36, 38]

$$\sigma_{\max} \varepsilon_a E = \left(\sigma_f'\right)^2 \left(2N_f\right)^{2b} + \sigma_f' \varepsilon_f' E \left(2N_f\right)^{b+c} \tag{11}$$

In order to save time and cost, it is often desirable to estimate fatigue life of a component or structure with a reasonable degree of accuracy using easily and quickly obtainable material properties such as hardness and tensile strength. Accordingly, many universally valid correlations between monotonic strength data and fatigue life have been proposed in the literature based on experimental data [31, 36]. Among these relations, the Modified Universal Slopes method proposed by Muralidharan and Manson is the best known and given by [31, 36, 38]

$$\frac{\Delta\varepsilon}{2} = \varepsilon_a = 0.623\left(\frac{S_{ut}}{E}\right)^{0.832}\left(2N_f\right)^{-0.09} + 0.0196\left(\varepsilon_f\right)^{0.155}\left(\frac{S_{ut}}{E}\right)^{-0.53}\left(2N_f\right)^{-0.56} \tag{12}$$

where S_{ut} is the ultimate tensile strength. Another universal relation based on Brinell hardness [31] is given by

$$\frac{\Delta\varepsilon}{2} = \frac{4.25\left(HB\right)+225}{E}\left(2N_f\right)^{-0.09} + \frac{0.32\left(HB\right)^2 - 487\left(HB\right)+191000}{E}\left(2N_f\right)^{-0.56} \tag{13}$$

The final two approximations do not require coefficients or exponents specific to a material. They use only hardness, ultimate tensile strength, and modulus of elasticity (in MPa) for strain-life calculations; all of which are commonly available, or easily measurable. These equations are applicable to a range of materials.

1.3. Geometry of the Spot Weld Joints

In this study, four commonly used joint types, tensile-shear (TS) modified tensile-shear (MTS), coach peel (CP), and modified coach peel (MCP), were considered. TS and MTS are made of three strips of sheets joined by two spot welds as shown in Figures 1.2 and 1.3 Unlike TS specimens, MTS specimens contain plates bent at their sides. This increases the flexural rigidity, and thus resistance to bending and buckling. CP and MCP joints are made of two strips of sheets joined by one spot weld as shown in Figures 1.4 and 1.5 Because automated-type spot welds are formed by pressing the plates at both sides, some of the molten material is squeezed out into the interface between the plates. The extent of the slag material pushed into the interface between the plates may reach up to 10-20% of the sheet thickness [36, 37, 39]. In order to be on the conservative side, the gap between the overlapping portions of the plates was taken as 0.2 mm

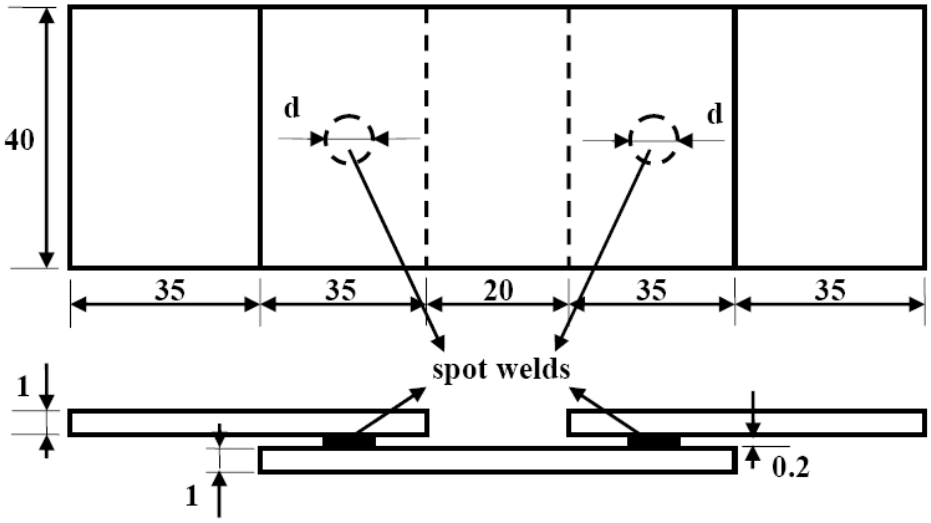

Figure 1.2. Geometry of the tensile shear (TS) specimens (bottom and side views).

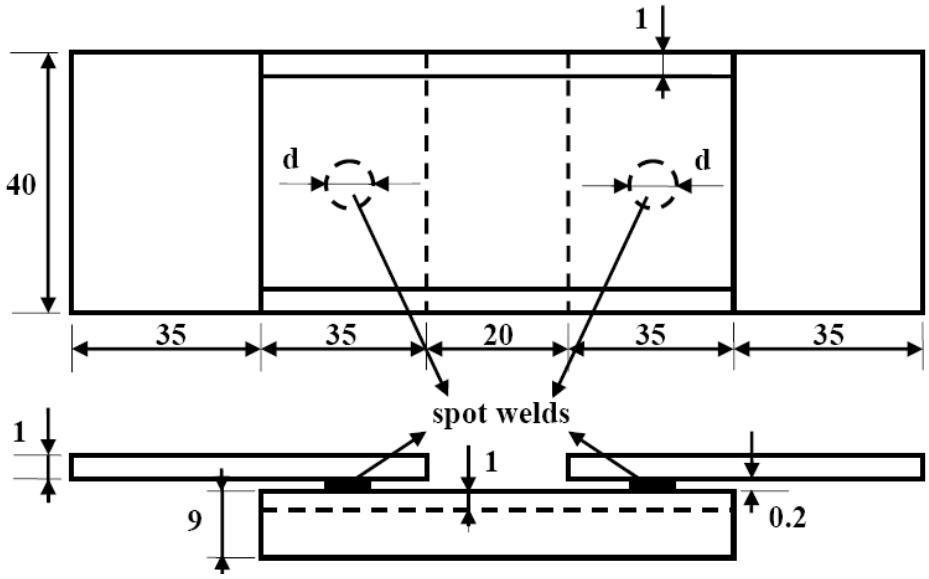

Figure 1.3. Geometry of the modified tensile shear (MTS) specimens (bottom and side views).

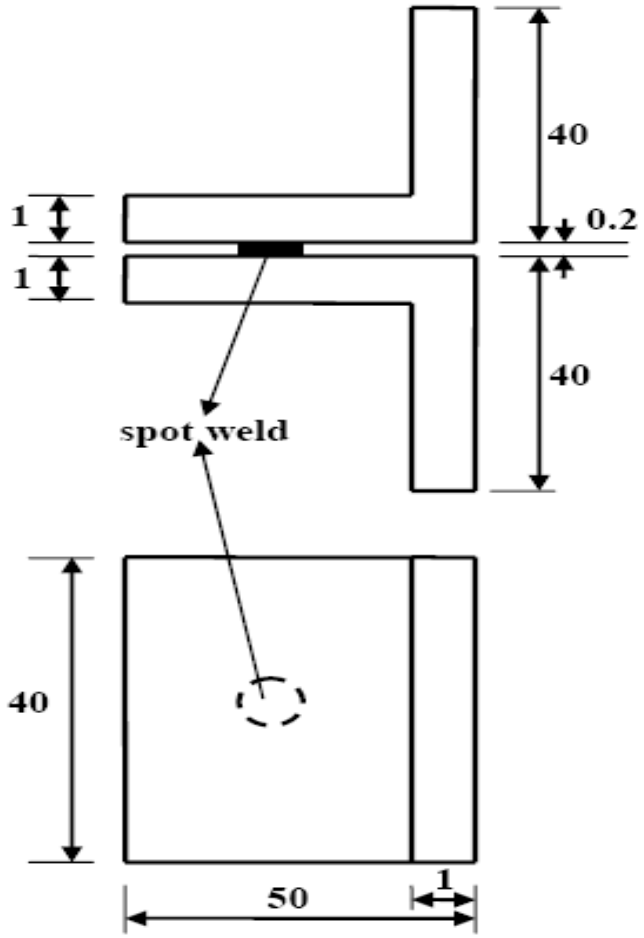

Figure 1.4. Geometry of the coach peel (CP) specimens (side and top views).

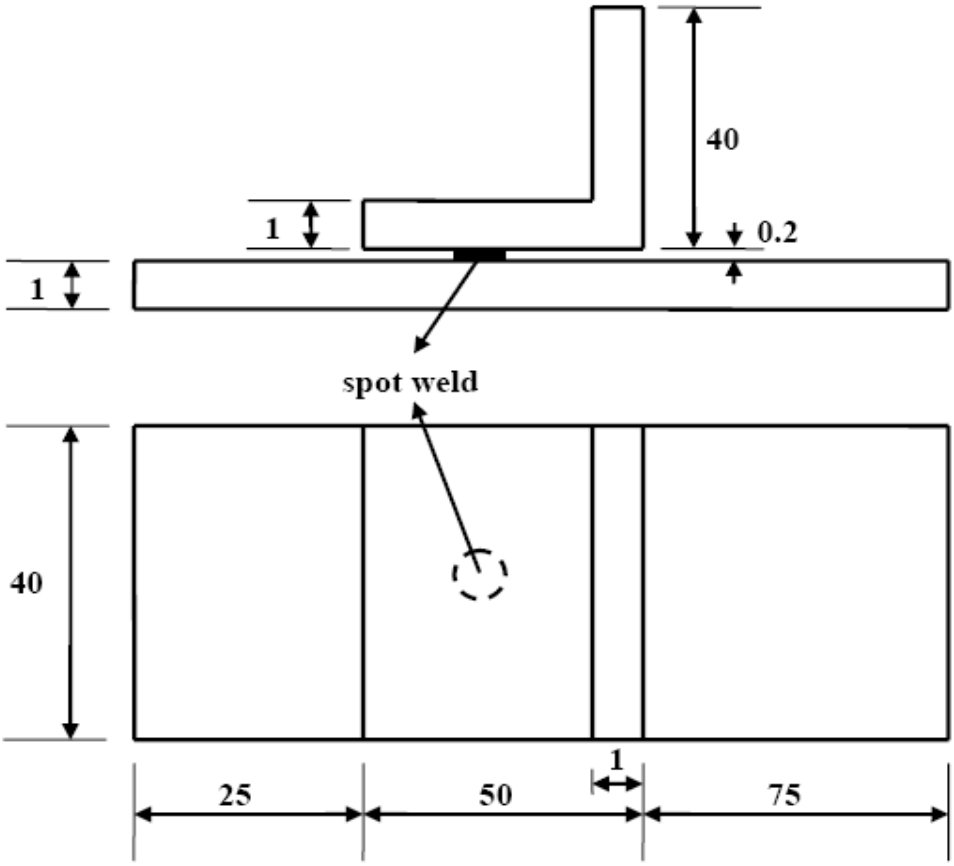

Figure 1.5. Geometry of the modified coach peel (MCP) specimens (side and top views).

1.4. Material Properties

In the FE model, the material properties of St 12 03 (DIN 1623), a low carbon steel, were used. The engineering stress-strain diagram is given in Figure 1.6. The average mechanical properties of St 12 03 are given in Table 1.1 [22]. Materials of this type are widely used in automotive industry, especially to construct body frames. Low carbon steels are cheaper and easier to process in comparison to high carbon steels. Although they have lower fatigue strength, they are less sensitive to notches and surface imperfections. Also, they weld evenly and easily, and hold paint well

A spot welded joint is composed of a nugget and base metal. Because heat treatment does not cause an appreciable change in elastic modulus and Poisson's ratio, it can be accepted that their magnitudes remain about the same throughout the specimen despite

melting during the formation of the nugget. Although the fatigue parameters and the nonlinear stress-strain relation of the material in and around the nugget are affected during the joining operation, this effect was neglected considering that the steel was not hardened and heat treated. In Table 1.1, the results of micro-hardness tests on base metal, HAZ, and nugget are given. Because the hardness levels at these locations are close to each other, one may assume that there is no significant change in mechanical properties of the material during welding. The engineering stress-strain curve of the base material (DIN 1623), shown in Figure 1.6, was assumed to be valid for the nugget and heat affected zone (HAZ).

Table 1.1. Mechanical properties of St 12 03 (DIN 1623) steel [22, 40].

Number of tests performed	4
Average tensile strength, (MPa)	319.64 (2.43*)
Average yield strength, (MPa)	217.41 (1.25*)
Average reduction of area, %	35.59 (2.71*)
Average hardness for base metal, (kgf/mm^2)	105.5
Average hardness for HAZ, (kgf/mm^2)	106.2
Average hardness for nugget, (kgf/mm^2)	112.6
Modulus of Elasticity, (GPa)	207
Poisson's ratio	0.25

* The values inside the parentheses show standard deviations of the values

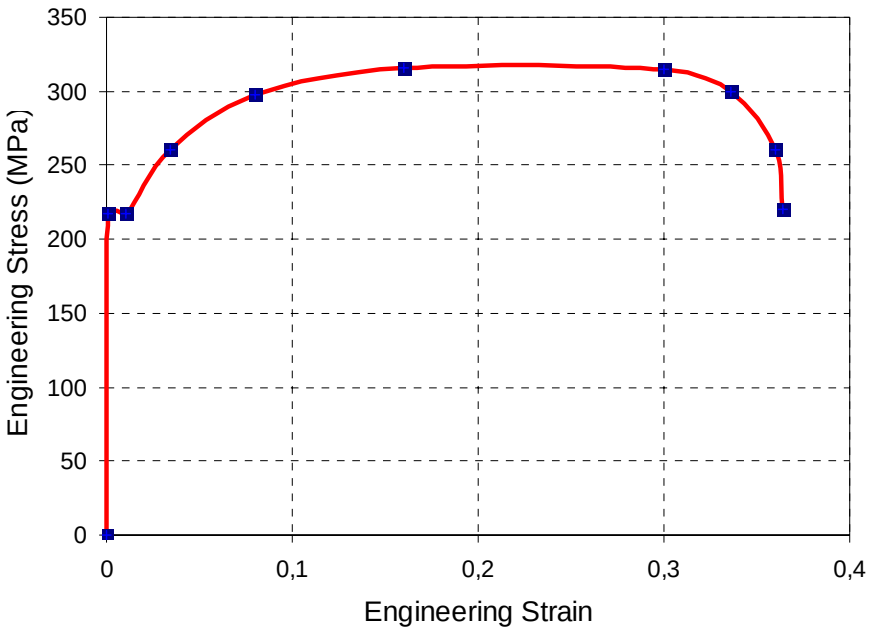

Figure 1.6. Engineering stress-strain curve [22, 40].

There are various industry standards for sizing a spot weld for a given sheet metal thickness. For instance, the American Welding Society (AWS), Society of Automotive Engineering (SAE), and the American National Standards Institute (ANSI), together recommend a weld nugget diameter for steels [5] given by

$$d \approx 4\sqrt{t} \tag{14}$$

where d and t are the weld nugget diameter and sheet thickness, respectively (in mm). This recommended formula is empirical in nature obtained through extensive experiments. Interestingly, this formula is valid independent of the varying properties of the materials [5, 41]. In this study, the specimens were made of a metal sheet having 1 mm thickness. In accordance with the formula, the spot weld nugget diameter was selected as 4 mm.

1.5. Fatigue Lives

As in the previous studies [19, 21, 36], the fatigue life was defined as the number of loading cycles it takes for the first crack to initiate and propagate through thickness of the sheet, and become visible from the outer side of the sheet. In that case, testing of the specimen was immediately terminated. After a through crack had appeared, the maximum deflection increased quickly indicating a significant decrease in the stiffness of the specimen. In order to aid in the visual detection of a crack, a small amount of machine oil was deposited between the specimen sheets before testing. When the crack grew through the sheet, it allowed the oil to seep through and appear on the outer surface of the sheet signaling failure.

Table 1.2 shows the tabulated data of the applied load ranges (P_{min}, P_{max}) and the corresponding experimental fatigue life ranges of the specimens [22]. Manual-type spot weld joints endured 30 percent to 45 percent shorter life in comparison to automated-type spot weld joints. Although sometimes porosities were observed in the manual spots, the nugget did not fail. On the contrary, cracks leading to fatigue fracture appeared close to the nugget edges and propagated through the thickness as in the automated welds. The reason

why the manual spots are weaker to fatigue loading may be attributed to higher stress concentration arising from non-symmetric weld geometry and sharper edges

Table 1.2. Average (or mean) fatigue lives of the specimens and the number of samples tested, *n* [22].

Manual-Type Spot				Automated-Type Spot			
P_{max}(N)	P_{min}(N)	*n*	N_f (cycles) range	P_{max}(N)	P_{min}(N)	*n*	N_f (cycles) range
3700	200	5	9800-10100	3700	200	5	13280-13450
3000	150	4	36500-41500	3000	150	4	58660-62970
2700	150	4	49000-55940	2700	150	4	90750-95000
2400	150	3	79650-102450	2400	150	3	159250-172300
2200	150	3	143456-185432	2250	150	2	265700-300600
2100	150	2	416474-450430	2150	100	1	633250

1.6. Statistical Analysis of the Experimental Data

The scatter in fatigue lives is large even under controllable and repeatable testing conditions. Lack of precision in testing equipment, loose tolerances in specimen dimensions, large variations in environmental conditions etc. may lead to unacceptably large scatter in data. For this reason, one should ensure that the scatter in experimental data is within the acceptable range and tests are conducted under controllable and repeatable conditions. This requires a statistical analysis of the data.

One of the ways to estimate the scatter in fatigue life is to calculate the coefficient of variation (COV) as given in Equation (15). The typical values of COV for mild steels range from 0.10 in low cycle fatigue to 0.5 in high cycle fatigue [42, 43]. High strength materials seem to exhibit larger scatter in fatigue life [43]. The COV values for welded joints are even higher [36]. Tables 1.3 and 1.4 show COV (δ_x) values of fatigue lives of spot weld joints corresponding to the load ranges indicated in Table 1.2. As seen in these tables, the fatigue life data experimentally obtained [22] have lower values of COV than the typical ones for all loading cases. This shows that the data are reliable and the testing conditions are repeatable and controllable. Variations in the data are then mostly attributable to the inherent characteristics of the material not to the testing conditions. One should also note that the values of COV for automated–type spot welds being somewhat lower imply that this type of specimens is more repeatable.

$$
\begin{aligned}
&COV = \delta_X = \frac{\sigma_X}{\mu_X} \\
&where \\
&\sigma_X = \sqrt{Var(X)} \\
&Var(X) = \frac{1}{n-1}\sum_{i=1}^{n}(x_i - \mu_X)^2 \\
&\mu_X = \frac{1}{n}\sum_{i=1}^{n} x_i
\end{aligned}
\tag{15}
$$

where σ_x and μ_x represent standard deviation and mean (average) value of the data, respectively, n is the number of data, μ_i is the mean value of the ith data, x_i is the ith data, $Var(x)$ is the variance of the data.

Table 1.3. Mean, standard deviation, and COV values for the automated-type spot welds.

Automated-Type Spot Weld			
Life Range	**Mean Value**	**Standard Deviation**	**COV**
13280-13450	13370	80.932	0.006
58660-62970	61190	1851.4	0.030
90750-95000	93480	1875.26	0.020
159250-172300	167100	6916.83	0.041
265700-300600	283150	24678.03	0.087
633250	633250	N/A	N/A

Table 1.4. Mean, standard deviation, and COV values for the manual-type spot welds.

Manual-Type Spot Weld			
Life Range	**Mean Value**	**Standard Deviation**	**COV**
9800-10100	9970	132.85	0.013
36500-41500	39000	2198.48	0.056
49000-55940	52470	3270.16	0.062
79650-102450	93550	12194.67	0.130
143456-185432	163546	21045.55	0.129
416474-450430	433452	24010.52	0.055

For relatively small sample size, n, cases, for instance, less than 10, the assumption that the sample variance is equal to the population variance is not appropriate [44]. In order to determine confidence interval for the mean assuming that the population standard deviation is not known in advance, Student's t-distribution can be used. In this point,

making the following probability statement given in Equation (16), the 95% confidence intervals for the mean of fatigue life data were calculated using Equation (17).

$$P\left(-t_{\alpha/2,n-1} \le \frac{\bar{X}-\mu}{S/\sqrt{n}} \le t_{\alpha/2,n-1}\right) = 1-\alpha \tag{16}$$

$$\langle \mu \rangle_{1-\alpha} = \left[\bar{x} - t_{\alpha/2,n-1}\frac{s}{\sqrt{n}} \; ; \; \bar{x} + t_{\alpha/2,n-1}\frac{s}{\sqrt{n}} \right] \tag{17}$$

where $1-\alpha$ is confidence level, $\bar{x}$ is sample mean, n is sample size, and s is standard deviation.

Tables 1.5 and 1.6 show the confidence interval for the mean assuming that the population standard deviation is not known in advance using the values of Student's t-distribution ($t_{\alpha/2,n-1}$).

Table 1.5. The 95% confidence interval of the mean for automated-type spot welded specimens using the values of Student's t-distribution.

Automated-Type Spot Weld			
Mean Value	**Standard Deviation**	**$t_{\alpha/2,\ n-1}$**	**Confidence Interval for Fatigue Life**
13370	80.932	2.776	[13270; 13470]
61190	1851.4	3.182	[58244; 64136]
93480	1875.26	3.182	[90496; 96464]
167100	6916.83	4.303	[149916; 184284]
283150	24678.03	12.706	[61430; 504869]
633250	N/A	N/A	N/A

Table 1.6. The 95% confidence interval of the mean for manual-type spot welded specimens using the values of Student's t-distribution.

Manual-Type Spot Weld			
Mean Value	**Standard Deviation**	**$t_{\alpha/2,\, n-1}$**	**Confidence Interval for Fatigue Life**
9970	132.85	2.776	[9870; 10070]
39000	2198.48	3.182	[35502; 42498]
52470	3270.16	3.182	[47267; 57673]
93550	12194.67	4.303	[63254; 123846]
163546	21045.55	4.303	[111262; 215830]
433452	24010.52	12.706	[217730; 649174]

In order to judge whether the scatter is within the acceptable range, one may also examine the regression coefficients obtained through a regression analysis of the experimental data. It is known that fatigue life data can typically be fitted to a power-law. Figure 1.7 shows the experimental data points and the fitted lines with their respective coefficient of determination (R^2) values for the manual-type and automated-type spot welds. The value of R^2 being close to 1.0 indicates that the linear line is a good fit for the data and the predictability of the regression is quite high.

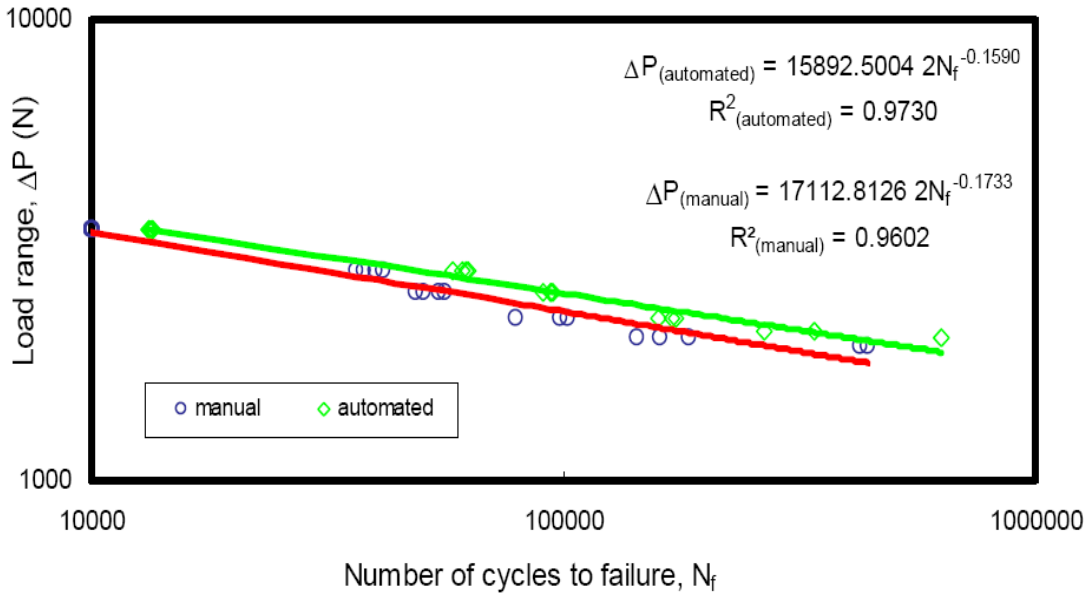

Figure 1.7. The resulting curve of the regression analysis for both the manual-type and the automated-type spot welds.

Tables 1.7 and 1.8 show the 95 percent and 99 percent confidence intervals (two-sided) of the mean for automated-type and manual-type spot welded specimens, respectively. Here the underlying distribution of experimental fatigue life data is normal.

Table 1.7. The confidence interval of the mean for automated-type spot welded specimens.

The confidence interval for the mean for the automated-type spot weld			
for the 95 percent interval		for the 99 percent interval	
13 299	13 441	13 277	13 463
59 376	63 004	58 802	63 578
91 642	95 318	91 061	95 899
159 273	174 927	156 797	177 403
248 948	317 352	238 129	328 171
N/A	N/A	N/A	N/A

Table 1.8. The confidence interval of the mean for manual-type spot welded specimens.

The confidence interval for the mean for the manual-type spot weld			
for the 95 percent interval		for the 99 percent interval	
9 854	10 086	9 817	10 123
36 845	41 155	36 164	41 836
49 265	55 675	48 250	56 688
79 750	107 350	75 385	111 715
139 731	187 361	132 197	194 895
400 175	466 729	389 649	477 255

1.7. Finite Element Model

Fatigue life prediction models require accurate calculation of stress and strain states developed in the structure. For this purpose, commercial FEA software, ANSYS (version 10), was used. Residual stresses developed during the formation of the spot weld were assumed not to affect the fatigue life and were not considered in the stress analysis. However, the residual stresses arising from non-uniform plastic deformations were determined through the nonlinear stress analysis. Dynamic effects were neglected and the load was assumed to be applied quasi-statically.

The actual behavior of the material may exhibit a combination of isotropic hardening and kinematic hardening characteristics. Assumption of purely isotropic hardening may lead to non conservative predictions. In the absence of full characterization of the material,

a kinematic hardening material model (KINH) was considered to be more appropriate to simulate the nonlinear deformation behavior. This model uses the Besseling formulation [35, 36, 46], which includes the Bauschinger effect, which refers to a property of material where the material's stress/strain characteristics change as a result of the microscopic stress distribution of the material, in cyclic loading. The data points were taken from the true stress-strain diagram, which was obtained by converting the engineering stress-strain diagram shown in Figure 1.6.

In the FE model, a 3D 10-node tetrahedral solid element, SOLID92 (Figure 1.8), was used for the sheet metal. This element has plasticity, creep, swelling, stress stiffening, large deflection, and large strain capabilities. The element also has ten nodes having three degrees of freedom at each node: translations in the nodal x, y, and z directions. Several types of models have been proposed in the literature for spot-weld nuggets: single-bar model [13], spoke-bar model [13, 29], multiple rigid-bar model [7, 13], and solid nugget model [6, 9, 13, 18, 19, 35, 45]. Modeling the beam using solid elements leads to difficulties in meshing because this requires matching of the meshes of different parts. Besides, since the length of the nugget is equal to the gap between the plates, which is very small, tiny solid elements should be generated for the nugget. This adds enormously to the computational time. For these reasons, a different approach was adopted in this study; the nugget was modeled using a two-node beam element, BEAM188 (Figure 1.9). Contact and target elements, TARGE170 (10) and CONTA175 (11), were created on the inner surfaces around the spots. The contact elements themselves overlay the solid elements describing the boundary of a deformable body and are potentially in contact with the target surface, defined by TARGE170. This target surface is discretized by a set of target segment elements (TARGE170) and is paired with its associated contact surface via a shared real constant set. For rigid target surfaces, these elements can easily model complex target shapes. For flexible targets, these elements will overlay the solid elements describing the boundary of the deformable target body [46]. The beam element, BEAM188, is based on Timoshenko beam theory. Shear deformation effects are included, which are especially important for short beams. This element has six degrees of freedom at each node. These include translations in the x, y, and z directions and rotations about the x, y, and z directions. This element is well-suited for linear, large rotation, and/or large strain nonlinear applications. The beam shares a single node on each plate. This element is

suitable for analyzing slender to moderately stubby/thick beam structures [46]. One should note that solid elements that are used to model the plates do not have rotational degrees of freedom unlike the beam element used for the nugget. In order to prevent relative rotation of plates with respect to spot weld at the connection points, the nodes on the plates that lie within the region of the spot weld radius are constrained to move within the plane perpendicular to the beam. Because the nugget experiences low stresses as reported in previous studies [21], its material model was chosen as linearly elastic.

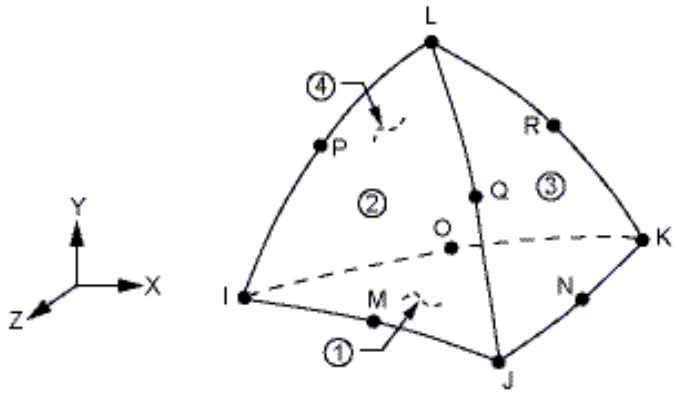

Figure 1.8. General geometry of SOLID 92 element [46].

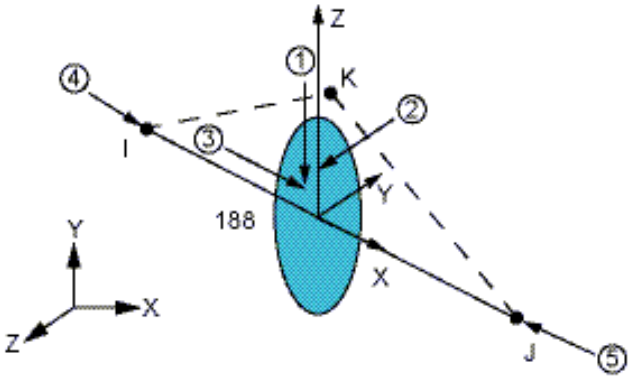

Figure 1.9. General geometry of BEAM 188 element [46].

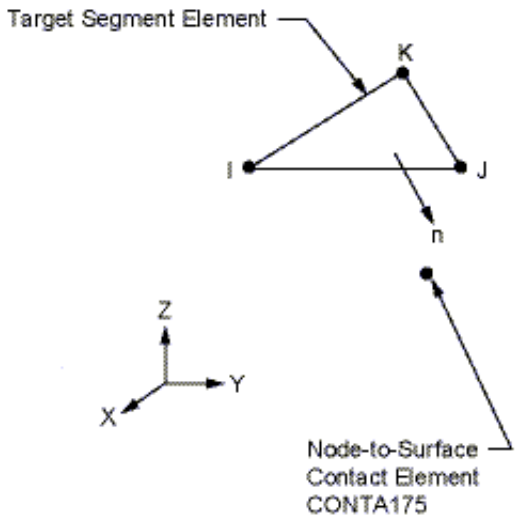

Figure 1.10. General geometry of TARGE170 element [46].

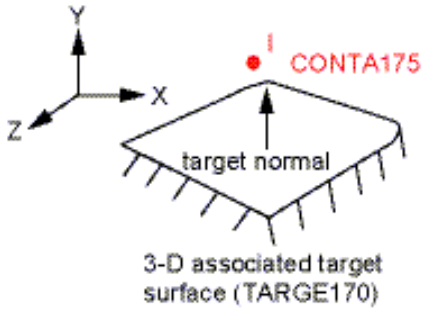

Figure 1.11. General geometry of CONTA175 element [46].

In order to obtain an appropriate mesh structure that may enable accurate calculation of the stress state, a convergence analysis was carried out for the element size. In the FE analysis, a load range of 150 N-2700 N was applied. Figure 1.11 shows the maximum tensile stress calculated using different element sizes. Convergence was obtained for 0.002 mm element size. The size of the elements used within and around the spot-weld nugget was chosen to be much smaller than 0.002 mm to correctly determine the stress state in this highly stresses region. Figure 1.13 shows the finite element mesh and Figure 1.14 depicts a detail of the mesh on the section passing through the middle of the right spot weld.

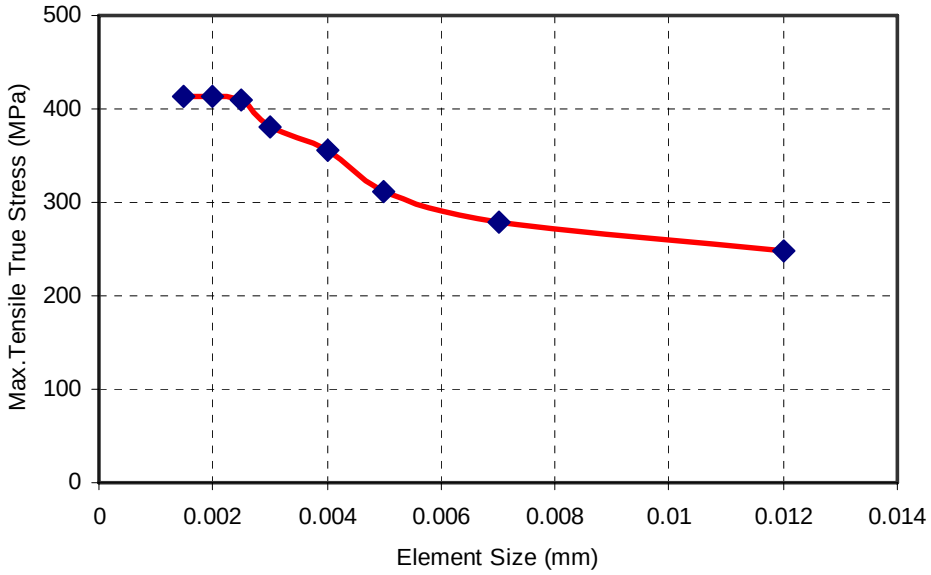

Figure 1.12. Convergence in terms of element size.

In ANSYS, a load step is applied in increments with a certain number of substeps. A convergence analysis was also performed to determine the number of substeps necessary for accuracy. As shown in Figure 1.15, 160 substeps are adequate for an accurate analysis.

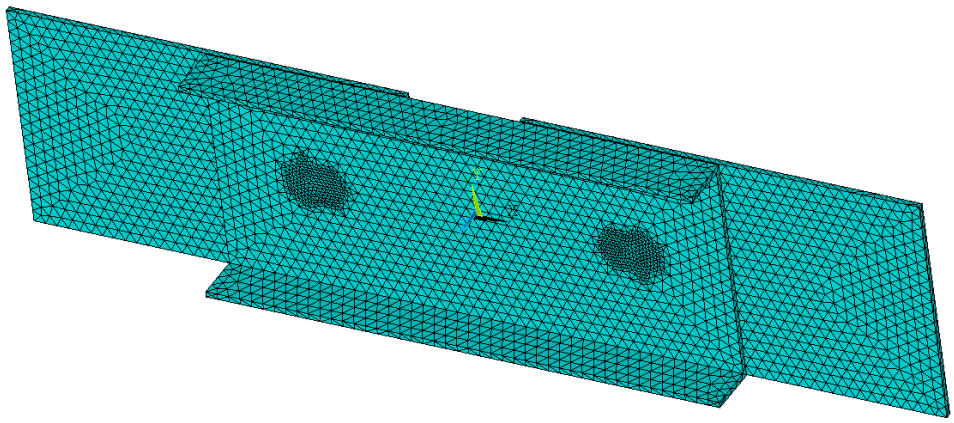

Figure 1.13. Finite element model for the MTS specimen.

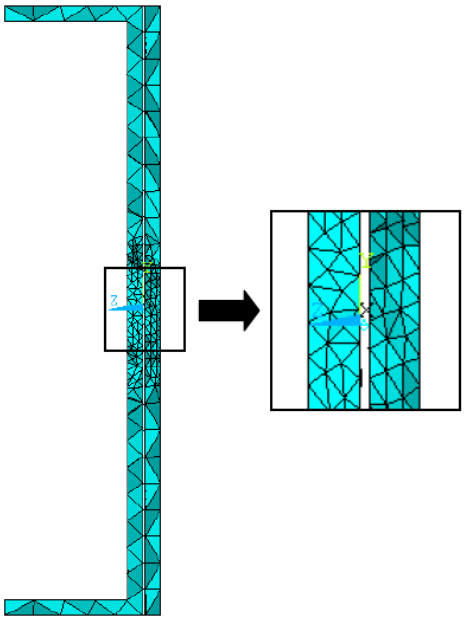

Figure 1.14. A detail of the mesh at and around the right spot weld of the specimen.

The space or gap between the overlapping portions of the plates was taken as 0.2 mm. Because different values were suggested in the literature (e.g. 0.02 mm in [47]), the effect of the extent of the gap on fatigue life was also investigated.

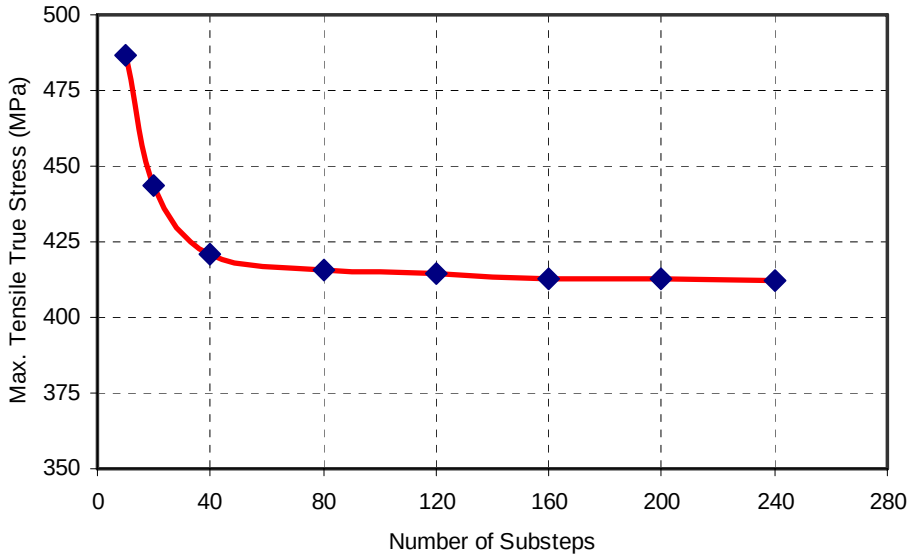

Figure 1.15. Convergence in terms of substeps.

1.8. Boundary Conditions

The boundary conditions in the FE model of TS and MTS specimens are shown in Figures 1.16 and 1.17, respectively. Displacements and rotations in all degrees of freedom are fixed at one end. The other end is subject to uniformly distributed in-plane load cycle in the *x*-direction, while the movement is prevented in the other degrees of freedom. The boundary conditions for MTS specimen are the same. The boundary conditions for CP and MCP are shown in Figures 1.18 and 1.19, respectively.

The cyclic loading was applied in two load steps. First, the load was incrementally increased to its maximum value, P_{max}, and the resulting stress state was obtained. In the second load step, the load was incrementally decreased to its minimum value, P_{min}. In the next load cycles, stresses were assumed to fluctuate between the stress values obtained for the maximum and minimum load levels in the first load cycle.

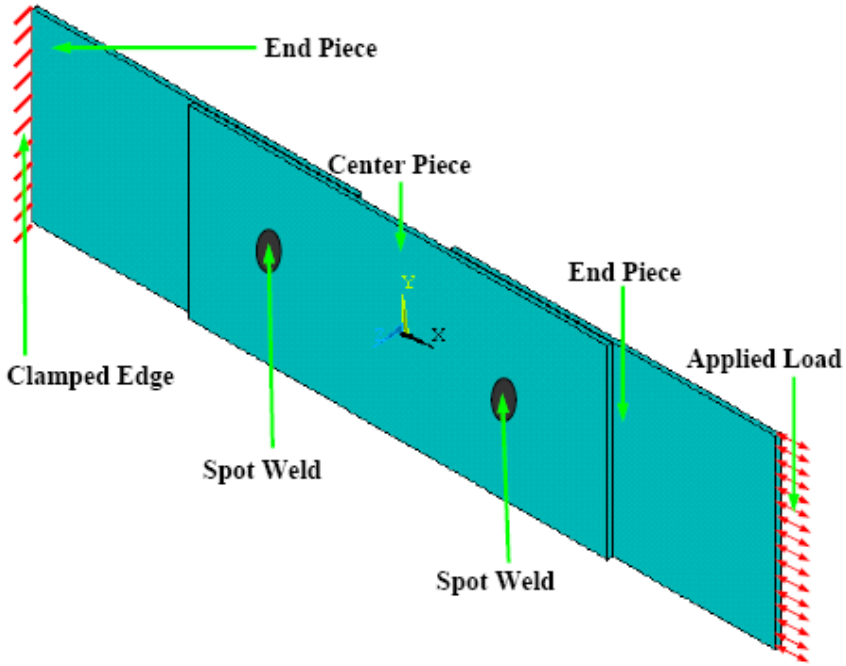

Figure 1.16. Boundary conditions of the finite element model of TS.

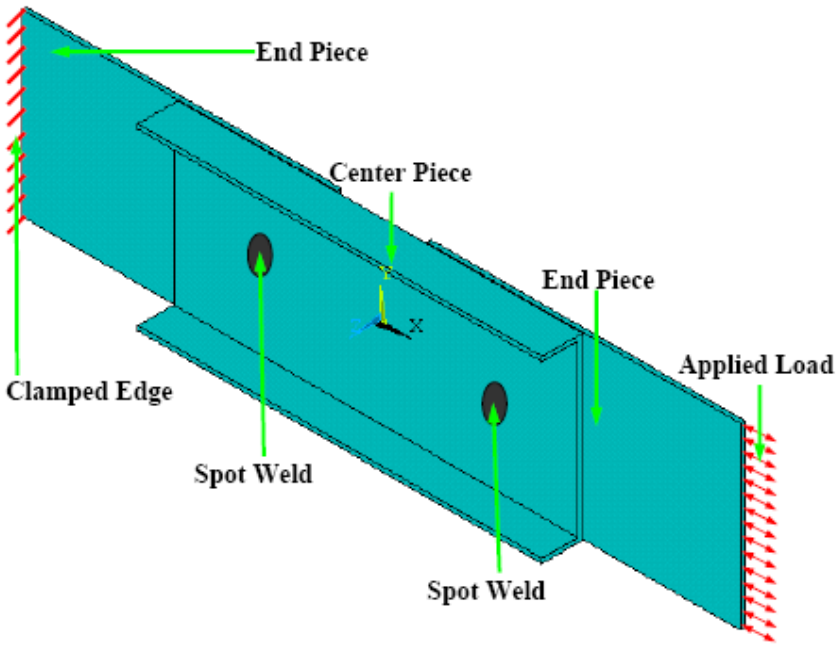

Figure 1.17. Boundary conditions of the finite element model of TS.

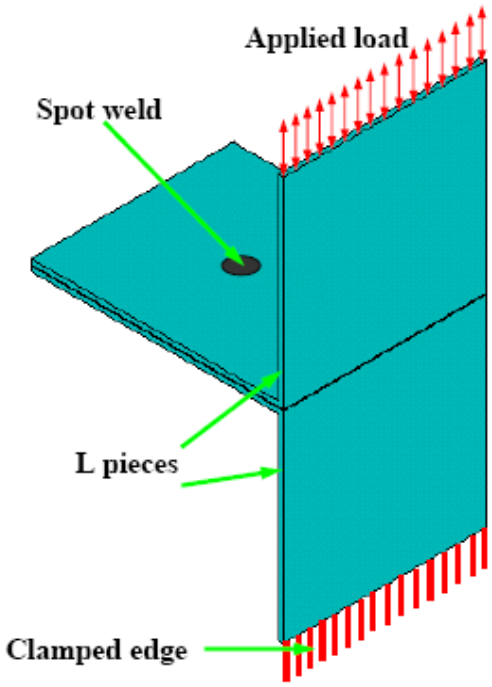

Figure 1.18. Boundary conditions of the finite element model of CP.

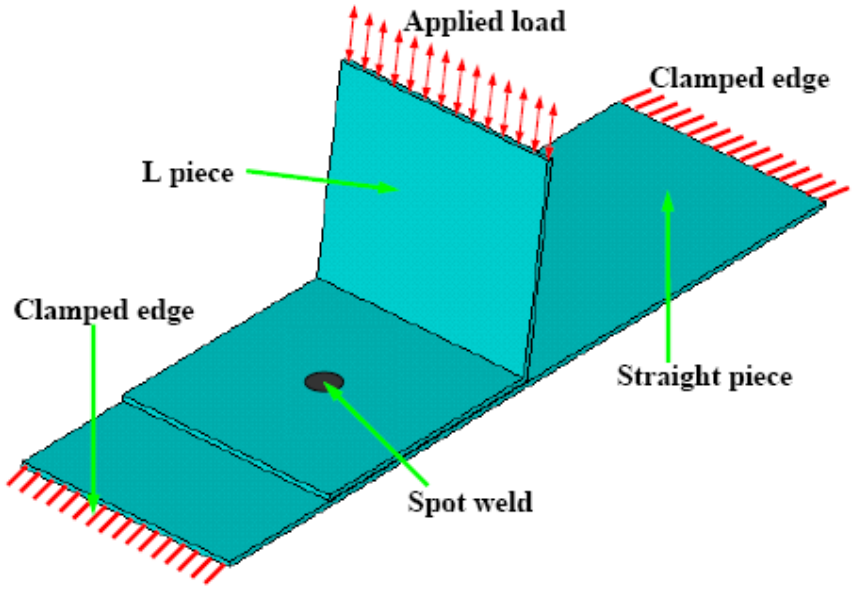

Figure 1.19. Boundary conditions of the finite element model of MCP.

1.9. Resulting Stress States

Figures 1.20-1.23 show the distributions of σ_{xx} component of stress on the inner and outer surfaces of central pieces of TS and MTS specimens developed after the maximum (2700 N) and minimum (150 N) loads are applied. High stresses develop on the inner surfaces of the sheets close to the peripheries of the spot weld nuggets. The peak tensile stress develops close to the spot weld but not on its circumference. The location of the high stress conforms to the fatigue crack initiation sites experimentally observed in previous studies [22, 40, 47, 48].

Because the minimum load is tensile and quite low (150 N), significant compressive stresses existing after unloading may only be attributed to residual stresses developed due to nonuniform plastic deformation. Although load transfer occurs through the spot weld joint, the nugget is subject to low stresses since its thickness is large in comparison to the sheet thickness. Besides, the nugget is mainly subject to shear loading and the plate is mainly subject to bending moment. Consequently, bending induces larger stresses. Due to the effect of bending, stresses change from tension to compression through the thickness as seen in Figures 1.20 and 1.22. For this reason, flexural rigidity of the plate, i.e. its

resistance to bending significantly affects the stress level even though the plates are subject to in-plane loading. The flanges of MTS specimens increase its flexural rigidity, but essentially at the sides. Considering also that the load is transferred through the middle region, one may see why stresses are more concentrated in the MTS specimen (Figure 1.22) in comparison to the TS specimen (Figure 1.20). However, the peak compressive residual stress in the minimum load case is larger for the TS.

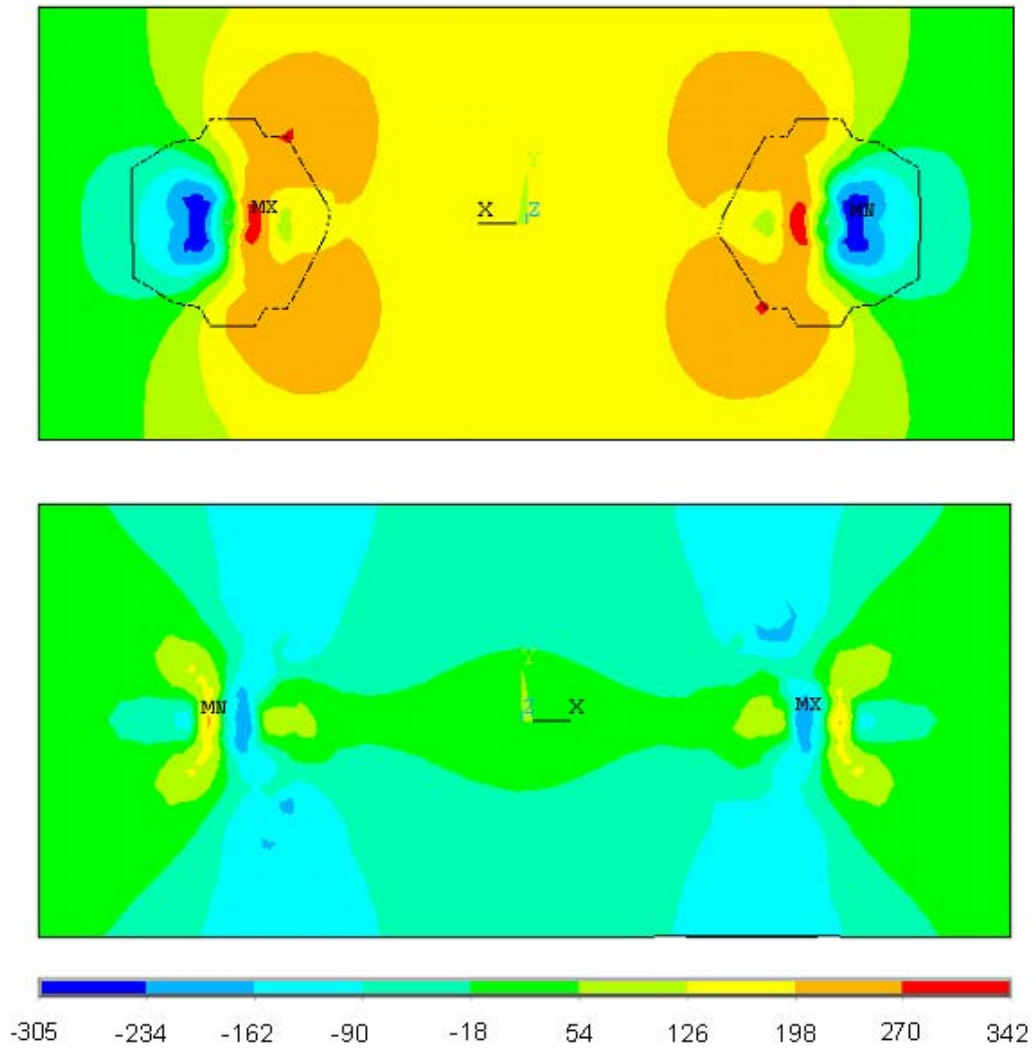

Figure 1.20. Distribution of σ_{xx} component of true stress (in MPa) on the inner and outer surfaces of the central plate of a TS specimen developed due to the maximum load. (t = 1 mm, d = 4 mm, number of spots = 2)

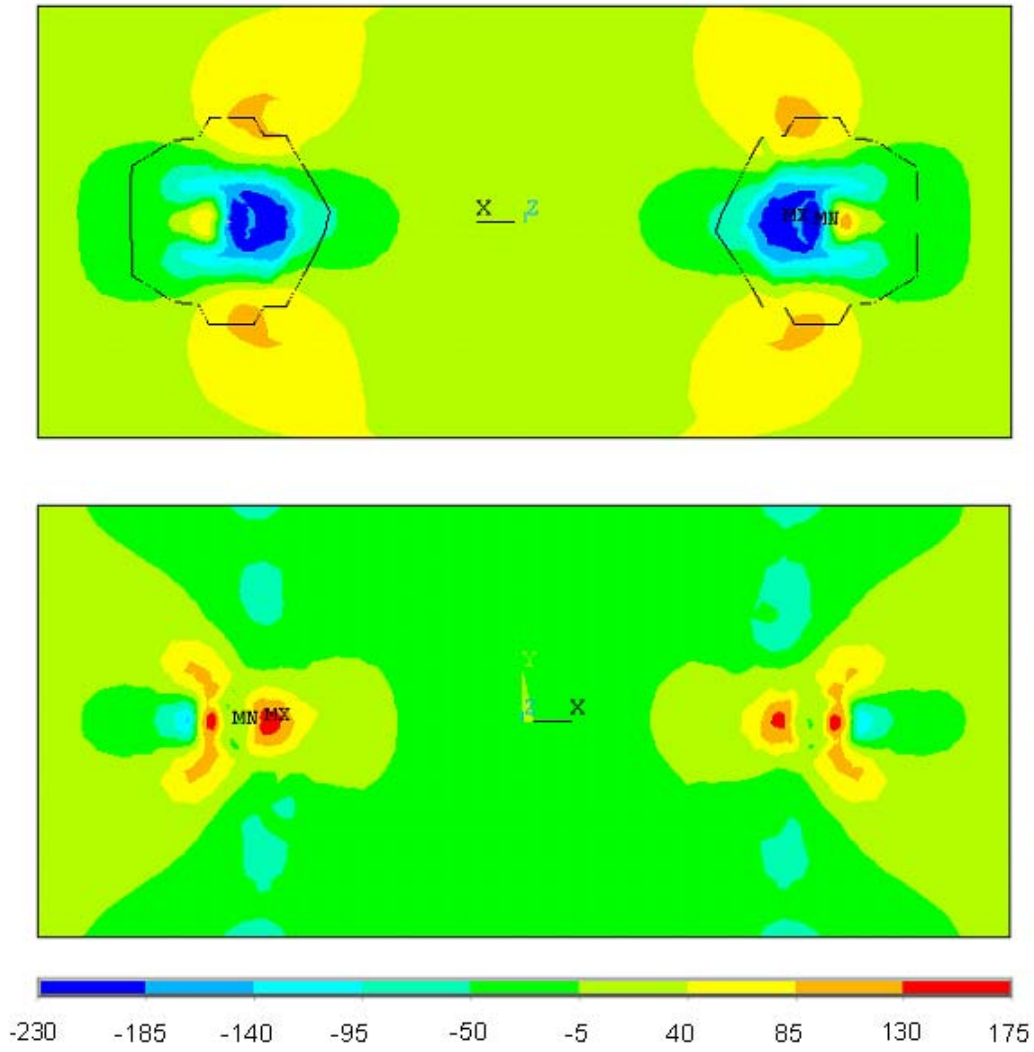

Figure 1.21. Distribution of σ_{xx} component of true stress (in MPa) on the inner and outer surfaces of the central plate of a TS specimen developed due to the minimum load. (t = 1 mm, d = 4 mm, number of spots = 2)

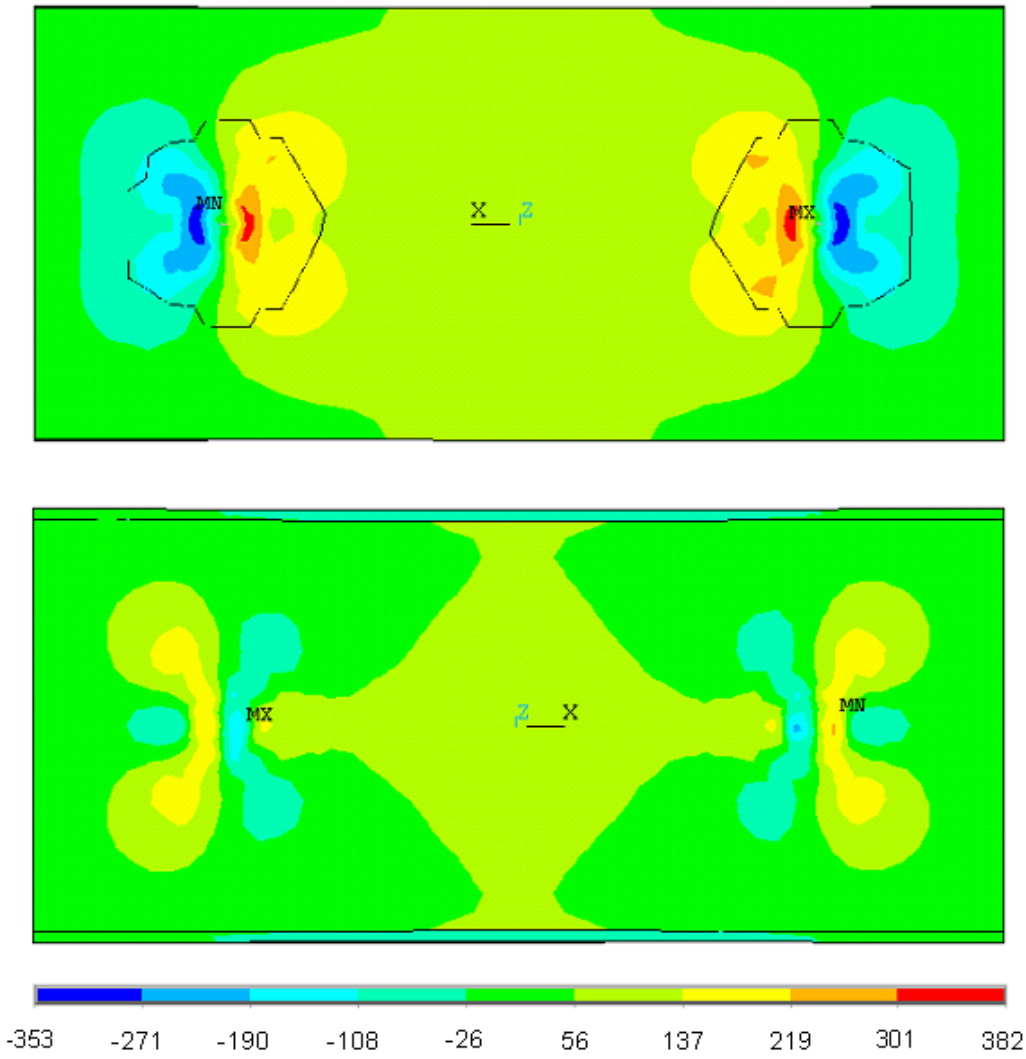

Figure 1.22. Distribution of σ_{xx} component of true stress (in MPa) on the inner and outer surfaces of the central plate of a MTS specimen developed due to the maximum load. (t = 1 mm, d = 4 mm, number of spots = 2)

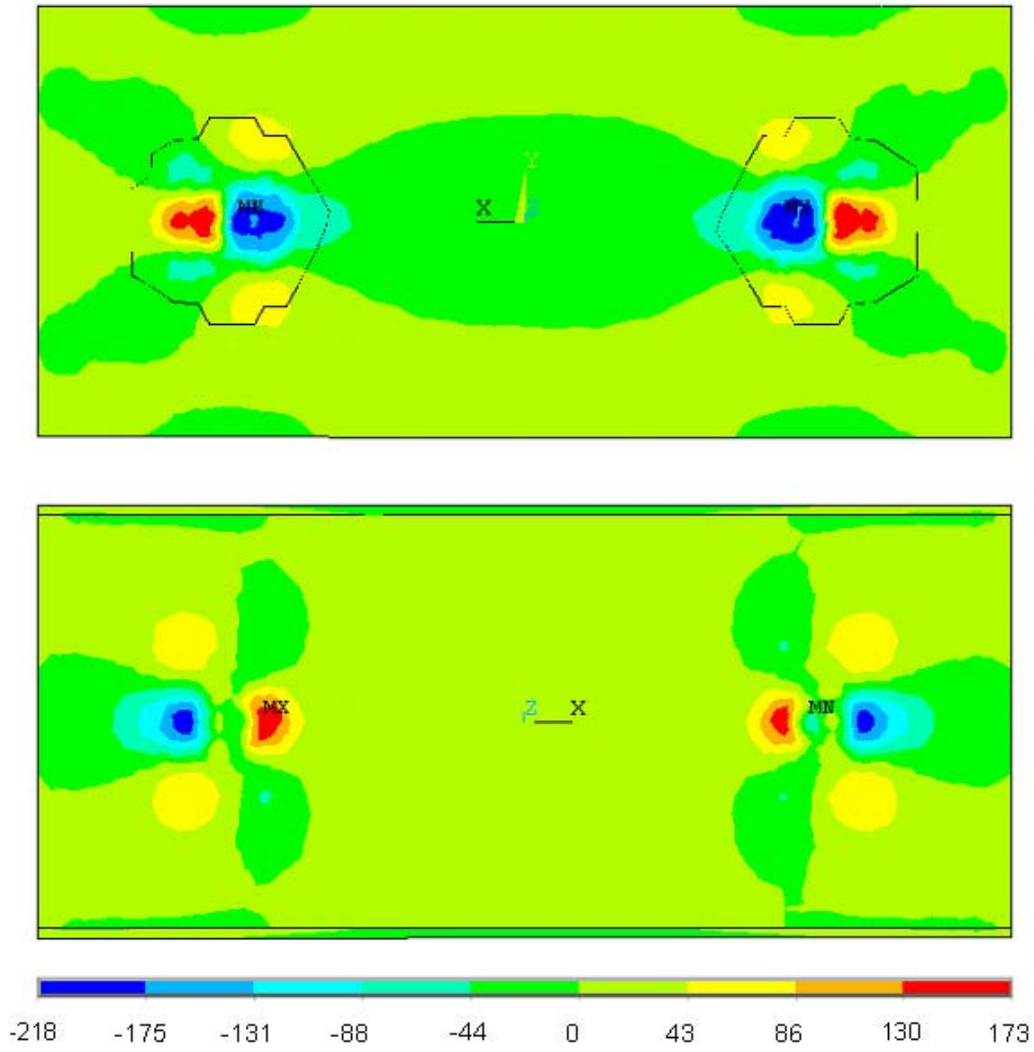

Figure 1.23. Distribution of σ_{xx} component of true stress (in MPa) on the inner and outer surfaces of the central plate of a MTS specimen developed due to the minimum load (t = 1 mm, d = 4 mm, number of spots = 2).

Figures 1.24 and 1.25 show the effect of nugget diameter on stress distribution after the maximum load (2700 N) is applied. If the diameter is reduced to 2 mm, the stresses become extremely concentrated. In the case of 6 mm diameter, stress concentration is relieved and the maximum stress is reduced.

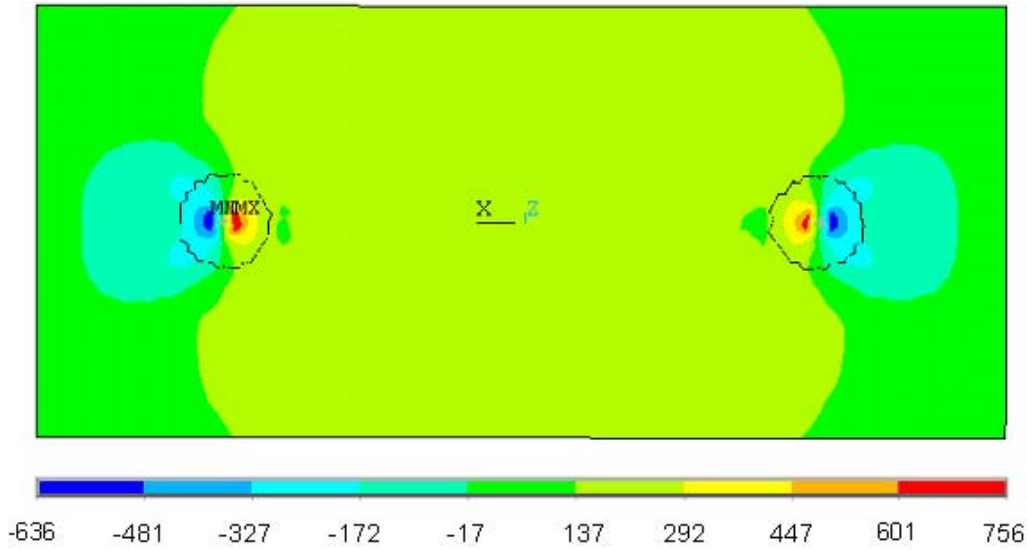

Figure 1.24. Distribution of σ_{xx} component of true stress (in MPa) on the inner surface of the central plate of a TS specimen developed due to the maximum load. (t = 1 mm, d = 2 mm, number of spots = 2)

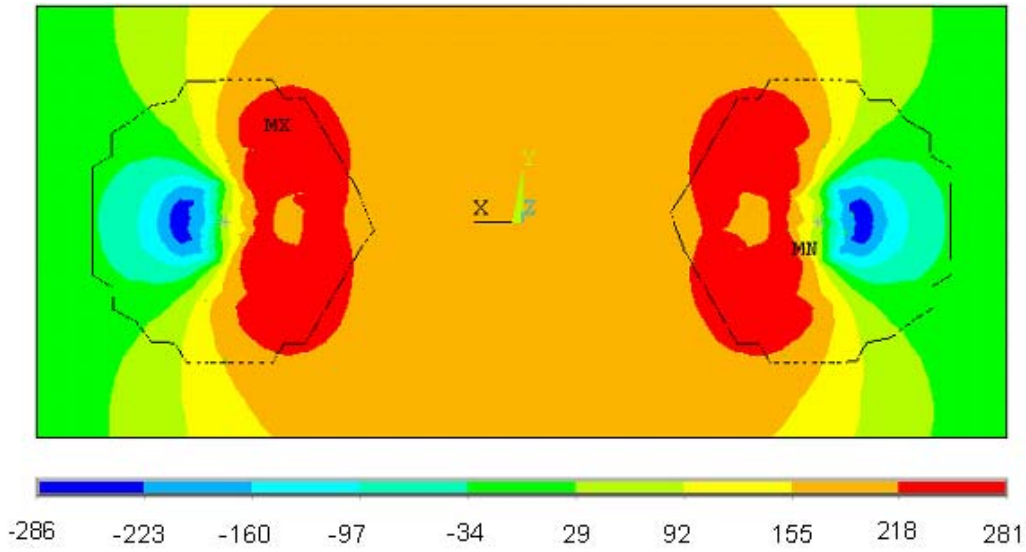

Figure 1.25. Distribution of σ_{xx} component of true stress (in MPa) on the inner surface of the central plate of a TS specimen developed due to the maximum load. (t = 1 mm, d = 6 mm, number of spots = 2)

Figure 1.26 shows the stress distribution on the inner surface of TS specimens with 2-mm plate thickness after the maximum (2700 N) load is applied. Comparing with the stress distribution for 1 mm given in Figure 1.20, one may see that the increase in thickness leads to a higher stress concentration, but a lower value for the highest stress. The reason for the more localized stress distribution may be attributed to the increased stiffness. Considering that a larger volume of material transfers the load, decrease in stress level is understandable. Increasing the thickness to 4 mm results in extremely high stress concentration as seen in Figure 1.27. For this reason, decrease in stress level is not observed in this case.

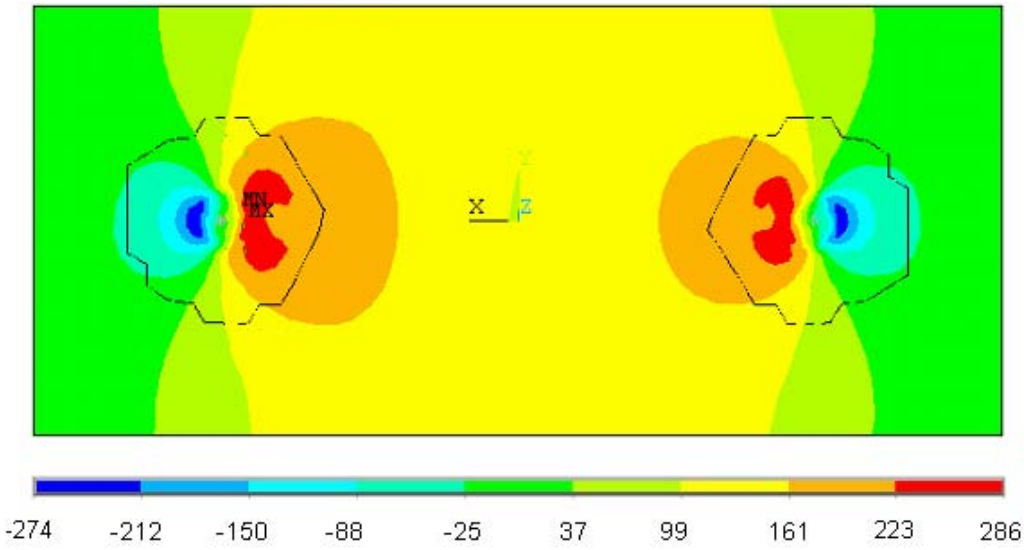

Figure 1.26. Distribution of σ_{xx} component of true stress (in MPa) on the inner surface of the central plate of a TS specimen developed due to the maximum load. (t = 2 mm, d = 4 mm, number of spots = 2)

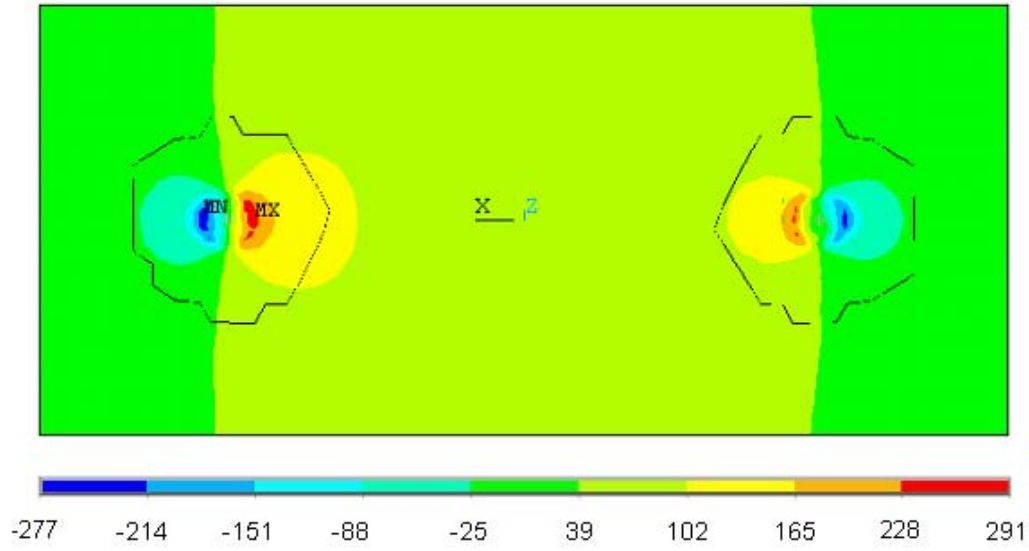

Figure 1.27. Distribution of σ_{xx} component of true stress (in MPa) on the inner surface of the central plate of TS specimen developed due to the minimum load. (t = 4 mm, d = 4 mm, number of spots = 2)

Figure 1.28 shows the distributions of σ_{xx} component of stress on the inner surface of central plate of a TS specimen developed after the maximum (2700 N) and minimum (150 N) loads are applied. This time, the plates are fastened using eight spots with 2 mm diameter, which have the same total cross sectional as that of two spots with 4 mm diameter (Figures 1.20 and 1.21). For this case, stresses are more uniformly distributed. Accordingly, residual stresses are reduced.

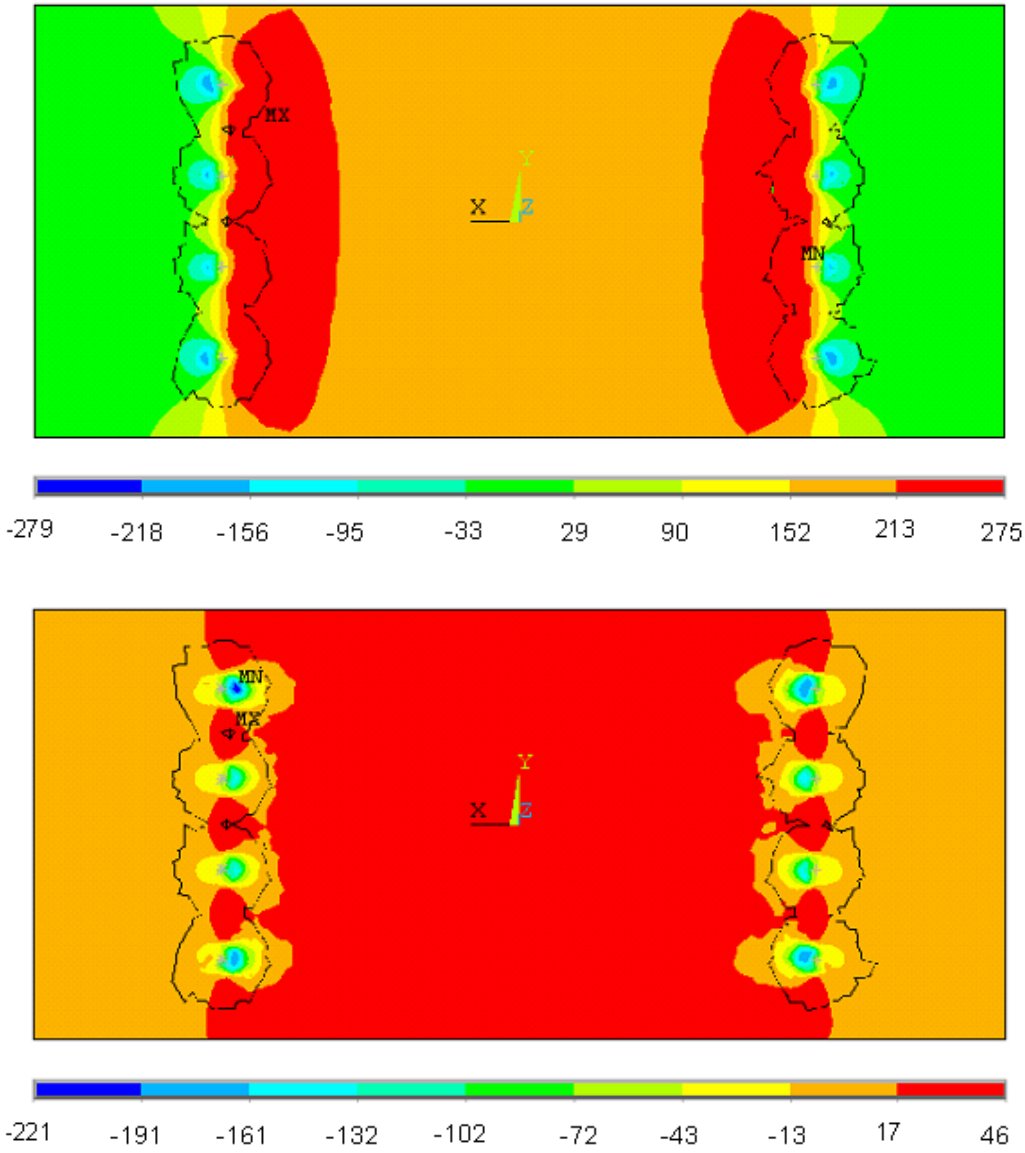

Figure 1.28. Distribution of σ_{xx} component of true stress (in MPa) on the inner surface of the central plate of TS specimen developed due to the maximum and minimum load. (t = 1 mm, d = 2 mm, number of spots = 8)

When the location of the point where the maximum tensile stress developed was examined, this point was observed to become closer to the nugget boundary with the decreasing load range. For the cases with the maximum load of 2700 N, 1750 N, and 750 N, the distance of the critical point to the nugget circumference was 0.42 mm, 0.39 mm, and 0.35 mm, respectively. This conformed to the trend that crack initiation sites were

closer to the nugget for low loads as observed in the experiments. The reason why the maximum stress develops at a farther distance from the nugget with a larger load may be attributed to an enlarged yield zone away from the nugget.

1.10. Estimated Fatigue Lives

1.10.1. Calculation of Fatigue Lives

In a mechanical component under fluctuating loads, the process of nucleation, growth and joining of micro-cracks is expected to take place in highly stressed regions. Fatigue crack growth is known to occur along planes where the tensile stress takes its maximum value. Accordingly, the fatigue life calculations were carried out using the stress and strain states in the element at which the maximum tensile stress develops for the given maximum loading case. This element is located at the faying surface or HAZ around the peripheries of the spot welds as indicated in Figures 1.20-1.23. The fatigue properties of the material used in the fatigue assessment models are given in Table 1.9 [36].

Table 1.9. Fatigue data of the material used in the fatigue assessment models [36].

σ'_f	σ_f	ε'_f	ε_f	b	c	HB
499 MPa	475 MPa	0.104	1.63	-0.06	-0.4	105.1

1.10.2. Comparison of the Predicted and Measured Fatigue Lives

The fatigue lives of the specimens were estimated using the available fatigue assessment models. Figure 1.29 shows the load range vs. number of cycles to failure obtained through the experiments and fatigue analyses. The fatigue lives given in the figure were predicted using the stress based approaches. The lines shown in the figure are fitted to the data. It should be noted that Figure 1.29 contains off-data; that means some of the data are outside the range shown in the figure. The best correlations were obtained via the Gerber's and Morrow's models. Nevertheless, their predictions were overly conservative for spot weld joints. This may be because these models do not adequately account for the effects of the highly localized plastic deformation around the spot weld nuggets.

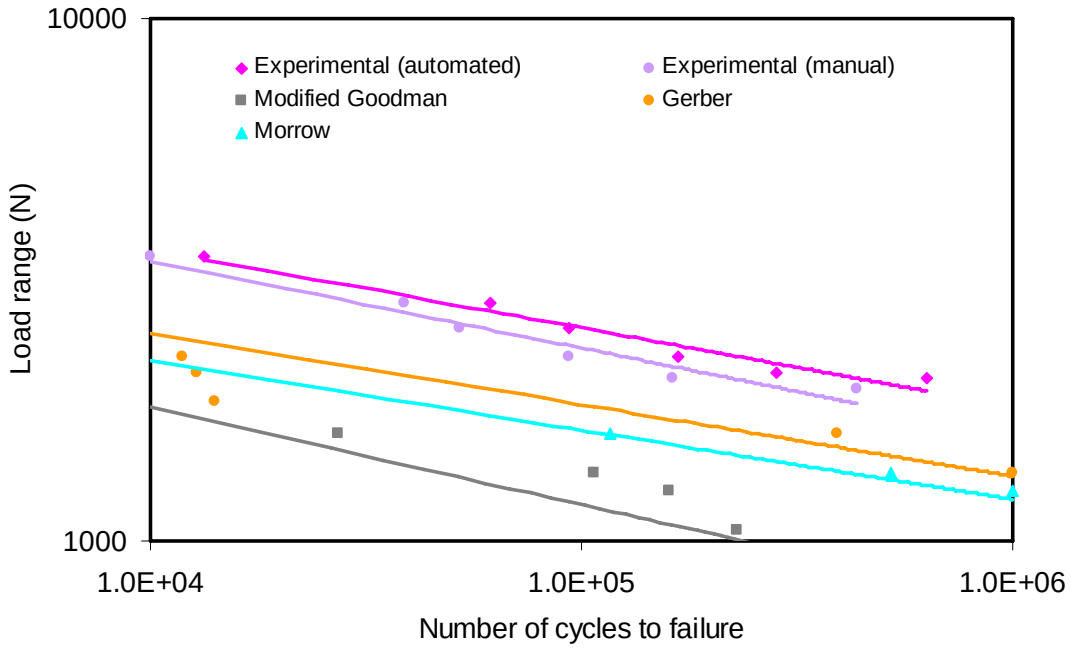

Figure 1.29. Comparison of the fatigue lives predicted using stress-based approaches and experimental results.

Figure 1.30 shows a comparison of the experimentally determined fatigue lives and the predictions based on the strain-based approaches. Coffin - Manson and Morrow's mean stress models yielded the best correlation. Considering the scatter in the data, the agreement with the experimental results was excellent for both low and high cycle fatigue. The models, especially Coffin – Manson, captured the increasing trend of fatigue life with decreasing load. Its predictions are close to the 99 percent confidence interval of the manual spot weld data given in Table 1.8. All of the models predicted a life greater than 1 $\times 10^6$ cycles for a maximum load of 1750 N. The fact that a better correlation was obtained via Modified Coffin-Manson model, which does not take into account the effect of mean stress, in comparison to Morrow's mean stress model implies that the influence of mean stress on fatigue life of spot welds is not significant in spot weld joints. This may be because plastic strains were not large. The maximum principal strain for the maximum and minimum peak loads of 3700 N and 2100 N were calculated as 0.107 and 0.028, respectively. No observed effect of mean stress also corroborates our assumption that residual stresses developed during the welding process have little effect on fatigue life since they mainly affect mean stress rather alternating stress. Accurate and consistent

predictions of the model for spot weld joints in which highly complex stress states develop imply that the model adequately reflects the effects of the basic underlying mechanisms leading to fatigue failure for typical engineering applications

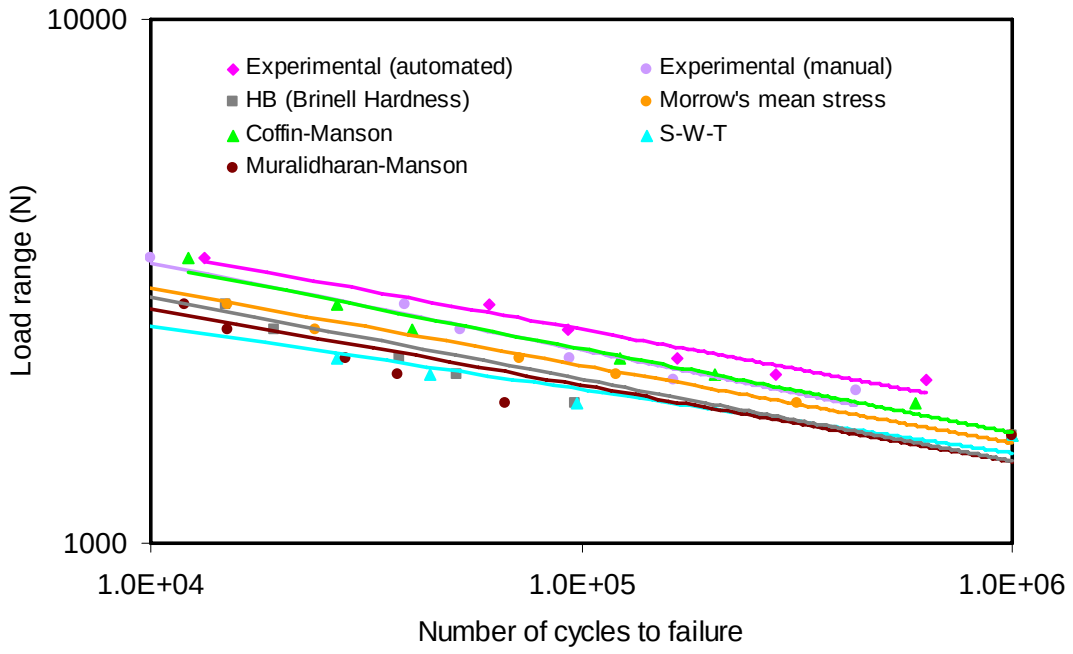

Figure 1.30. Comparison of the fatigue lives predicted using strain-based approaches and the experimental results.

In order to apply the models, which account for fatigue failure only in uniaxially loaded parts, we need to find equivalent stress and strain values representing the multiaxial stress and strain states that developed in the spot weld joint. There are mainly three approaches: The maximum principal strain, the maximum shear strain, and the octahedral shear strain. Figure 1.31 shows the fatigue lives predicted by Morrow's mean stress method using different equivalent strain approaches. As seen in the figure, the octahedral shear strain and the maximum principal strain better represent the effect of multiaxial strain state.

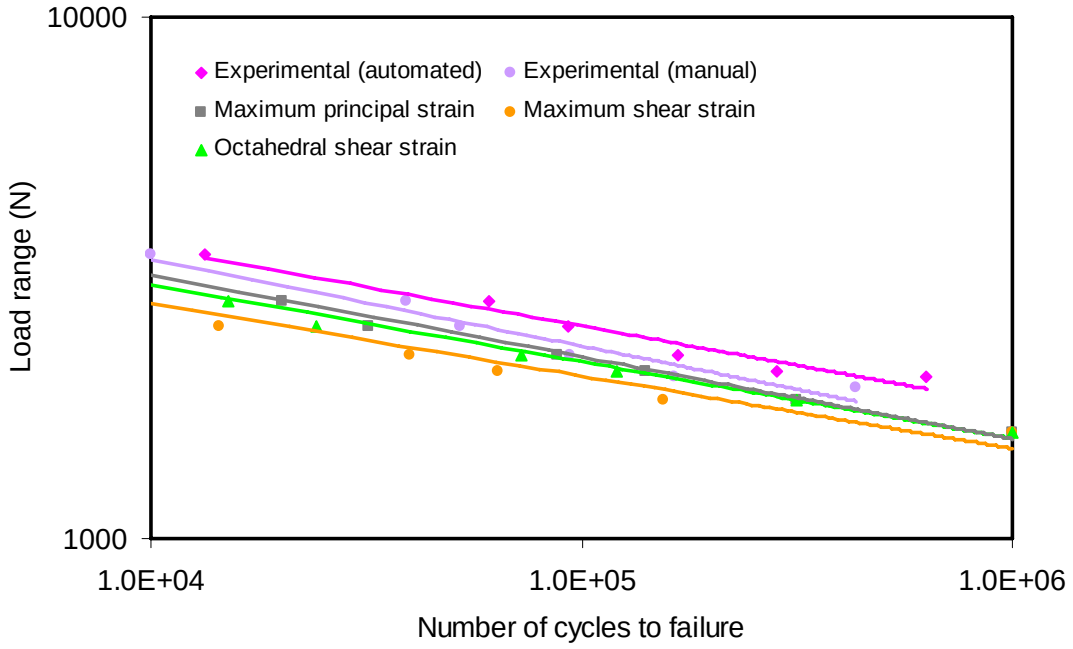

Figure 1.31. Comparison of the fatigue lives predicted using Morrow's mean stress model with different equivalent strain approaches.

As mentioned earlier, the fatigue lives were calculated based on the stress and strain states at the point where the maximum tensile stress developed. Alternatively, the points where the maximum shear stress or Von Mises stress developed were also tried. However, non-conservative predictions were obtained for high cycle fatigue. Thus, the criterion initially adopted to determine the critical point turned out to be appropriate.

The gap between the overlapping portions of the MTS specimen depends on a number of factors; gripping force, intensity of welding current, sheet thickness etc. This in turn affects the resulting stress state. Figure 1.32 shows the predicted effect of the gap on fatigue life. Understandably, the larger the gap, the larger the stresses and the shorter the fatigue life since increased distance between the plates leads to larger bending moments.

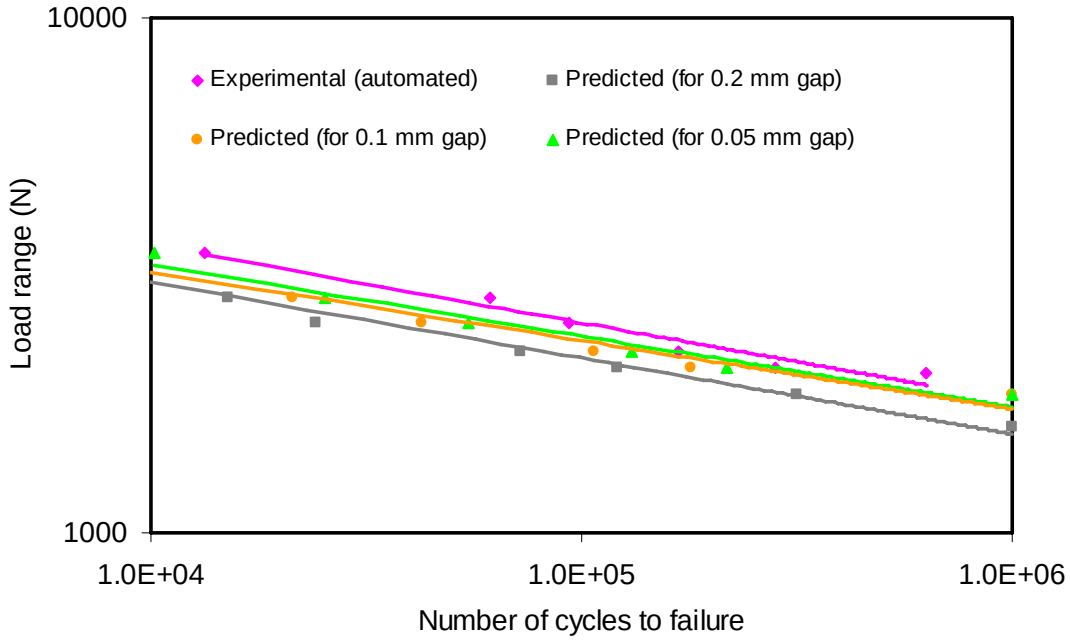

Figure 1.32. Comparison of the fatigue lives predicted for different gap values using Morrow's mean stress approach and experimental results.

The accuracy of the fatigue life predictions was verified by comparing them with the fatigue lives of MCP and MTS specimens experimentally obtained [18, 19] and [22]. The FE calculations were carried out using the material properties, loading, and geometry of the specimens provided in those studies. The tested specimens were made of two different types of low carbon steels. In MTS specimens, the weld nugget was basically subject to shearing force. On the other hand, in MCP specimens, the spot weld was subject to an out-of-plane separating force. Comparisons were made for different load ranges. Fatigue lives were predicted using modified Coffin-Manson (the total strain life equation) and Morrow's mean stress models. As seen in Figures 1.33-1.35, the results compare quite well. Correlation of Modified Coffin-Manson model with the experimental data is better. It should also be noted that better correlation obtained with the data provided [18, 19] in comparison to the data provided [22] may be attributed to the use of the material properties of the HAZ in the former case rather than the properties of base metal in the other case.

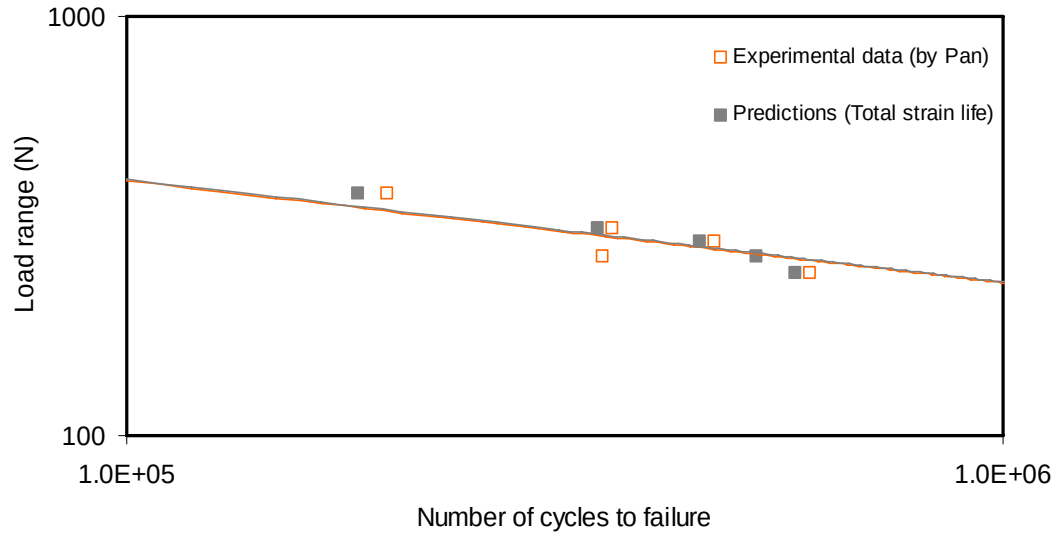

Figure 1.33. Comparison of predicted fatigue lives with experimental results obtained by Pan (for DQSK MCP specimens) [18, 19].

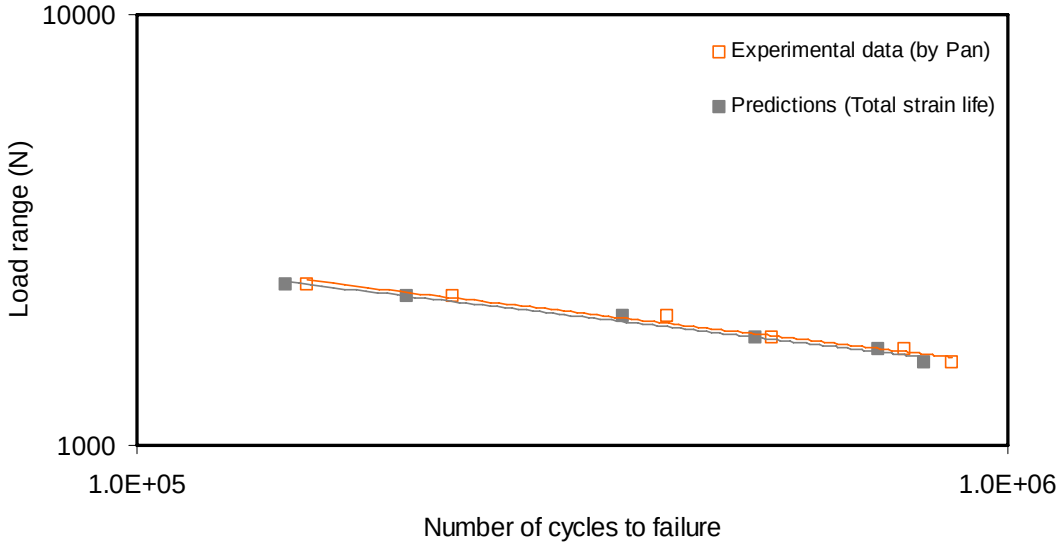

Figure 1.34. Comparison of predicted fatigue lives with experimental results obtained by Pan (for DQSK MTS specimens) [18, 19]

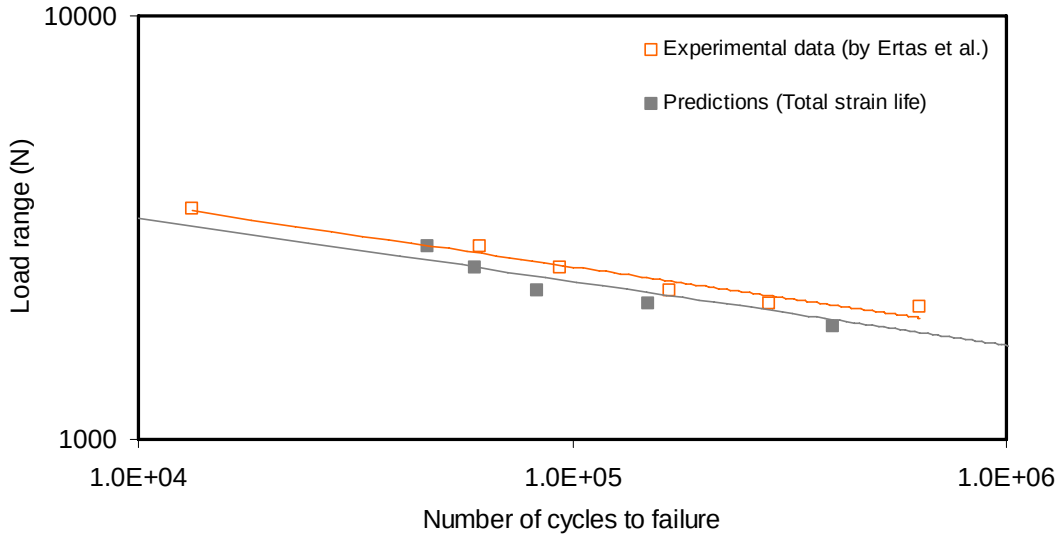

Figure 1.35. Comparison of predicted fatigue lives with experimental results obtained by Ertas *et al.* (for DIN 1623 MTS specimens) [22].

1.10.3. Results and Discussion

A parametric study was conducted to determine the effects of design variables on fatigue life. The basic geometry was chosen as a TS specimen with 4-mm diameter spot weld and 1-mm thick sheet. In order to see the effects of a variable, only one variable is changed while the others are kept constant. Accordingly, fatigue lives of TS and MTS specimens with three different spot weld diameters (4 mm, 5 mm, and 6 mm) and three different plate thicknesses (1 mm, 1.5 mm, and 2 mm) were calculated using Modified Coffin-Manson model. Figures 1.36-1.39 present the results. As shown in Figure 1.36, joints with large spot weld diameters have much higher fatigue strength. This is because a larger region transmits the applied load, which reduces stress concentration as indicated in Figures 1.24 and 1.25. The improvement obtained by increasing the diameter from 5 mm to 6 mm is less pronounced.

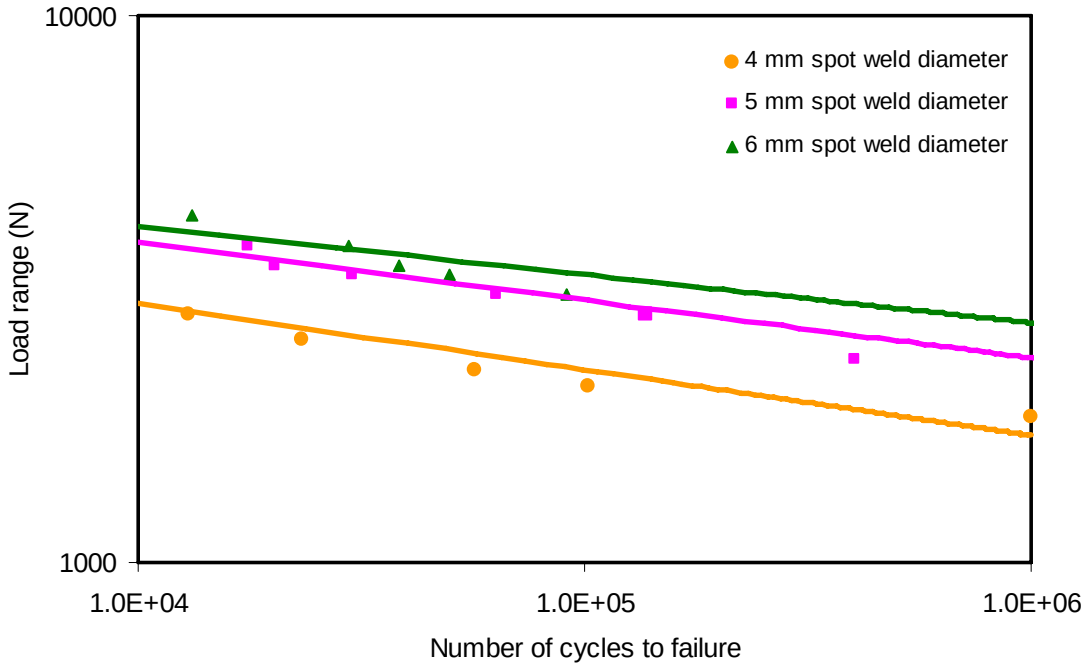

Figure 1.36. Fatigue lives predicted using Modified Coffin-Manson approach for TS specimens with 1-mm thickness and different spot weld diameters.

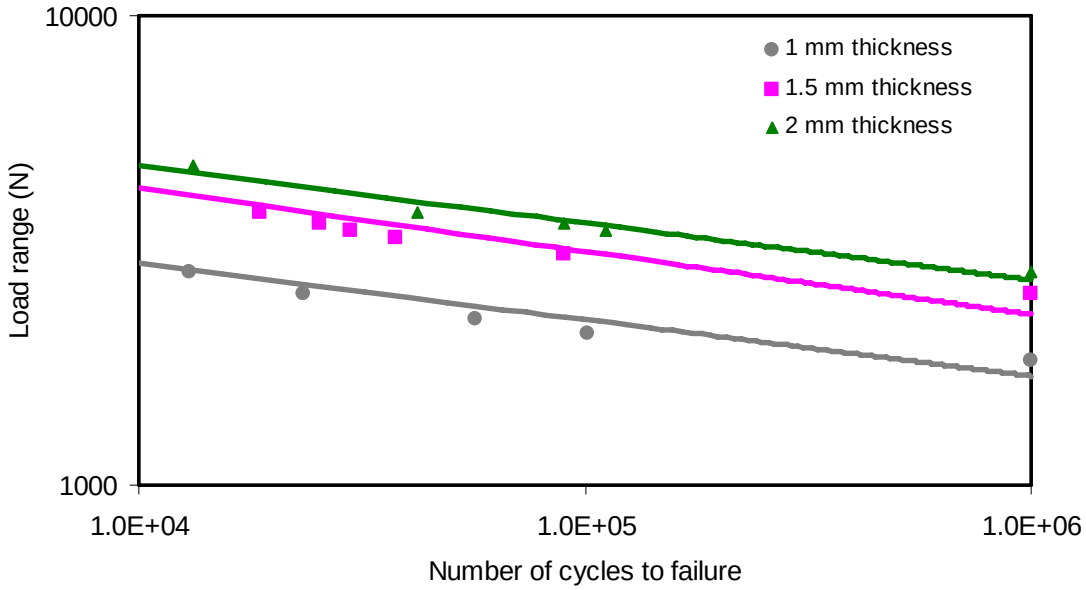

Figure 1.37. Fatigue lives predicted using Modified Coffin-Manson approach for TS specimens with 4-mm spot diameter and different metal sheet thicknesses.

As seen in Figure 1.37, the fatigue strength is significantly improved when the thickness is increased from 1.0 mm to 1.5 mm due to the reduction in the maximum stress level as seen in Figures 1.20 and 1.26. However, there is relatively small increase in fatigue strength when the thickness is increased from 1.5 mm to 2.0 mm. This means that this design change, which increases material cost and weight by 33%, does not considerably improve the performance of the joint.

Figures 1.38 and 1.39 show a comparison of the fatigue behaviors of MTS and TS specimens for different sheet thicknesses and different spot-weld diameters, respectively. Although MTS specimen has a larger flexural strength, its fatigue strength is not greatly improved because of a higher stress concentration. The fatigue strength of MTS is better for small thickness and diameters. For large diameters and thicknesses, they have comparable strengths. This may be due to the increased contribution of thickness to flexural rigidity in comparison to that of the flange of the MTS specimen.

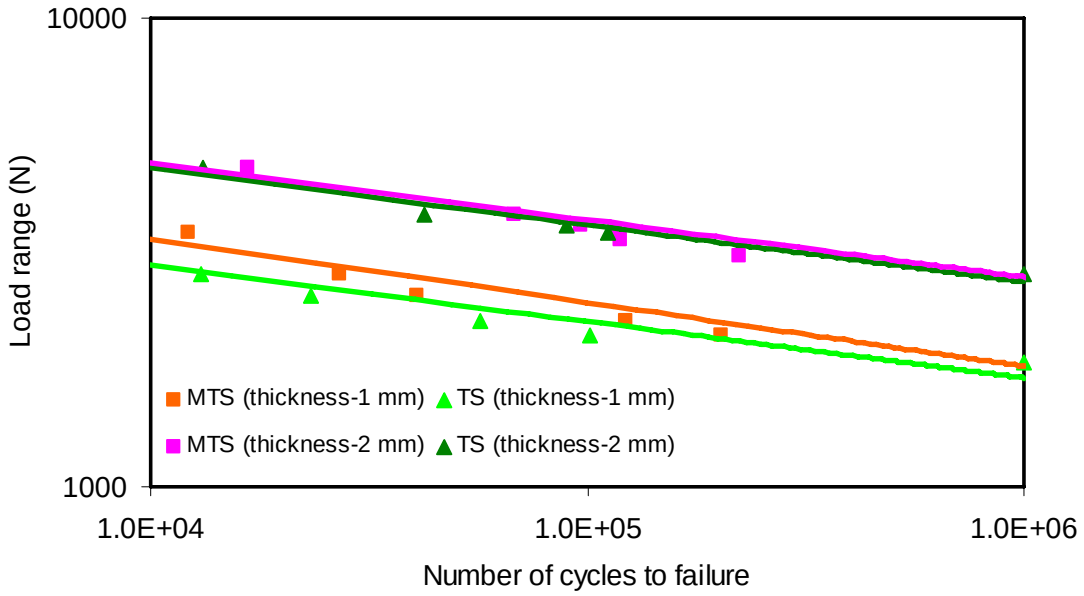

Figure 1.38. Comparison of fatigue lives predicted using Modified Coffin-Manson approach for MTS and TS specimens with 4-mm spot diameter and different metal sheet thicknesses.

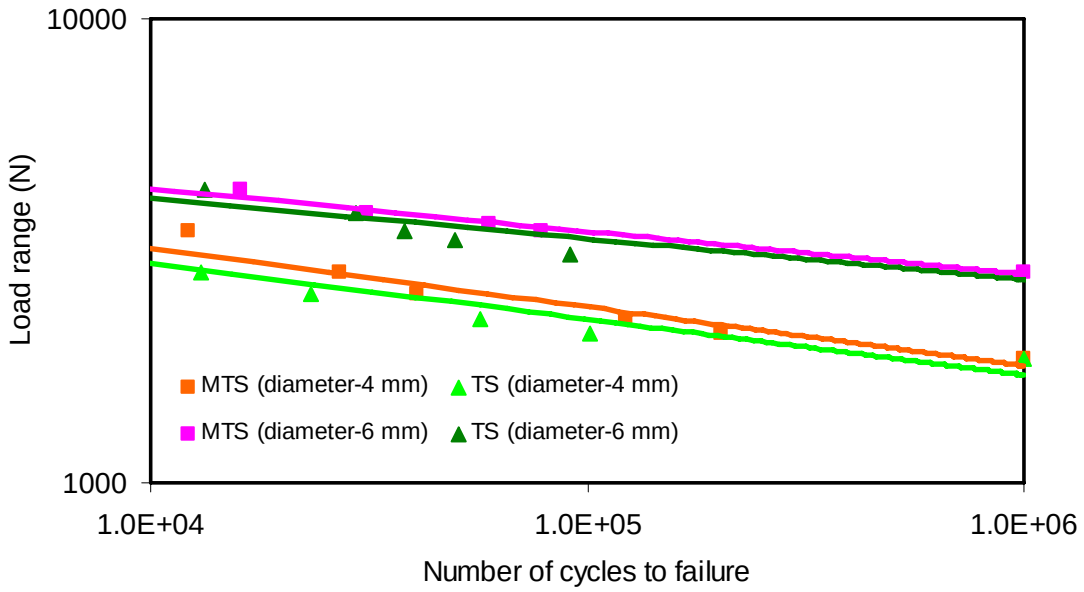

Figure 1.39. Comparison of fatigue lives predicted using Modified Coffin-Manson approach for MTS and TS specimens with 1-mm thickness and different spot-weld diameters.

Table 1.10 gives a comparison of fatigue lives of different joint types for different load ranges. CP provides the weakest connection among all; therefore it should be avoided if possible. CP may be used if the plates cannot be gripped from both sides due to space limitations. Even in that case, one may prefer a TS joint with manuals spot welds because they are achieved by touching the electrode on one surface of the plate without applying force. MCP is weaker in comparison to TS and MTS for the load case of 200N/150N. However, when the load is increased deterioration in fatigue life is less pronounced for MCP. This is because when the load is increased the yield zone expands, but the maximum stress slightly increases.

Table 1.10. Comparison of the fatigue lives (number of cycles to failure) of different joint types (t = 1 mm and d = 4 mm).

	Load range		
Specimen type	2700N/150N	2250N/150N	2000N/150N
CP	2357	2704	13053
MCP	29663	181200	192184
TS	15288	68997	>1 x 10^6
MTS	24227	120964	>1 x 10^6

Tables 1.11 and 1.12 give fatigue lives of TS specimens connected by different numbers of spot welds having different diameters. As seen in Table 1.11, the joint with eight spots having 2-mm diameter is much stronger than that with two spots having 4-mm diameter even though the total cross sectional areas are the same. Similarly, the joint with four spots having 4-mm diameter is stronger than that with two spots having 5.66-mm diameter, which have the same total cross sectional areas (Table 1.12). This implies that a joint with larger but fewer number of spots is weaker than a joint with smaller but larger number of spots. This means that instead of increasing the nugget diameter, it is better to increase the number of spots if the increase in manufacturing time can be tolerated.

Table 1.11. Fatigue lives of TS specimens with different numbers and diameters of spots (t = 1 mm and d = 4 mm).

		Load range		
No of spots	Diameter	5000N/200N	3700N/200N	3000N/150N
2	4 mm	3162	3930	8194
8	2 mm	4687	21072	>1 x 10^6

Table 1.12. Fatigue lives of TS specimens with different numbers and diameters of spots (t = 1 mm and d = 5.66 mm).

		Load range		
No of spots	Diameter	4500N/200N	3700N/200N	3500N/200N
2	5.66 mm	5659	31967	53637
4	4 mm	5856	33911	56409

2. OPTIMIZATION OF MONOLITHIC MATERIALS: DESIGN OPTIMIZATION OF SPOT WELDED PLATES FOR MAXIMUM FATIGUE LIFE

2.1. Introduction

Resistance spot welding is the most preferred and widely used method for joining metal sheets in automotive and many other industrial assembly operations. Spot-welded joints are usually susceptible to fatigue failure. Increasing the fatigue strength of the joints through some changes in geometry will also increase the overall integrity of the structure

Because spot weld joints provide localized connection, and thus lead to high stress concentration in the joined plates, any improper design may result in excessively high stresses and premature failure. The critical failure mode under fluctuating loads is mainly fatigue. Knowing that fatigue crack initiation is very sensitive to stress level, that means increase in stress level dramatically increases the likelihood of fatigue failure. Designers may significantly boost fatigue strength of a component by introducing changes in its geometry that will reduce the level of stress in highly stressed regions. The geometry and material of a joint can be tailored to obtain optimal performance and the most effective use of material. The design variables for spot welded structures are locations of spot welds, length of the overlapping region of plates, material, plate thickness, diameter and number of the spot welds. In this study, positions of spot welds and overlapping length of the plates were considered as design variables to maximize the fatigue life. Sheet thickness and material were assumed to be predetermined according to the strength requirements of the structure.

In this part of the study, a methodology is proposed to find the optimum locations of spot welds and the optimum overlapping length of the joined plates for maximum fatigue life. Minimum weld-to-weld and weld-to-edge distances recommended by the industry are considered as side constraints. Modified Coffin-Manson model is used to predict the fatigue life. This fatigue assessment model requires the strain state developed in the

structure. For this purpose, a nonlinear finite element analysis is carried out, taking into account residual stresses due to localized plastic deformations around the spots. Nelder-Mead (Sequential Simplex) is employed as the search algorithm in the optimization procedure. A number of problems were solved to demonstrate the effectiveness of the proposed method

2.2. Literature Survey

In the literature, there are a few studies about optimization of spot welded structures. Zhang & Taylor [29] optimized the positions of two spot welds in a tensile shear specimen. They formulated two optimization problems: one was to maximize the stiffness of the structure under fatigue life constraints and the other was to seek the maximum fatigue life of the structure. The objective function to be minimized was the maximum radial stress, which was assumed to be correlated with fatigue life. Chae et al. (2002) investigated optimal locations of spot welds under static and impact loading to maximize safety factors of spot welds. Rui et al. (1996) used a topological optimization algorithm to minimize stress intensity factor of spot welds, which is a control parameter for the fatigue life of the structure, in a spot-welded structure. Finally, Liangheng et al. (2003) proposed a method to reduce the number of welds in automobile bodies subject to rigidity requirements.

In the present optimization procedure, the fatigue life is directly calculated and maximized. Because of high stress concentration, nonlinear and plastic deformation is likely to occur around the spots even at low load levels. These stresses control the failure behavior of the joint and thus the whole structure. Strain based models are known to better assess fatigue life of plastically deformed parts. Accordingly, the total strain life equation (or modified Coffin-Manson equation) was used, which was observed [40, 52] to be better in predicting fatigue life of spot welded joints in comparison to other strain based models. In addition to choosing a reliable fatigue assessment model, another requirement for accurate predictions is that one should correctly determine the change in the strain state under cyclic loading. For this purpose, a nonlinear finite element analysis was carried out using nonlinear material properties and contact elements on the inner surfaces of the plates. Plastic deformations and residual stresses developed after unloading were taken into

account. The fatigue assessment model and FE model were verified before for various types of spot welded structures [40, 52] by comparing the results with experimental data.

It should be noted that processing parameters like welding current, welding time, clamping force, electrode diameter, hold time and process conditions like clamping conditions, welding sequence have significant effect on the quality of the spot-weld joint in terms of fatigue strength and geometric distortions. In order to ensure the integrity of the joint, one should therefore consider these factors. However, the present study focuses only on design optimization.

2.3. Problem Statement

In this part of the study, a common geometry, tensile-shear (TS) joint with two or three spot welds (Figure 2.1), was considered and optimized for various in-plane loads. The variables of the design optimization process were chosen to be x and y coordinates of the spot welds, x_i, y_i, and the length of the contacting surface between the joined metal sheets, ℓ. The origin of the coordinate axes was taken to be the center of the overlapping region. Spot weld diameter, d, metal sheet thickness, t, and width of the plate, w, were predetermined to be 4 mm, 1 mm, and 40 mm, respectively,

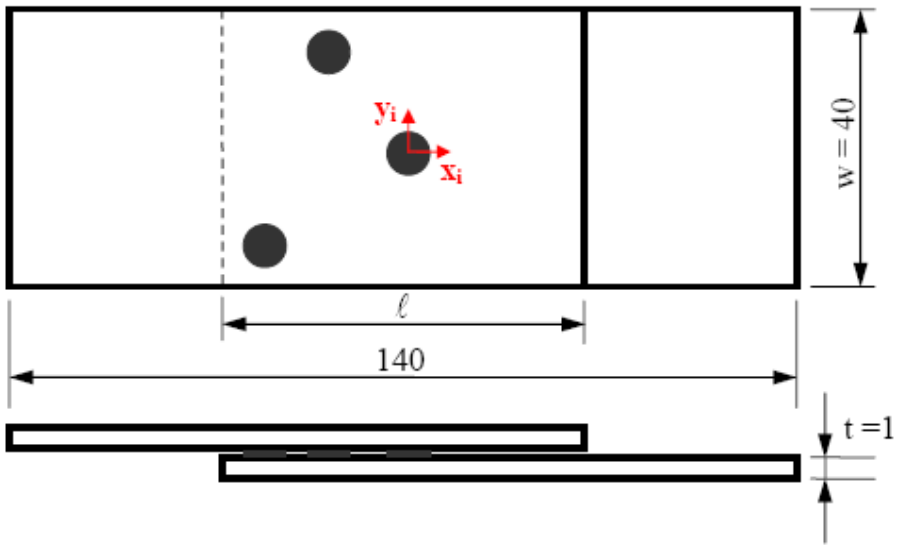

Figure 2.1. Geometry of the joint with three spot welds (top and side views).

The objective of the design optimization problem is to maximize the fatigue life, $2N_f$, of the joint.

$$\text{maximize } N_f \tag{18}$$

The design variables are subject to a number of side constraints. The spot welds should be prevented from interfering with each other and getting close to the plate boundaries; this means that the design should conform to the standards related to weld-to-weld spacing and weld-to-edge distance. According to industrial organizations like Precision Metalforming Association (PMA) and American Welding Society (AWS) the distance between an edge and the center of a spot weld should be greater than one spot weld diameter, *d*. Accordingly, the constraint equations are given as

$$-(\ell/2 - d) \le x_i \le \ell/2 - d \tag{19}$$

$$-(w/2 - d) \le y_i \le w/2 - d \tag{20}$$

Besides, the distance between the centers of the spot welds should be greater than twice the spot weld diameter as recommended by the industry. Then,

$$s_{ij} \le 2d \tag{21}$$

where s_{ij} is the distance between spot welds *i* and *j*.

2.4. Methodology

2.4.1. Objective Function

In the optimization procedure, if the value of a design variable is outside its feasible range, a penalty value is calculated and added to the value of the objective function. The penalty value was chosen as the difference between constraint limit and the value of the

design variable. By using penalty functions, the constraint optimization problem was transformed into an unconstrained one for which the chosen search algorithm was suitable. The objective function then becomes

$$f_{obj} = \frac{c_1 N_f}{N_r} + \frac{c_2 \ell}{w} + c_3 \sum_i P_i \tag{22}$$

where N_r is the reference life used to normalize the fatigue life, N_f, c_i are suitable coefficients, and P_i are penalty values. The overlapping length, ℓ, was normalized by the width of the plates, w. In this way, fatigue life is maximized with an effective use of material.

2.4.2. Optimization Algorithm

In optimization problems one may use zero, first or second order search algorithms [53, 54]. Considering that the value of the objective function in the present problem is numerically calculated using FE analysis, calculating its first or second order derivatives is difficult. For this reason, a zero order algorithm, Nelder-Mead (see Appendix A), which required only the values of the objective function for the given set of design variables, was chosen. Because this is a local search algorithm and structural optimization problems contain many locally optimum configurations, the optimization process was repeated many times starting from different configurations for each problem to avoid locally optimum designs with a high objective function value. Figure 2.2 describes the methodology followed in this part of the study. The details of FE analysis and optimization are described in the following sections.

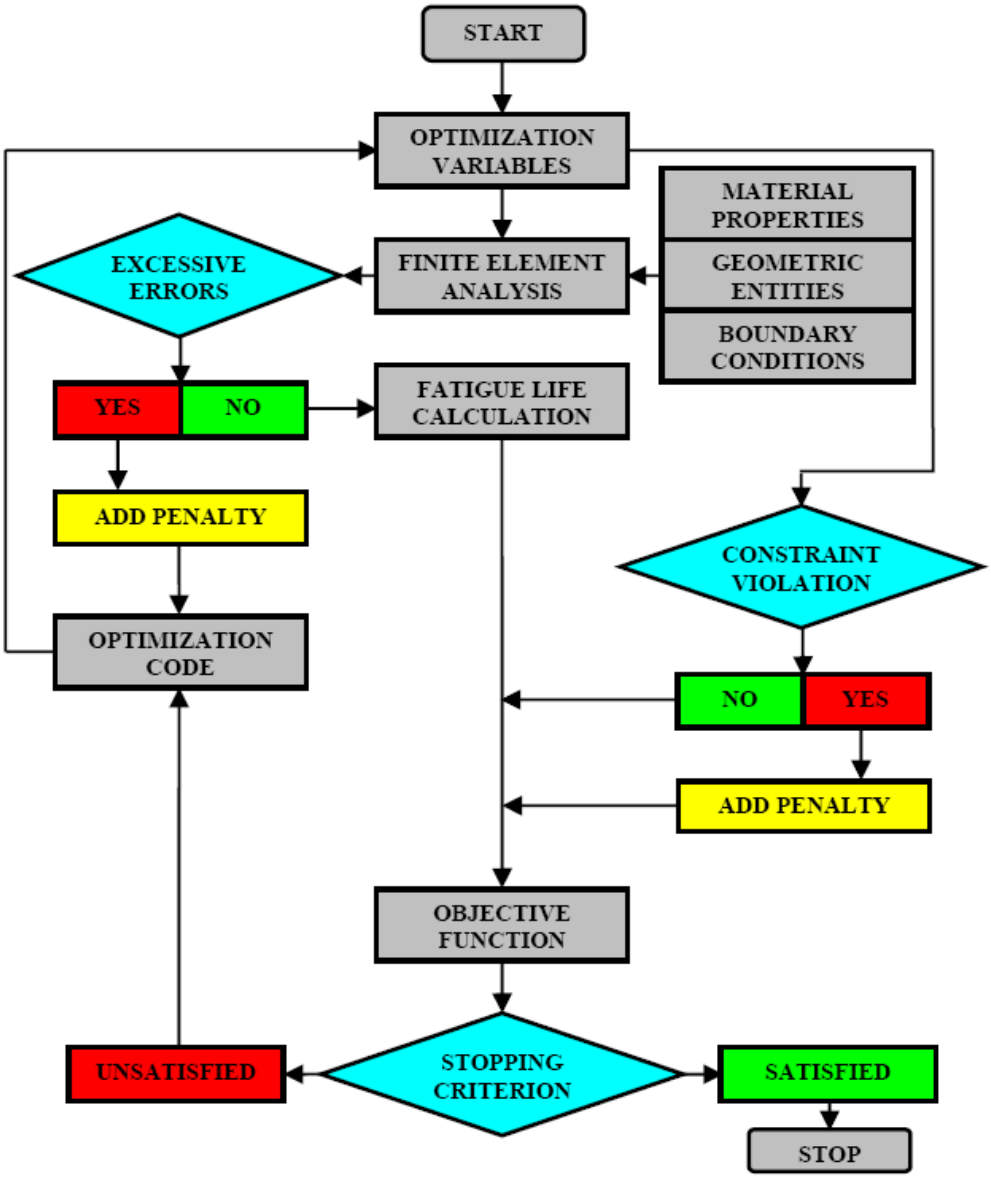

Figure 2.2. The optimization procedure.

2.4.3. Finite Element Analysis

In order to determine the strain states developed in the structure, a nonlinear analysis was carried out using commercial FEA software, ANSYS. A kinematic hardening material model (KINH) was used to simulate the nonlinear stress-strain relation. This model

includes the Besseling formulation, which takes into account the Bauschinger effect in cyclic loading. The base metal was modeled using 3D 10-node tetrahedral solid elements, SOLID92. This element has plasticity, stress stiffening, large deflection, and large strain capabilities. The spot weld nugget was modeled using a two-node beam element, BEAM188, which has six degrees of freedom at each node. Because this element is based on Timoshenko beam theory, shear deformation effects are included, which are especially important for short beams. Contact elements were defined on the interfaces between the plates around the spot welds. Relative rotation of the region around the spot welds with respect to the beam element is prevented through constraint equations.

Because high stress concentration occurs in the vicinities of the spot welds, much smaller elements were used within and around the spot-welds in comparison to that of the base metal. Figure 2.3 shows the finite element model of two spot-welded TS joint as an example. The details of the FEA and the material properties used in the models can be found in [40, 52].

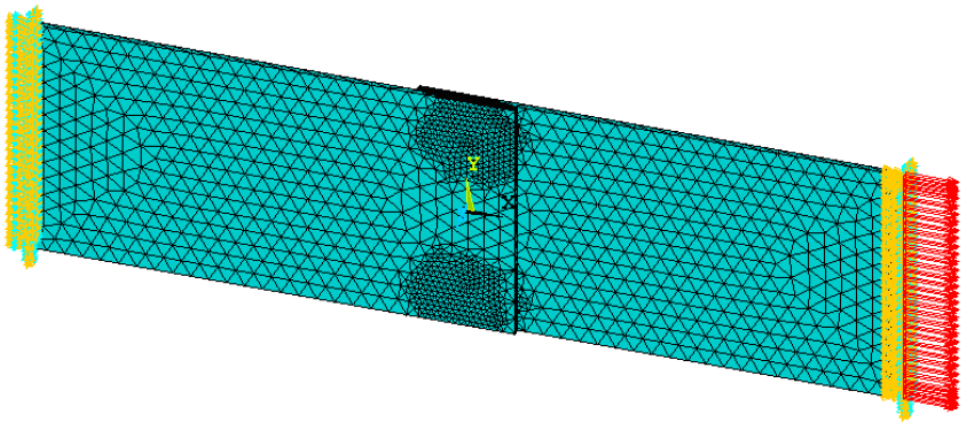

Figure 2.3. Finite element model for two spot-welded TS joint.

Boundary Conditions: The boundary conditions in the FEA model are shown in Figures 2.3, 2.4 and 2.5. In one loading case, displacements and rotations in all degrees of freedom are fixed at one end; the other end is subject to uniformly distributed in-plane load cycle between 3 kN and 1 kN in the *x*-direction, while the movement is prevented in other degrees of freedom. The boundary conditions for the other loading case are the same

except that the right end is not restrained in the *y*-direction; instead a load is applied fluctuating between 2 kN and 1 kN.

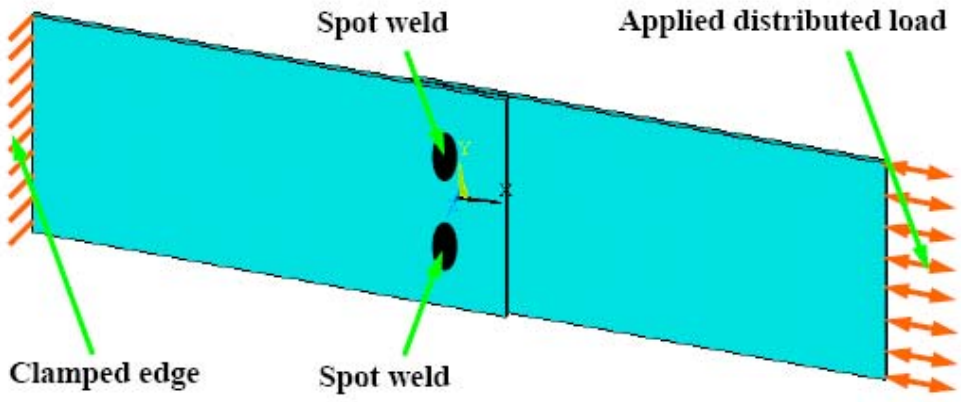

Figure 2.4. Boundary conditions of the finite element model for the axial loading case.

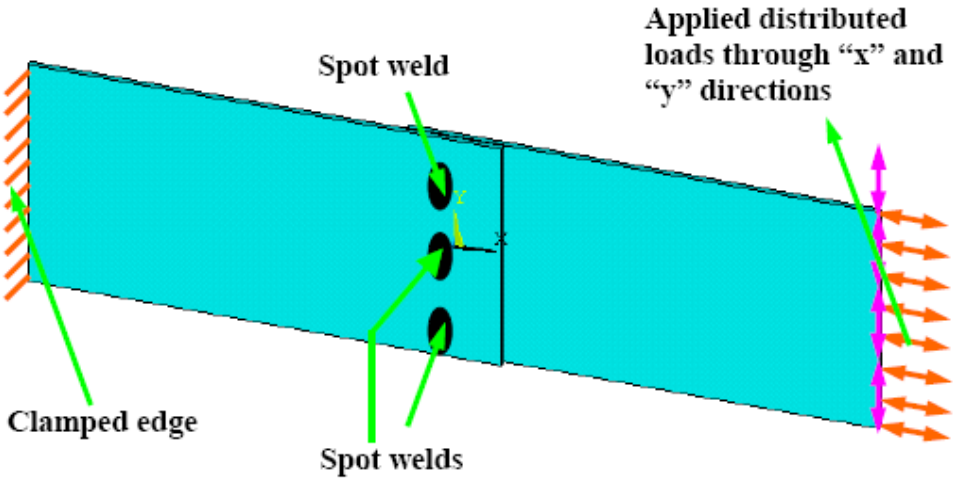

Figure 2.5. Boundary conditions of the finite element model for the axial and transverse loading case.

The cyclic loading was applied in two load steps. First, the load was incrementally increased to its maximum value, P_{max}, and the resulting strain state was obtained. In the second load step, the load was incrementally decreased to its minimum value, P_{min}. In the next load cycles, stresses were assumed to fluctuate between the stress values obtained for the maximum and minimum load levels in the first load cycle.

The process of nucleation, growth and joining of micro-cracks is expected to take place in highly stressed regions. Depending on the material and loading conditions, fatigue crack growth occurs along planes where the tensile stress or shear stress takes the maximum value [55]. In this study, the fatigue lives were calculated based on the stress and strain states at the points where the maximum shear stress, tensile stress and Von Mises stress developed. The predictions were similar; but the life calculated at the point where the maximum tensile stress developed was on the conservative side, others, on the other hand, were on the non-conservative side. For this reason, the fatigue life was calculated ,Equation (5), using the stress and strain state in the element at which the maximum tensile stress develops. This element is located at the faying surface in the heat affected zone around the peripheries of the spot welds.

2.5. Results and Discussions

In the finite element (FE) model, the material properties of DIN 1623 were also used. The engineering stress-strain diagram is given in Figure 1.6 and the related material properties of the material are given in Table 1.1.

2.5.1. Optimization of a Joint with Two Spots under Cyclic Axial Loading

First, a two-spot-welded joint subject to an axial load cycle with constant load amplitude were optimized in which *y* coordinate of the spot welds and overlapping length were chosen as design variables. Starting from different initial designs, the optimization process was repeated many times. In one of these trials, initial coordinates of the spot welds were (0, 16) mm and (0, -16) mm and the overlapping length (ℓ) was 80 mm. Critical stresses developed on the inner surfaces of the plates. Figure 2.6 shows the distribution of

σ_{xx} component of stress (before optimization) on the inner surface of one of the plates corresponding to the minimum and the maximum loads, respectively. Dashed lines show the boundaries of the contact region around the spot welds. The nuggets caused bending of the plates such that highly localized tensile and compressive stresses above yield point developed around them. The corresponding fatigue life of the joint was calculated as 12,047 cycles. After 66 iterations, the fatigue life reached to its maximum value, 64,705 cycles, corresponding to the optimal coordinates (0, 11.84) mm, (0, -11.84) mm and optimal overlapping length of 18.48 mm.

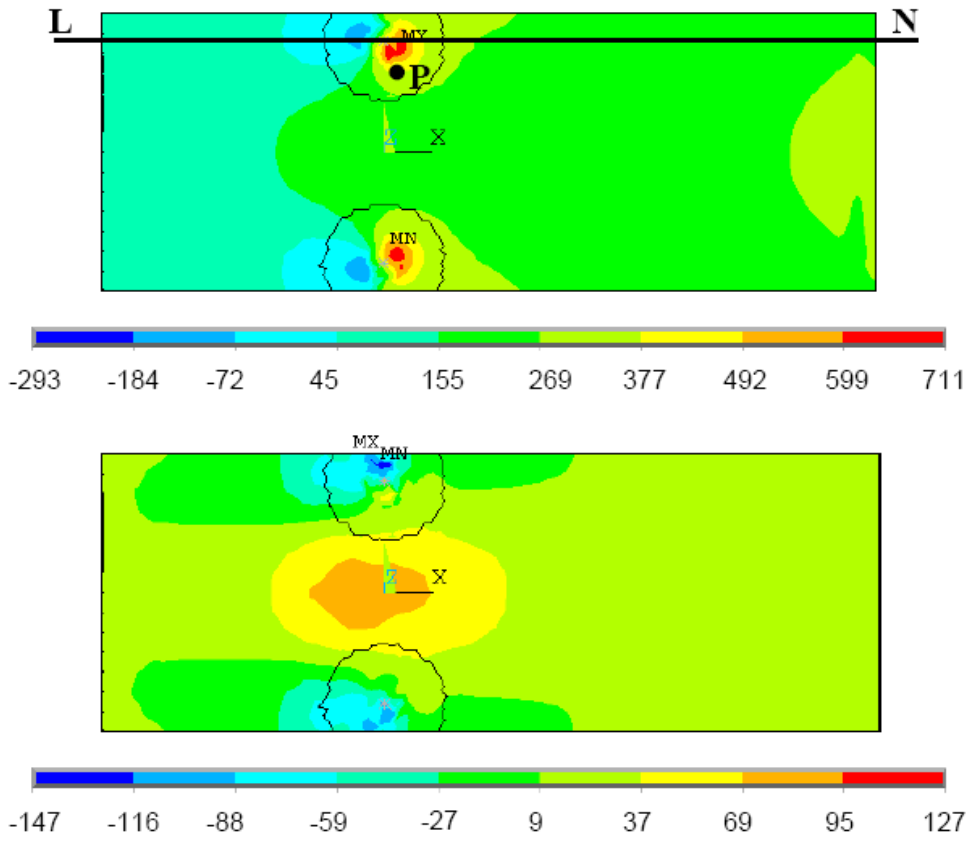

Figure 2.6. Distribution of σ_{xx} component of stress (in MPa) on the inner surface of one plate with two spot welds subject to the maximum axial load (upper figure) and the minimum axial load (lower figure) for the initial design.

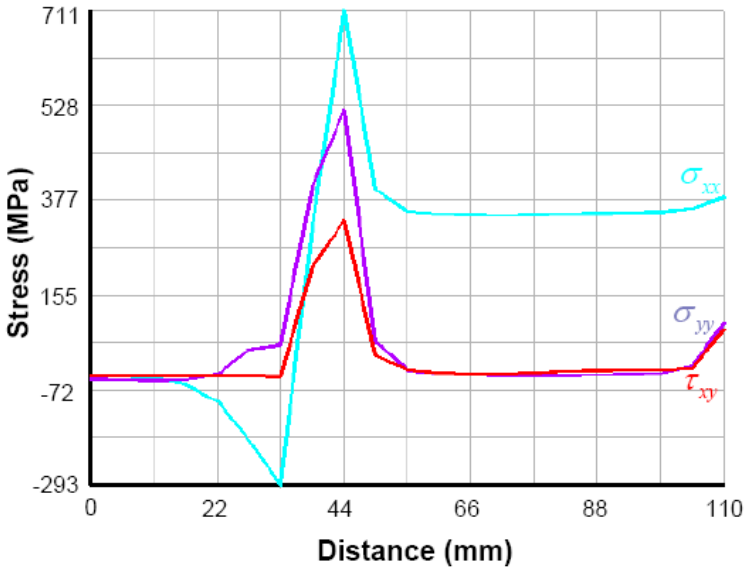

Figure 2.7. Distribution of the stress components σ_{xx}, σ_{yy}, and τ_{xy} along the line L-N shown in Figure 2.6, which passes through one of the spot welds, for the maximum axial loading condition and for the initial design.

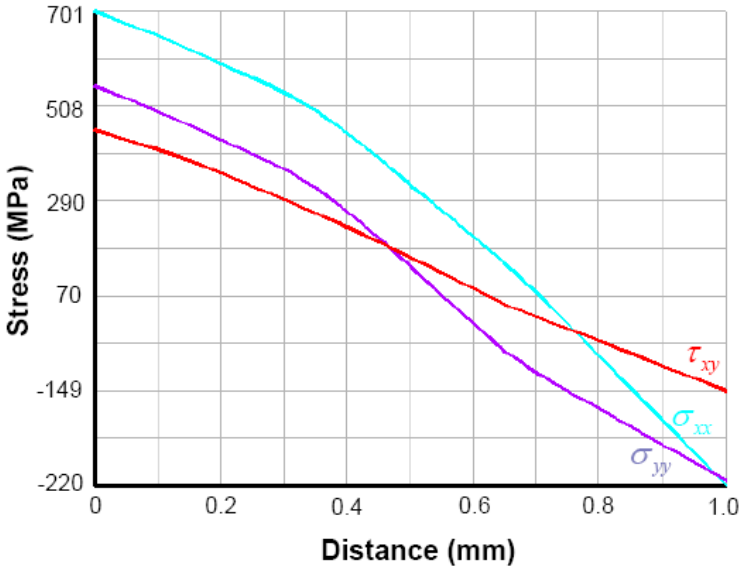

Figure 2.8. Distribution of the stress components σ_{xx}, σ_{yy}, and τ_{xy} (in MPa) through the thickness along a line passing through the point P in Figure 2.6 for the maximum axial loading condition for the initial design.

Nelder-Mead algorithm used n+1 current configurations, n being the number of design variables. Figure 2.9 shows the change in the objective function value of the best of these configurations generated during the optimization process. Figure 2.10 shows the resulting stress distributions in the optimally designed plate. As seen in Figures 2.6 and 2.10, stress concentration is considerably reduced through the optimization. Figures 2.7 and 2.8 show the multiaxial stress distribution along the length of the plate (L-N in Figure 2.6) and through the thickness (P in Figure 2.6) for the initial design of the plate, respectively. Figures 2.11 and 2.12 show, on the other hand, the multiaxial stress distribution along the length of the plate (L-N in Figure 2.10) and through the thickness (P in Figure 2.10) for the optimized plate, respectively. As seen in Figures 2.6-2.10, the highest stresses develop on the faying surface at the periphery of the spot weld. This conforms to the fatigue crack initiation locations observed in the experiments [6].

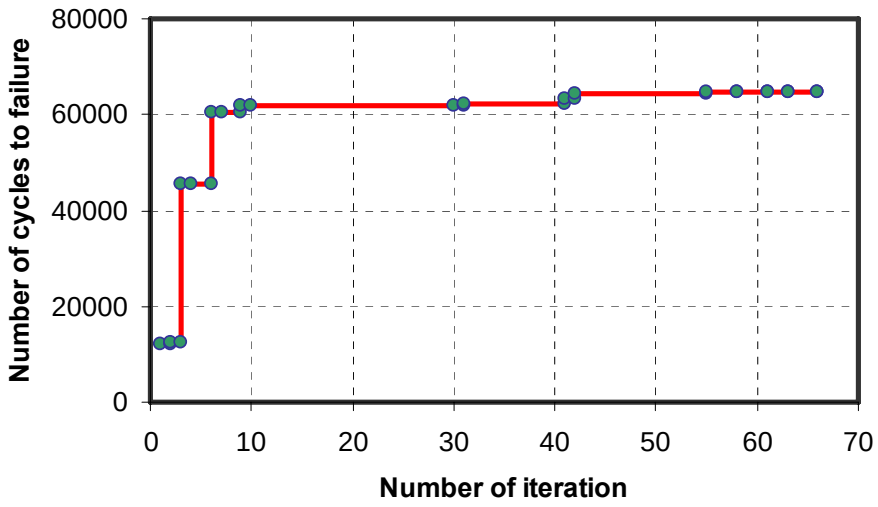

Figure 2.9. Fatigue life of the best current configuration generated during the optimization process.

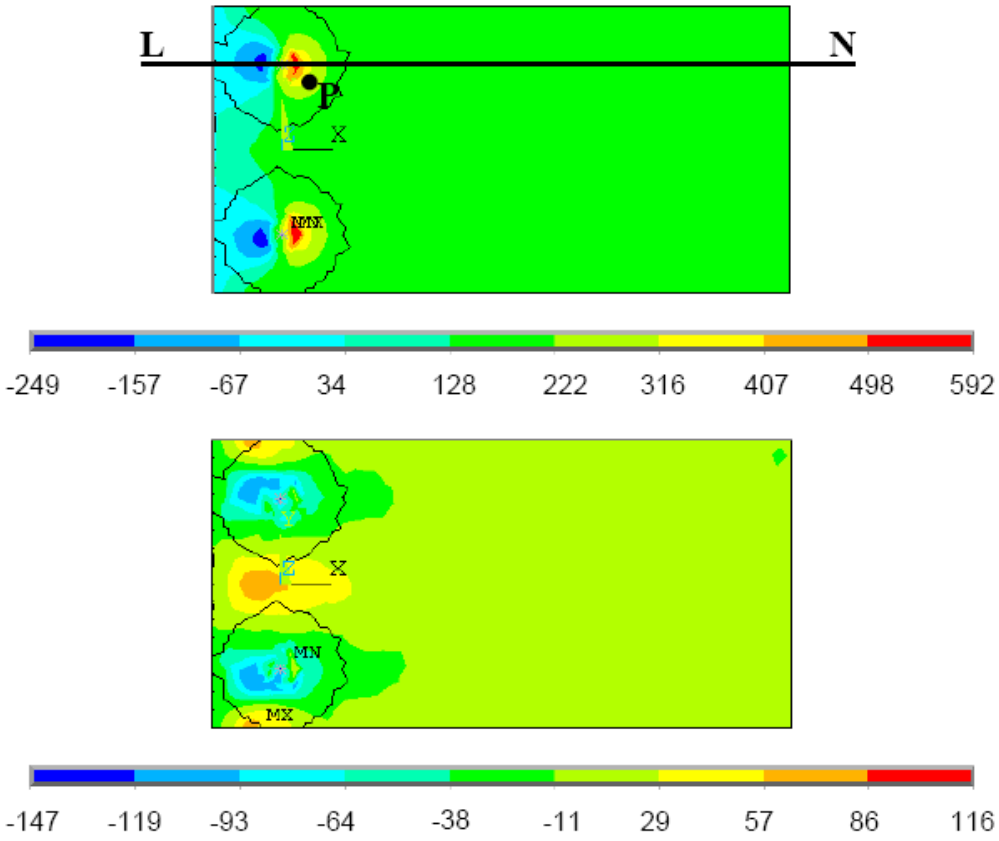

Figure 2.10. Distribution of σ_{xx} component of stress (in MPa) on the inner surface of one plate with two spot welds subject to the maximum axial load (upper figure) and the minimum axial load (lower figure) for the optimized design.

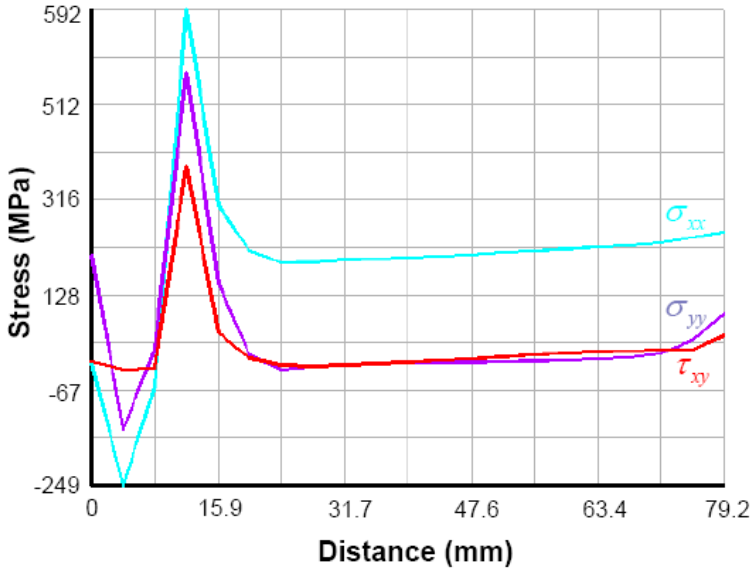

Figure 2.11. Distribution of the stress components σ_{xx}, σ_{yy}, and τ_{xy} along the line L-N shown in Figure 2.10, which passes through one of the spot welds, for the maximum axial loading condition and for the optimized design.

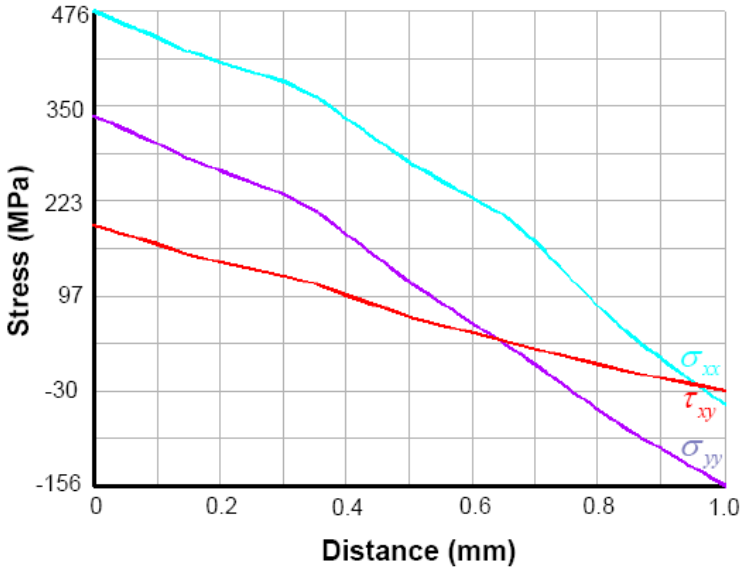

Figure 2.12. Distribution of the stress components σ_{xx}, σ_{yy}, and τ_{xy} (in MPa) through the thickness along a line passing through the point P in Figure 2.10 for the maximum axial loading condition for the optimized design.

Table 2.1 lists some of the optimization results obtained starting from different initial configurations. There are a number of near global optimums and worse local optimums.

Table 2.1 Results of maximum fatigue life optimization of the joint with two spots under cyclic axial loading

Optimization results for joints with two spots under axial load cycle									
	Initial coordinate values (mm) for simplex								
	First point		Second point		Third point		Optimized values (mm)		Fatigue life (cycles)
	y	ℓ	y	ℓ	y	ℓ	y	ℓ	N_f
1	16	80	15	90	14	100	11.84	18.48	64705
2	6	34	5	22	8	40	13.62	21.51	64650
3	17	90	10	80	13	100	13.35	20.25	62903
4	18	50	15	70	13	60	13.96	20.68	62256
5	9	64	9	102	14	60	13.68	22.63	61950
6	14	76	14	98	6	54	14.05	19.96	60032
7	18	10	17	12	16	14	13.52	20.58	45620
8	15	16	14	18	13	20	13.68	20.69	41259
9	12	22	11	24	10	26	11.01	25.23	28596
10	5	10	10	54	7	78	10.26	39.32	19265
11	8	36	9	38	7	34	9.91	40.45	26956
"y" represents the coordinate of the spots on "y" axis									
"ℓ" represents the length of the overlapped portion of the joint									
"y" coordinate of the second spot is the same but different sign with the first spot									

2.5.2. Optimization of a Joint with Two Spots under Cyclic Axial and Transverse Loading

In this case, a joint with two spot welds subjected to both an axial and a transverse load cycles with constant load amplitude (Figure 2.13) was optimized (Figure 2.15) in which x and y coordinates of the spot welds and overlapping length, ℓ, were chosen as design variables. In one of the optimization runs, initial coordinates of the spot welds were (15, 6) mm and (-10, -6.5) mm and overlapping length was 90 mm. Figure 2.13 shows the distribution of σ_{xx} component of stress for the initial design. The corresponding fatigue life of the joint was 4,428 cycles. After 117 iterations, 19,865 cycles of fatigue life were obtained corresponding to the optimal coordinates (6.62, 12.98) mm, (-5.1, -9.71) mm and optimal overlapping length of 35.06 mm. Figure 2.14 shows the change in the objective function value of the best of these configurations generated during the optimization process. Figure 2.15 shows the resulting stress distributions on the optimally design plate.

In this case, in order to determine the global optimum design, the optimization process was repeated 14 times starting from different points.

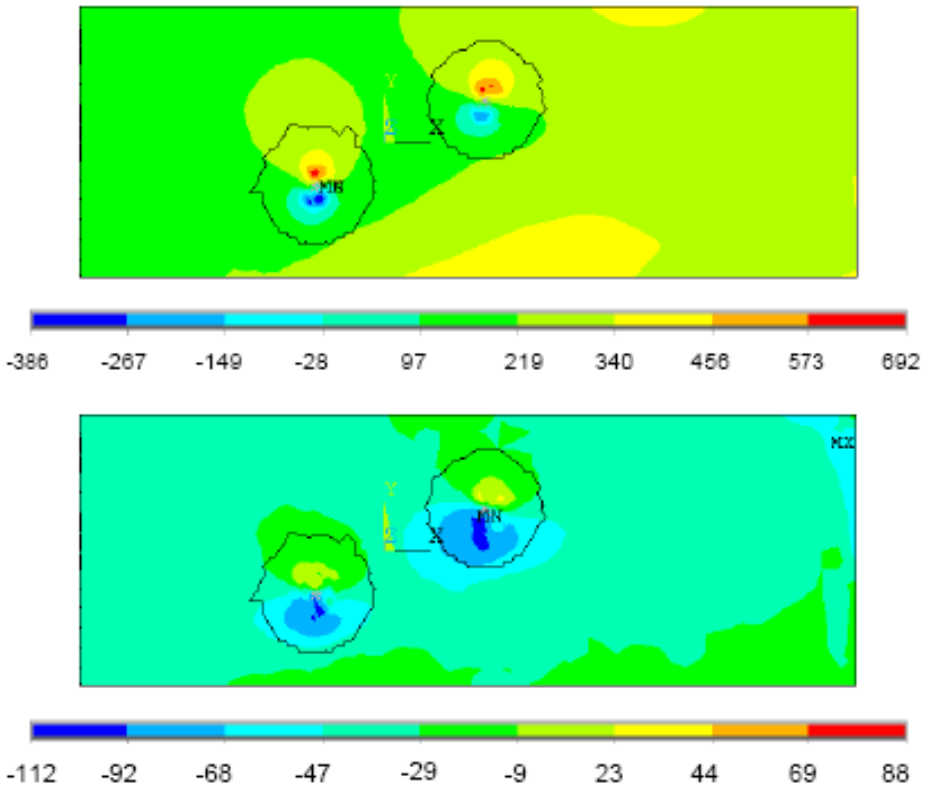

Figure 2.13. Distribution of σ_{xx} component of stress (in MPa) on the inner surface of one plate with two spot welds subject to the maximum axial and transverse loads (upper figure) and the minimum axial and transverse loads (lower figure) for the initial design.

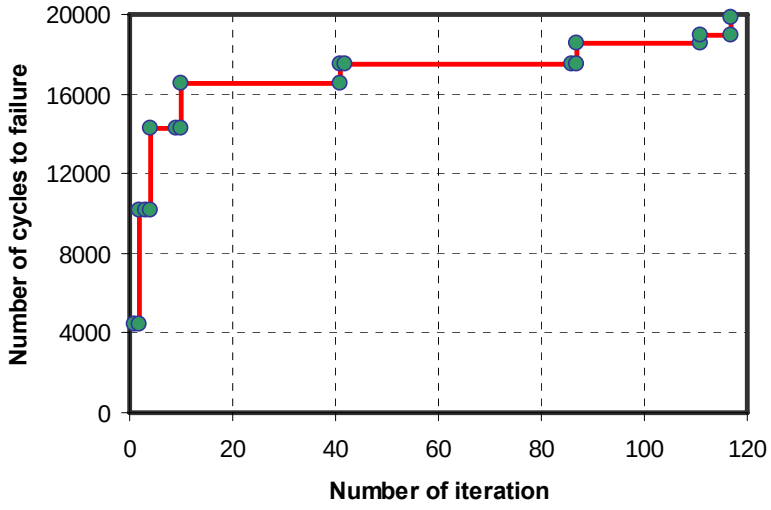

Figure 2.14. Fatigue life of the best current configuration generated during the optimization process

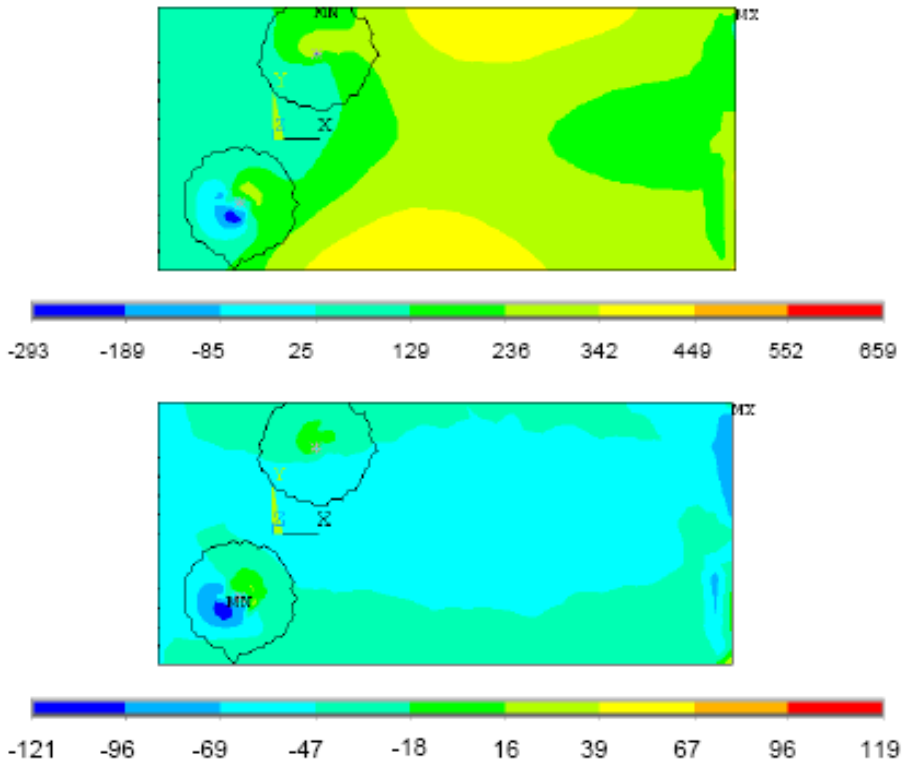

Figure 2.15. Distribution of σ_{xx} component of stress (in MPa) on the inner surface of one plate with two spot welds subject to the maximum axial and transverse loads (upper figure) and the minimum axial and transverse loads (lower figure) for the optimized design.

2.5.3. Optimization of a Joint with Three Spots under Cyclic Axial Loading

In this case, three spot-welded joints subject to an axial load cycle with constant load amplitude were optimized. One of the spot welds was positioned at the center of the joint and its location was not changed during the optimization while the others were free to move. In one of the trials, initial coordinates of the spot welds were (21, 15) mm, (0, 0) mm and (11, -12) mm and overlapping length (ℓ) was 110 mm. Figure 2.16 shows the distribution of σ_{xx} component of stress. The corresponding fatigue life of the joint was 425,791 cycles. After 69 iterations, a fatigue life of 1,391,655 cycles was obtained for the optimal coordinates of (0, 14.35) mm, (0, 0) mm, and (0, -14.26) mm and optimal overlapping length of 16.50 mm. Figure 2.17 shows the change in the objective function value of the best of these configurations generated during the optimization process. Figure 2.18 shows the resulting true stress distributions on the optimal design plate.

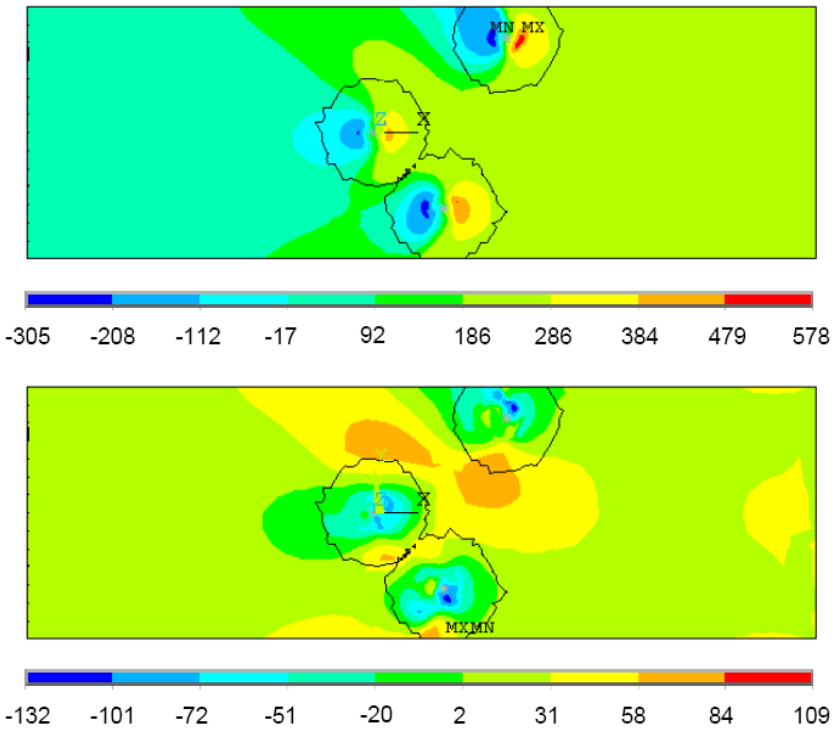

Figure 2.16. Distribution of σ_{xx} component of stress (in MPa) on the inner surface of one plate with three spot welds subject to the maximum axial load (upper figure) and the minimum axial load (lower figure) for the initial design.

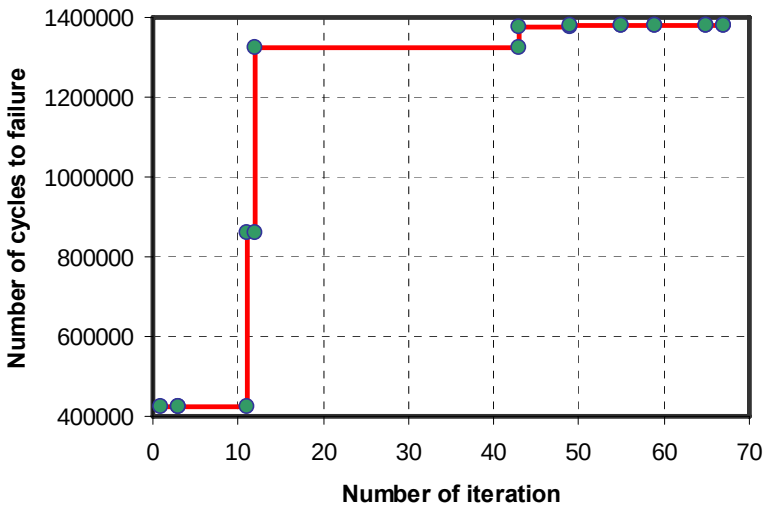

Figure 2.17. Fatigue life of the best current configuration generated during the optimization process.

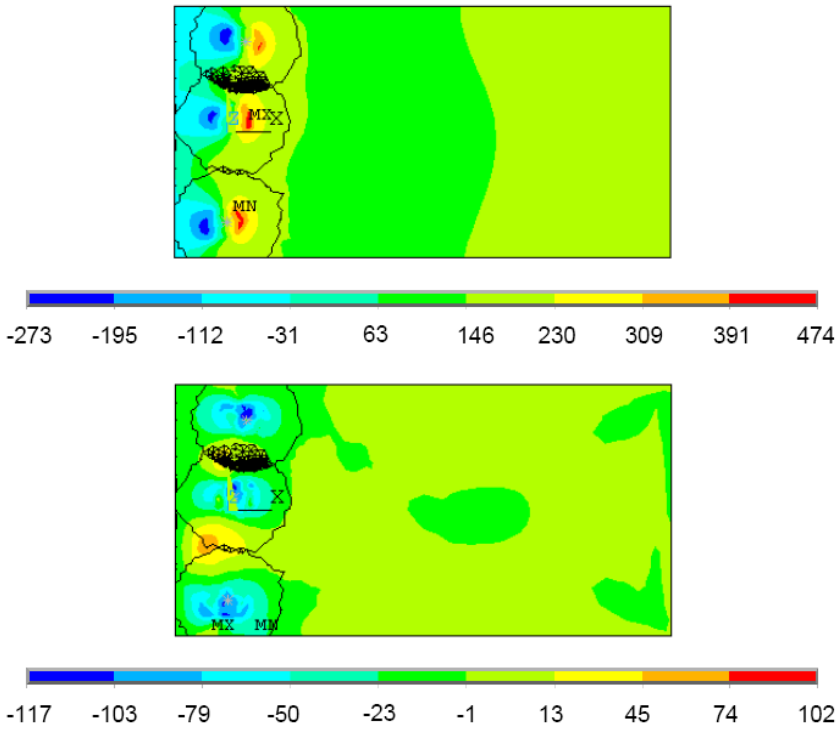

Figure 2.18. Distribution of σ_{xx} component of stress (in MPa) on the inner surface of one plate with three spot welds subject to the maximum axial load (upper figure) and the minimum axial load (lower figure) for the optimized design.

2.5.4. Optimization of a Joint with Three Spots under Cyclic Axial and Transverse Loading

In this case, a joint with three spot welds subject to both an axial and a transverse load cycle with constant load amplitude were optimized. Also for this problem, centrally positioned spot weld was fixed and the positions of the other two were optimized. In one of the optimization runs, initial coordinates of the spot welds were (-14, 13) mm, (0, 0) mm and (13, -14) mm and overlapping length (ℓ) was 100 mm. Figure 2.19 shows the distribution of σ_{xx} component of stress for the initial design. The corresponding fatigue life of the joint was 6,168 cycles. After 73 iterations, a fatigue life of 168,356 cycles was obtained for the optimal coordinates (13.51, 12.12) mm, (0, 0) mm, and (-13.25, -14.24) mm and optimal overlapping length of 65.58 mm. Figure 2.20 shows the change in the objective function value of the best of these configurations generated during the optimization process. Figure 2.21 shows the resulting stress distributions on the optimal design plate.

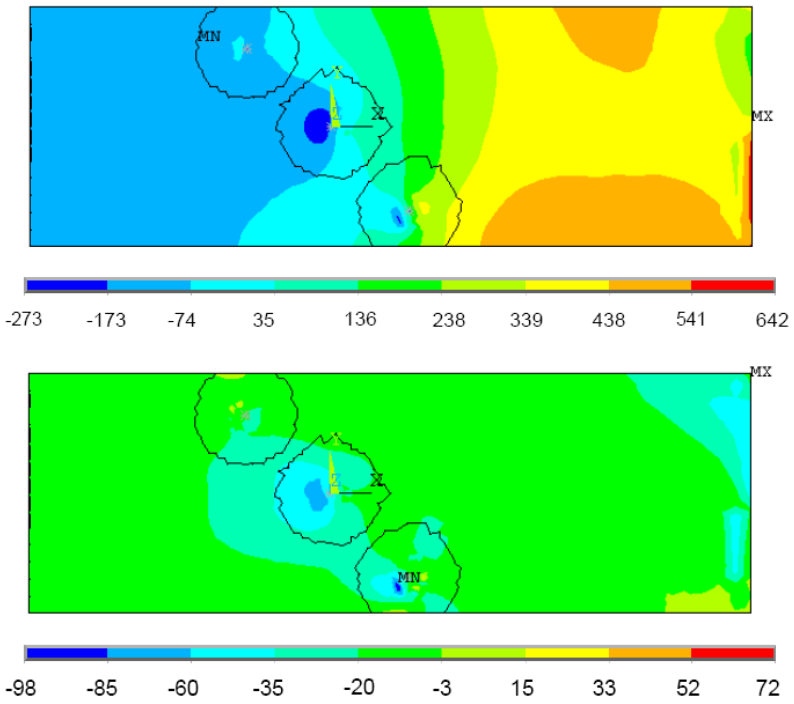

Figure 2.19. Distribution of σ_{xx} component of stress (in MPa) on the inner surface of one plate with three spot welds subject to the maximum axial and transverse loads (upper figure) and the minimum axial and transverse loads (lower figure) for the initial design.

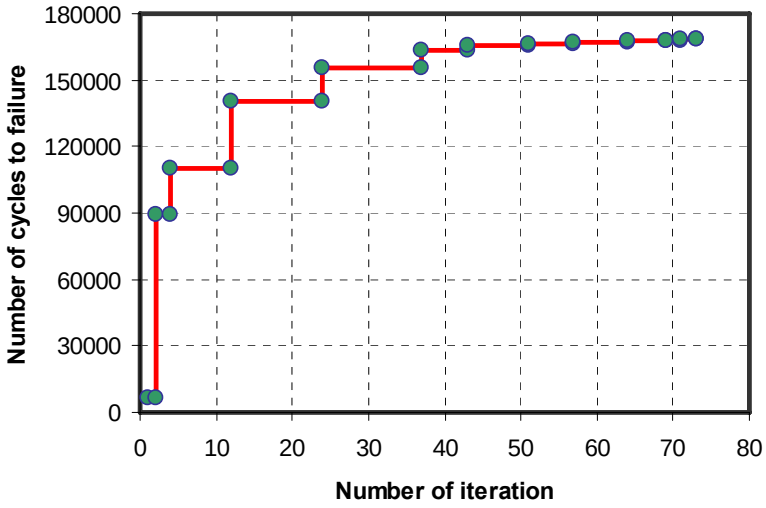

Figure 2.20. Fatigue life of the best current configuration generated during the optimization process.

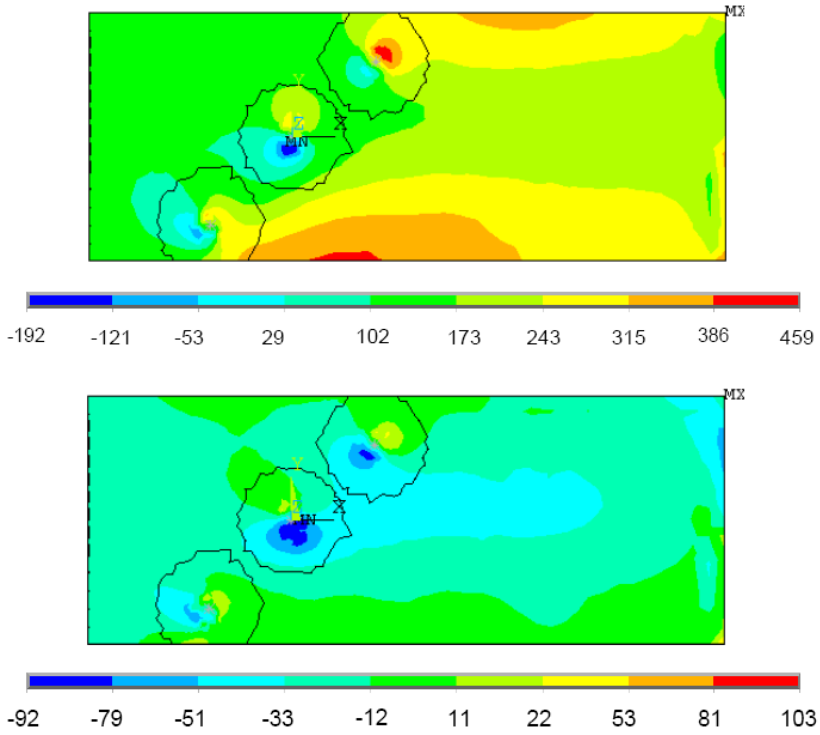

Figure 2.21. Distribution of σ_{xx} component of stress (in MPa) on the inner surface of one plate with three spot welds subject to the maximum axial and transverse loads (upper figure) and the minimum axial and transverse loads (lower figure) for the optimized design.

3. OPTIMIZATION OF COMPOSITE MATERIALS: DESIGN OPTIMIZATION OF FIBER REINFORCED LAMINATES FOR MAXIMUM FATIGUE LIFE

3.1. Introduction

Composites are used in many structural applications ranging from airplanes, ships to sporting goods due to their superior properties, e.g., stiffness-to-weight or strength-to-weight ratios. In addition, composites are less sensitive to fatigue than metals. As a further advantage, composite structures offer great flexibility in design, allowing change of the material system in many ways like number of fibers, different lay-up configurations, etc.

The durability of a structure is defined as its ability to maintain mechanical performance throughout its service life. Durability is an economical consideration because maintenance, repair, or modification costs over the service life depend on maintaining adequate durability. In composites, fatigue is the main damage growth mechanism under service loading. The growth and accumulation of fatigue cracks through the laminate thickness is often the sequence of events that leads to failure and the loss of structural integrity [56].

The extensive research [23, 57-87] on composite materials, on the other hand, revealed that their fatigue behavior is more complex than that of metals. In a metal, fatigue damage develops through initiation and propagation of sharp cracks, which can be reasonably well predicted by fatigue and fracture analysis. Fatigue damage in composite materials, on the other hand, specifically can take the form of any, or all, of the following: fiber-splitting, fiber-breakage, transverse microcracking, matrix microcracking, matrix crazing, fiber/matrix debonding, void growth, and delaminations [65]. It is known that after initiation, the propagation of the crack is responsible for final fatigue failure in metals, while accumulation of cracks leads to failure in composite materials [65]. When the first ply failure occurs, then transverse microcracks through the thickness of the ply ensue and then delamination damage follows; finally, fiber breakage occurs [62, 65, 88-90]. A

catastrophic failure may thus occur at the last stage of the failure. A catastrophic failure may also occur through microcracking and delamination damage without fiber breakage [62, 65, 88-90]. These micro-structural mechanisms of damage accumulations occur sometimes independently and sometimes interactively, and the predominance of one or other may be strongly affected by both materials variables and testing conditions [65]. In other words, even for unidirectional reinforced composites under the simple loading case such as tension loading along the direction of fibers, fatigue cracks may initiate at different locations and in different directions. Cracks can initiate in the interface along the directions of fibers between the fibers and matrix because of the debonding; cracks can also initiate in the matrix, perpendicular to the direction of loading [65, 88, 89, 91, 92]. The fatigue behavior of one constituent may be significantly affected by the presence of other constituents and the interfacial regions between fibers and matrix. Fatigue failure behavior in laminated composite structures is highly dependent on the properties of fiber orientation, the constituent material properties, nature of the loading, stacking sequence, environmental conditions like temperature and humidity, etc [62, 65, 88-90].

Previously, structural optimization was restricted to just sizing optimization. However, today there are three general problem areas that the scientists face: The first one is shape optimization. This area involves finding the best profile for a structure under various constraints imposed by the requirements of the design. Hence, the objective may be to minimize weight or maximize mechanical performance of the structure. The second area is topology optimization, which involves finding the best configuration or layout for a structure. The last one is composite optimization. By optimizing the material system itself such as fiber orientations, filler or fiber volume fraction, ply thickness, stacking sequence, better performance may be obtained [93, 94].

Locating globally optimum structural designs is a difficult problem, which requires sophisticated optimization procedures. In typical structural optimization problems, there may be many locally optimal configurations. Hence, a downhill-proceeding algorithm, e.g. Sequential-Simplex, in which a monotonically decreasing value of objective function is iteratively created, may get stuck into a locally optimal point other than the globally optimal solution. Therefore, researchers adopted global search algorithms like simulated annealing in structural optimization problems [94], especially for composites.

The purpose of composites optimization is to find the best design for a composite materials system according to a chosen criterion under various constraints imposed by the requirements of the design. The optimum design provides either the most efficient and effective use of material or the best performance.

However, because of the contexture, analyzing of composite materials is difficult. For example, when a multidirectional laminate is loaded uniaxially, the resulting stress distributions in its individual laminae are inherently multiaxial. As a result, these multiaxial stresses will considerably weaken a laminate as they act on planes transverse to the reinforcement directions promoting progressive failure in the matrix and interface between the fibers and matrix. Upon such failure, the transfer of load between the fibers in the same lamina and adjacent plies through shear stresses is no longer uniform, and the resulting stress concentrations lead to a premature failure of the laminate. This makes the examination of composites hard [76, 77]

The use of Fiber Reinforced Materials (FRM) can be accelerated if the ability of the prediction of fatigue failure life under various loading conditions accurately. This can be achieved either through experimental characterization or by using predictive tools. Experimental studies related to fatigue behavior of composite materials are very expensive and time consuming processes. Moreover, it is not easy to generalize the experimental results. Hence, even if most of the existing investigations are primarily experimental, modeling is generally attractive way for saving time and expenses in the fatigue design of composite laminates. In the past, many theories have been proposed for the prediction of static failure of FRM's [56, 78, 82, 95]. In contrast, very little work has been done in the area of predicting multiaxial fatigue failure.

There are numerous experimental studies [8, 56, 66, 71, 74, 76, 79, 80, 85, 96-114] on the fatigue failure of composites. On the other hand, the analytical studies are relatively scarce. Because of the difficulties in obtaining reliable fatigue life predictions, large factors of safety are adopted in the designs. In other words, composite structures that are susceptible to fatigue failure are generally over-designed to eliminate catastrophic failure and are therefore less than optimum [65]. Researchers faced considerable difficulties in

modeling fatigue damage in composite materials. Modeling fatigue behavior of a composite can be accomplished using existing single crack type approaches of monolithic materials, but these do not necessarily work with all composite laminate geometries because the damage by fatigue often results in multiple, distinctly different, interacting damage types [65, 88, 89, 92, 115].

There have been a lot of studies on predicting fatigue life in composites which have led to the development of theoretical equations such as Residual Strength Degradation and Stiffness Reduction. In addition, there are many empirical relationships for predicting fatigue life such as Basquin's Law (power law), straight line fits to S-N curves, Miner's rule, and Coffin-Manson Law. Some models show good agreement with experimental data. However, three is no single model which predicts fatigue life in composite structures reliably [65, 90].

Configurations of a laminate, i.e. fiber orientation, ply thickness, stacking sequence, type and volume fraction of reinforcement can be tailored to make a better use of material or attain a desired property, e.g. strength, elastic modulus, thermal and electrical conductivity, thermal expansion coefficient. One may thus significantly decrease the weight of a structure by optimizing the design of the composite material itself, or increase its performance using the same amount of material. For this reason, optimum design of composites has drown the attention of many researchers [66, 67, 71, 85, 100, 116].

In literature, optimization of composites has been examined widely, e.g. minimization of thickness under static loading [8, 84, 96-98, 102, 103, 106-108, 110], weight optimization [18, 90, 116, 117], optimization of buckling strength [101, 106, 108, 109, 111, 118, 119]. However, the analytical studies on fatigue damage of composites are very few [23, 74-77], moreover, there is not a general fatigue life prediction model which is not limited to a special geometry, lay-up, loading case, boundary condition, material property etc. In this study, a parametric fatigue life prediction model, Fawaz-Ellyin model, was used with the Direct Simulated Annealing (DSA) optimization algorithm to obtain maximum fatigue life configuration of the composite structure under biaxial loading. In order to optimize a composite structure, some of its features affecting the objective function are allowed to be changed. There should be some design variables. In this study,

the aim is to maximize the fatigue life of the laminated composite structures taking fiber orientation angle as the so called design variable of the composite structure.

3.2. Problem Statement

The problem is to design a composite laminate reinforced by continuous fibers subject to in plane loads. The objective is to find the optimum design of the laminate to attain the maximum fatigue life. The number of distinct fiber orientation angles, m, and the number of plies each lamina contains, n_k, are given. The orientation angles, θ_k, are to be determined in the design process. Accordingly, the number of design variables is m.

The orientation angles take discrete values; they are chosen from a given set of angles. First, as possible fiber orientation angles 0°, 45°, and 90° were chosen, then 0°, 30°, 60°, and 90°, then 0°, 15°, … and 90°, and then 0°, 5°, 10°, 15°, …, and 90°. They can take either a positive or a negative value.

3.3. Fatigue Life Assessment Models for Composite Materials

Fatigue life prediction models for composite materials are mainly classified into five categories, namely cumulative and progressive damage [57, 59, 60, 88, 104], probabilistic [57, 86, 100, 120], phenomenological/empirical [66, 72, 74-78, 80, 83, 87], artificial neural network [98, 121], and meso/micromechanics [65, 81, 89, 92, 115]. In cumulative and progressive damage methods, the term “damage” is generally used for all kinds of physical deterioration of the material depending on the used model. For instance, “damage” may be defined as matrix and fiber cracking sequences, the resulting strength degradation, matrix cracks, stiffness degradation, debonding of fibers from the matrix, matrix cracks etc. In probabilistic models, the reasons of the fatigue life dispersion of composite laminates are analyzed. It is accepted generally that the inner original defects, which derived from the manufacturing process of composite laminates, are the major and common reason of causing the random distributions of the fatigue life. With the study of statistical relationship between the fatigue loading and the fatigue life in the uniform confidence level and the same survival rate of applied stress versus fatigue life curves of material, the relationship between the fatigue life distributions are then obtained and used to describe the

distributions of fatigue life of composites. Phenomenological/emprical models describe strength or stiffness degradation due to constant amplitude fatigue loading and use these descriptions in load-fatigue life predictions. Extensive experimental data are required to construct the models. Artificial neural network system has been used especially in the last years. In this model, a database contains different applied stress versus fatigue life data is used to predict a fatigue life corresponding to an unknown applied stress. Micromechanical models, on the other hand, attempt to describe composite degradation due to fatigue from the constituent properties.

In [87], the model based on the classical lamination theory uses three experimentally measured properties, which are the static strengths of the composite and the slope of the linear fatigue life curve for the laminate, and applied to unidirectional and cross-ply woven fiber reinforced polymer materials. In [75], a fatigue model, which is applied to uniaxial and some angle ply glass fiber-reinforced plastic composites, includes the effects of load stress ratio and load frequencies was proposed. This model, in addition to material constants obtained by the uniaxial tests, requires experimental load versus fatigue life data to establish a set of characteristic fatigue curves for a given composite. In [66], a fatigue failure criterion is employed to determine the failure load. A symmetric angle-ply laminate, which is E-glass fiber reinforced epoxy material, under in-plane cyclic loads are investigated for different fiber orientation, layer thickness and fiber content. In [77], a general model is presented which predicts the fatigue failure of fiber reinforced materials under multiaxial stresses. Different fiber orientations with respect to the loading directions are examined. Using related experimental data, the model was applied to unidirectional and bidirectional fiber reinforced materials. In this model, in addition to the material properties, two additional non-dimensional entities, which are the static strength and the stress ratio correlation factors, obtained via experimental data are necessary. It is shown that the model succeeds in accurately predicting fatigue failure of different unidirectional and bidirectional fiber reinforced materials subject to uniaxial and biaxial stresses and different cyclic stress ratios.

In [87] there is a simple model to predict fatigue life of fiber reinforced polymer materials. The model needs three experimentally determined constants. Even if the model is basic and easy to use, it is not reliable in predicting the fatigue life of composites in all

cases. It is only accurate when the fatigue damage mechanisms and failure mode of the composite are not changed significantly by the through-thickness reinforcement. As a result, a limitation of the model is that a deep knowledge of the fatigue damage process of the composite is needed before it can be used with confidence.

In [122] there is a model accounting for different damage modes for low cycle fatigue (LCF) of composite laminates. At the ply level, a damage-sensitive-model which is based on a family of S-N curves is described for fatigue damage.

In [59-61] a progressive fatigue damage model was proposed to simulate the fatigue behavior of laminated composite materials under in-plane fatigue loading conditions. Using the idea of the traditional progressive damage model, the fatigue damage model was developed. The model is actually an integration of three major components of stress analysis, failure analysis, and material property degradation rules. Authors developed a 3-D, nonlinear, finite element technique for the stress analysis.

Noda et al. (2007) investigated the applicability of the statistical linear cumulative damage (SLCD) rule for predicting the fatigue life under variable cyclic loading for Carbon Fiber Reinforced Plastics (CFRP) laminates [57].

Huang (2001) examined laminated epoxy composites subjected to fatigue loads. The theoretical prediction for the laminate fatigue strength was made using a general methodology, which is a combination of the classical lamination theory and introducing micromechanics model which states that the internal stresses in the constituent fiber and matrix materials of the lamina at every load level are explicitly related to the overall applied load using the constituent properties and the fiber volume fraction only. In this study, the stresses sustained by each lamina layer in the laminate were determined according to the classical lamination theory, whereas the internal fatigue stresses generated in the fiber and matrix materials of the lamina were obtained by the aid of the bringing model.

Epaarachchi et al. (2003) proposed a fatigue model for Graphite Fiber Reinforced Plastics (GFRP) composites that has stress ratio and testing frequency as independent

variables. The model can be used to predict the fatigue behavior of a composite material using a well-defined minimum number of tests.

Wu et al. (1996) investigated the fatigue damage and fatigue life of a batch graphite/epoxy composite laminate. Residual stiffness was selected as a parameter in order to describe the degradation behavior of the composite laminates. In addition to the residual stiffness degradation, a Markov chain model is also used to predict the probability distribution of loading cycles for the residual stiffness to degrade to a certain amount.

Kassapoglou (2007) and Miki et al. (1997) investigated composite structures which under constant amplitude loading to predict fatigue life values and a related approach was presented. This approach is based on the assumption that the cycles to failure are a function of the probability of failure during any given cycle.

Liu et al. (2005) proposed a damage accumulation model for fatigue life prediction of composite laminates with the computational methodology for fatigue life prediction and reliability evaluation. In this model, the fatigue life is predicted using experimental results of the unidirectional laminates. The methodology for probabilistic fatigue life prediction and reliability calculation is also presented.

Fuqiang et al. (2008) have investigated fatigue behavior of the composite laminates from probabilistic point of view using static strength data. They analyzed static strength and fatigue life dispersions of composite laminates. They found that there is a correlation between the failure probability of the specimen being subject to the fatigue cycles for a given fatigue strength and the failure probability of the specimen being subjected to fatigue strength for a given fatigue life. With the study of statistical relationship between the fatigue loading and the fatigue life in the uniform confidence level and the same survival rate $S-N$ curves of material, they obtained the relationship between the static strength distribution and the fatigue one through a material $S-N$ curve model.

3.4. Fawaz & Ellyin's Parametric Fatigue Life Prediction Model

The so called parametric model developed by Fawaz and Ellyin [76, 77] was used in this study to optimize composite laminates under fatigue loading. This model predicts the fatigue life of continuous fiber-reinforced materials (FRM's) under plane stress conditions subject to biaxial loading. This proposed methodology considerably reduces the number of parameters to be determined experimentally. The predictions of the model were compared with published experimental fatigue data and they were found to correlate well for different unidirectional and bi-directional FRM's subjected to uniaxial and biaxial loading conditions [76, 77]. In both unidirectional and biaxial loading applications, in addition to the material properties, only two additional non-dimensional entities, the static strength and the stress ratio correlation factors, obtained via experimental data are necessary. Hence this model considerably reduces the number of parameters to be determined experimentally.

Design optimization of composite laminates for maximum fatigue strength requires a reliable fatigue assessment model that accounts for all the factors affecting fatigue life. The fatigue strength of a given fiber-reinforced laminate depends primarily on the type of constituent laminae and the fiber orientation angle (θ) with respect to the loading directions [56, 76, 77, 79, 80], and magnitude of the cyclic stress as cyclic stress ratio [55, 74]. Besides, use of the model should not require extensive experimental data. Fawaz and Ellyin [77] have attempted to formulate a general multiaxial fatigue failure theory for FRM's that reduced the need of experimentally obtained data to a minimum. The resulting model, which has been used in this study, based on physically observed behavior of FRM's, can be fully established using only basic and easily obtained material properties. General loading parameters such as the biaxiality ratios, the minimum to maximum cyclic stress ratio, and the off-axis angle have been accounted for. The model first has been introduced using the concept of elementary blocks and unidirectional laminae as an elementary block. Then, it has been modified by taking a bi-directional woven laminate as the elementary block (laminae) [76, 77].

Fawaz and Ellyin started with the assumption that a semi-log linear relationship exists between the stress versus fatigue life of a fiber-reinforced laminae as the following [77]:

$$S = m\log(N) + b \tag{23}$$

where S is the alternating stress along a chosen reference direction, m and b are two parameters whose values depend on material properties and loading conditions, and N is the number of cycles to failure at the applied stress.

First the relation is established for the reference direction as the following:

$$S_r = m_r \log(N) + b_r \tag{24}$$

where the subscript r denotes parameters related to the reference line. Using the empirical data, i.e. measured fatigue lives corresponding to different levels of load in the reference direction, m_r and b_r are determined by curve fitting.

The relations between the two sets of material parameters in Equations (23) and (24) are defined by

$$\begin{aligned} m &= f(a_1, a_2, \theta)\, g(R)\, m_r \\ b &= f(a_1, a_2, \theta)\, b_r \end{aligned} \tag{25}$$

where f and g are non-dimensional entities and named as the static-strength and the stress ratio correlation factors, respectively; R is the stress or load ratio; a_1, which is equal to $a_1 = \sigma_{yy}/\sigma_{xx}$, and a_2, which is equal to $a_2 = \tau_{xy}/\sigma_{xx}$, are the first and second biaxial ratios, respectively; x and y represent the global coordinate system; θ is the fiber orientation angle with respect to the global coordinate system as seen in Figure 3.1. Substituting Equation (25) into Equation (23), the relation between the cyclic stress and fatigue life is obtained as [77]

$$S(a_1, a_2, \theta, R, N) = f(a_1, a_2, \theta)\left[g(R) m_r \log(N) + b_r\right] \tag{26}$$

where the non-dimensional entities, f and g, can be defined as the following:

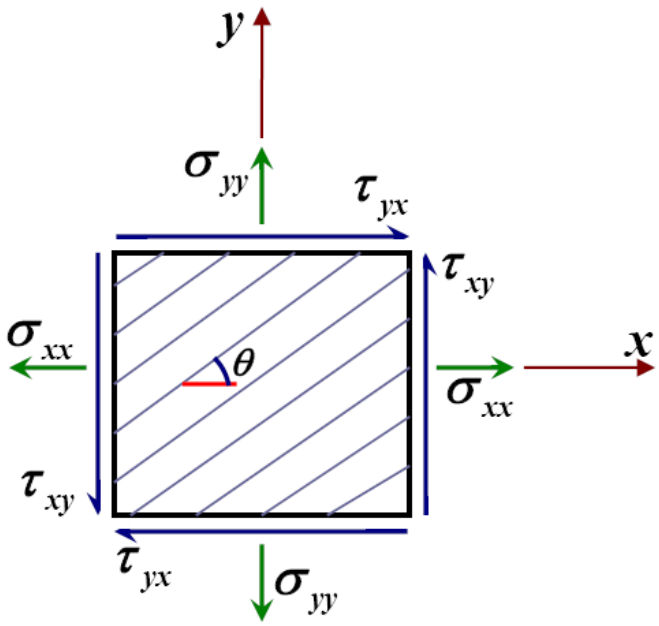

Figure 3.1. A representative geometry of a laminae showing stresses and fiber orientation angle

The model, expressed by Equation (26) can be used to determine the fatigue life of any fiber-reinforced laminate as long as the static strength and the stress correlation factors, f and g, are known for this specific laminate. f and g, are defined as

$$f(a_1, a_2, \theta) = \frac{S_x(a_1, a_2, \theta)}{X_r(a_{1r}, a_{2r}, \theta_r)} \tag{27}$$

$$g(R) = \left(\frac{\sigma_{\max}}{\sigma_{(\max)r}}\right)\left(\frac{1-R}{1-R_r}\right) \tag{28}$$

where S_x is the static strength along the x-direction corresponding to the actual loading parameters of a_1 and a_2, and actual fiber angle θ; X_r is the static strength along the x direction corresponding to the reference loading parameters of a_{1r}, a_{2r}, and θ_r; $\sigma_{\max}$ is the maximum stress occurs on the x-direction; $\sigma_{(\max)r}$ is the maximum stress occurs on the reference direction; R is the stress or load ratio along the x-direction; R_r is the stress or load ratio along the reference direction. f and g account for the differences in the actual and reference conditions in terms of static strength and stress ratio, respectively.

f and g are calculated depending on whether the lamina is unidirectional or bidirectional as follows:

3.4.1. Unidirectional Laminae

In order to calculate strength correlation factor, f, static strength, S_x, along x direction is required. For this purpose, a static failure criterion like Tsai-Hill can be used. According to this criterion critical failure is predicted if the following equality is satisfied.

$$\left(\frac{\sigma_1}{X}\right)^2+\left(\frac{\sigma_2}{Y}\right)^2-\frac{1}{X^2}\sigma_1\sigma_2+\left(\frac{\tau_{12}}{S}\right)^2=1 \tag{29}$$

where X, Y, and S are the in-plane normal, transverse and shear strengths in the material directions. Here, the principal stress components leading to initial failure, σ_1, σ_2, and τ_{12} can be expressed in terms of stress components with respect to global coordinate, S_x, S_y, and S_{xy}, as the following:

$$\sigma_1=S_x\left(\cos^2\theta+a_1\sin^2\theta+2a_2\sin\theta\cos\theta\right) \tag{30}$$

$$\sigma_2 = S_x\left(\sin^2\theta + a_1\cos^2\theta - 2a_2\sin\theta\cos\theta\right) \tag{31}$$

$$\tau_{12} = S_x\left[\left(a_1 - 1\right)\sin\theta\cos\theta + a_2\left(\cos^2\theta - \sin^2\theta\right)\right] \tag{32}$$

Substituting Equations (30), (31), and (32) in Equation (29) yields:

$$\left(\frac{S_x\left(\cos^2\theta + a_1\sin^2\theta + 2a_2\sin\theta\cos\theta\right)}{X}\right)^2 + \left(\frac{S_x\left(\sin^2\theta + a_1\cos^2\theta - 2a_2\sin\theta\cos\theta\right)}{Y}\right)^2 - \frac{1}{X^2}\left[S_x\left(\cos^2\theta + a_1\sin^2\theta + 2a_2\sin\theta\cos\theta\right)\right]\left[S_x\left(\sin^2\theta + a_1\cos^2\theta - 2a_2\sin\theta\cos\theta\right)\right] + \left(\frac{S_x\left[\left(a_1 - 1\right)\sin\theta\cos\theta + a_2\left(\cos^2\theta - \sin^2\theta\right)\right]}{S}\right)^2 = 1 \tag{33}$$

Then, if Equation (33) is substituted into Equation (27), the static strength correlation factor, f, is obtained as the following:

$$f\left(a_1, a_2, \theta\right) = \pm\left(X/X_r\right)\left\{\begin{array}{l}\left[\cos^2\left(\theta\right) + a_1\sin^2\left(\theta\right) + 2a_2\cos\left(\theta\right)\sin\left(\theta\right)\right]^2 - \\ \left[\cos^2\left(\theta\right) + a_1\sin^2\left(\theta\right) + 2a_2\cos\left(\theta\right)\sin\left(\theta\right)\right] \\ \left[\sin^2\left(\theta\right) + a_1\cos^2\left(\theta\right) - 2a_2\cos\left(\theta\right)\sin\left(\theta\right)\right] + \\ \left(X^2/Y^2\right)\left[\sin^2\left(\theta\right) + a_1\cos^2\left(\theta\right) - 2a_2\cos\left(\theta\right)\sin\left(\theta\right)\right]^2 + \\ \left(X^2/S^2\right)\left[\left(a_1 - 1\right)\cos\left(\theta\right)\sin\left(\theta\right) + a_2\left(\cos^2\left(\theta\right) - \sin^2\left(\theta\right)\right)\right]^2\end{array}\right\}^{-1/2} \tag{34}$$

where the negative and positive signs refer to compressive and tensile failure stresses, respectively.

3.4.2. Bidirectional Laminae

Some composite laminates are composed of bidirectional plies having fibers that run perpendicular to each other. Fawaz and Ellyin [77] benefiting from symmetric geometry and assuming $a_2 = 0$, rewrote Equation (26) as

$$S(a,\theta,R,N) = f(a)T(\theta)\left[g(R)m_r \log N + b_r\right] \tag{35}$$

where a is the biaxial stress ratio and defined as $a = \sigma_{yy}/\sigma_{xx}$; f and T are non-dimensional parameters. Here, dependence on biaxial stress ratio, a, and fiber orientation angle, θ, are uncoupled.

In Equation (35), the non-dimensional entities, f and T, can be expressed as the following:

$$f(a) = 1 + \left[\left(\frac{S_x(\alpha) - X}{X\left(\alpha\nu_{xy} - 0.5\alpha^2\right)}\right)\left(\nu_{xy}a - 0.5\nu_{xy}a^3\right)\right] \tag{36}$$

$$T(\theta) = \frac{\left[X - S_x'(\beta)\left(\pi\theta + 2\theta^2\right)\right]}{\left[X_r - S_x'(\beta)\left(\pi\theta_r + 2\theta_r^{\,2}\right)\right]}$$

$$\textit{where} \tag{37}$$

$$S_x'(\beta) = \frac{\left(S_x(\beta) - X\right)}{2\beta^2 - \pi\beta}$$

where $S_x(\alpha)$ and $S_x(\beta)$ are the x component of a biaxial stress obtained for a biaxial ratio at $a = \alpha$, and the off axis strength parameter obtained at $\theta = \beta$, respectively.

In conclusion, the number of experimental data needed in the model varies depending on the nature of the experiments, uniaxial or biaxial. Basic static failure

parameters; which are in-plane normal strength, X, in-plane transverse strength, Y, and out-of-plane shear strength, S, obtained along with a reference curve which is to be determined using one static failure result, (X_r), and the linearity of that reference curve, at least two fatigue results at different stress levels are required for both uniaxial and biaxial cases. For bidirectional materials, two additional parameters; the x component of a biaxial stress obtained for a biaxial ratio at $a=\alpha$, $S_x(\alpha)$, and the off axis strength parameter obtained at $\theta=\beta$, $S_x(\beta)$, are also necessary [77]. In short, first of all, using uniaxial cyclic test results which fibers can orient between 0^0 and 90^0, the reference line is obtained. Then, using $S_x(\alpha)$ and $S_x(\beta)$ which are obtained from again uniaxial stress test results, the non-dimensional parameters, static correlation factor, $f(a)$, stress correlation factor, $g(R)$, and fiber orientation angle correlation factor, $T(\theta)$, can be obtained. Hence, all the components of the fatigue model are defined. Once the necessary experimental parameters are obtained, the model will predict the failure of any FRM's under any arbitrary set of loading conditions.

For example, Fawaz and Ellyin [77] proposed a reference line relationship using experimental data conducted by Smith [64] for a woven E glass fiber reinforced isophtholic polyester as the following:

$$S = f(a)T(\theta)\left[89.2 - 10.2\log(N)\right] \tag{38}$$

where the non-dimensional entities (the static strength correlation and fiber orientation angle correlation factors), $f(a)$ and $T(\theta)$, are expressed:

$$f(a) = 1 + 0.12a - 0.24a^2 \tag{39}$$

$$T(\theta) = 1.85 - 2.31\theta + 1.56\theta^2 \tag{40}$$

3.4.3. Experimental Correlation of the Model

Fawaz & Ellyin have also compared the model with different experimental data which exist in the literature. Figures 3.2 and 3.3 show the comparison of the Fawaz-Ellyin model with the results of Hashin and Rotem [80] on unidirectional Glass/Epoxy for different fiber orientation angle and the results of Smith [64] on bidirectional woven Glass/Epoxy for different stress ratios, respectively.

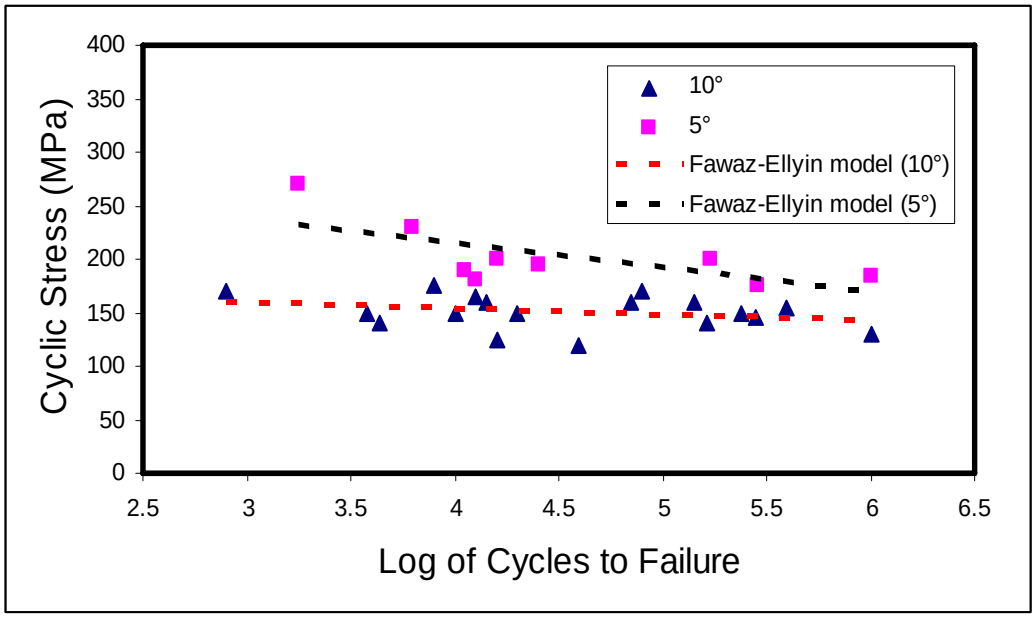

Figure 3.2. Comparison of the Fawaz & Ellyin's model with the results of Hashin and Rotem [80] on unidirectional Glass/Epoxy for different orientation angles [77]

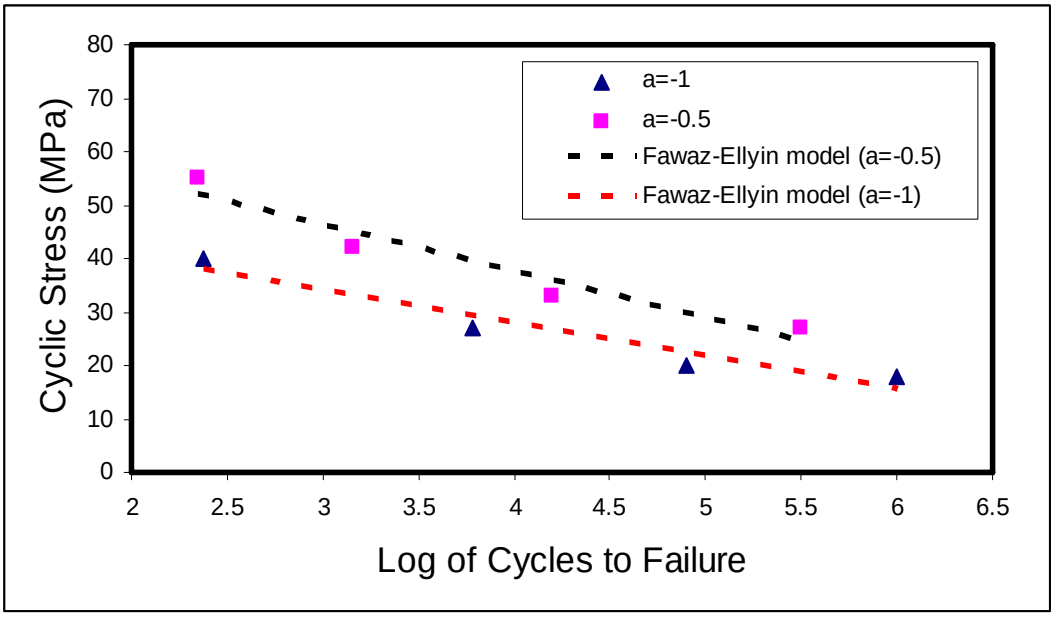

Figure 3.3. Comparison of the Fawaz & Ellyin's model with the results of Smith [64] on biaxial Glass/Epoxy for $\theta = 45^0$ and different stress ratios [77]

As seen in Figures 3.2 and 3.3, the model succeeds in accurately predicting fatigue failure of different unidirectional and bidirectional fiber reinforced materials subject to uniaxial and biaxial stresses and different stress ratios.

3.5. Structural Optimization using Simulated Annealing

Although composite materials offer great flexibility in product design with a large number of design variables, this feature also leads to an immense number of locally optimum designs. Locating globally optimum designs for composite structures is a difficult problem requiring sophisticated optimization procedures. Locating the globally optimal material design with a local search algorithm is almost a hopeless enterprise. For this reason, many researchers preferred global search algorithms like simulated annealing algorithm [94].

The origin of the Simulated Annealing (SA) algorithm is in statistical mechanics. The idea of using the annealing method in optimization problems is due to Kirkpatrick et al. (1983). Since then, SA and its variants are applied to numerous combinatorial and

continuous optimization problems. The algorithm tries to simulate the physical process of ***annealing***, where atoms rearrange themselves randomly during cooling to form a crystal structure having lowest energy state.

3.5.1. The SA Algorithm

SA gets its name from the physical process whereby the temperature of a solid is raised to a melting point, where the atoms can move freely and then slowly cooled. The method attempts to model the behavior of atoms in forming arrangements in solid material during annealing. Although the atoms move randomly, as their natural behavior they tend to form lower-energy configurations. However, this is a time-driven process. When a material is crystallized from its liquid phase, it must be cooled slowly if it is to assume its highly ordered, lowest-energy, perfect crystalline state. At each temperature level during cooling, the material should reach equilibrium. As the temperature decreases, the arrangement of the atoms gets closer and closer to the lowest energy state. This process continues until the temperature finally reaches freezing point.

There is an analogy between a physical annealing process and an optimization process. Different configurations of the problem correspond to different arrangements of the atoms. The cost of a configuration corresponds to the energy of the system. Optimal solution corresponds to the lowest energy state. Just in the same manner, the atoms find their way to build a perfect crystal structure through random movements, the global optimum is aimed to be reached through a search within randomly generated configurations.

In SA, an arbitrary initial design is selected and systematically updated until a stopping criterion is satisfied. Updating is based on an iterative procedure. In each iteration, an arbitrary design is generated in the neighborhood of the current configuration. If the cost function of the new design has a smaller value compared to that of the current design, it is accepted. The new design then replaces the old one. On the other hand, if the new cost function has a larger value, the acceptability of the design is decided according to the probability of Boltzman distribution. The calculation of this probability depends on a temperature parameter, T, which is referred to as temperature, because it plays a similar

role in the optimization process as the temperature in the physical annealing process. The temperature is kept constant for a number of trials and then reduced. The rate of reduction should be slow so as not to get trapped at a locally minimum point. At initial stages of the algorithm (at high temperatures), the probability of accepting worse designs is higher but later on at low temperatures, this probability becomes lower and lower so that in the end the designs having a higher cost are almost never accepted.

DSA differs from SA in two ways. Firstly, DSA keeps a set of current configuration rather than one current configuration. Hence, DSA starts with a set of N configurations, A. Secondly, it always retains the best configuration. In a way, this property imparts a sort of memory to the optimization process. If a newly generated configuration is accepted, it just replaces the worst configuration. For the optimization problem, the initial set of N different configurations is selected randomly within the search domain, S, without any regard to cost. Their costs are calculated and stored. The highest and lowest cost function values are denoted as f_h and f_ℓ. The number of these configurations depends on the dimension of the problem.

$$N = 7(n+1) \tag{41}$$

where n is the dimension of the problem, i.e. the number of design variables.

In each iteration, first, a configuration is randomly selected from the set of current configurations, and then random fiber orientations are given to the laminate, resulting in a new configuration. Acceptability of a new configuration depends on the value of its cost function, f_t; its acceptability, A_t, is calculated by

$$A_t = \begin{cases} 1 \text{.....if} & f_t \le f_h \\ \exp((f_h - f_t)/T_k) \text{.....if} & f_t > f_h \end{cases} \tag{42}$$

here f_h is the highest cost function value in A. This means every new design having a cost lower than the cost of the worst design is accepted. But, if the cost is higher, the trial

configuration may be accepted depending on the value of A_t. If it is greater than a number randomly generated between 0 and 1, the trial configuration is accepted, otherwise rejected.

If the trial function is accepted, it replaces the worst configuration. The best configuration, thus, always remains in A. In each iteration, f_h and f_ℓ are updated. At high temperatures it is unlikely that A will form a dense cluster. At low temperatures, because the likelihood of accepting a worse configuration is low, A will shrink to form a dense cluster.

The simulated annealing process consists of first "melting" the system being optimized at a high "temperature", T, then lowering the temperature slowly until the system "freezes" and no further changes occur. Here, temperature, T, has no physical meaning; it is just a control parameter. Melting corresponds to the initial stage at which configurations are generated within the solution domain, S, without much regard to the cost. At high temperatures, the probability of acceptance is high as Equation (42) implies. Accordingly, configurations that have even very high cost values may be accepted, just as in the physical annealing process the atoms in the melting state may form configurations having very high energy. At low values of temperature parameter, acceptability becomes low and acceptance of worse configurations is then unlikely, just as the atoms become stable, and do not tend to change their arrangements at low temperatures. The cooling schedule in SA controls the convergence of the algorithm to the global minimum just as the cooling scheme in the physical annealing process controls the final microstructure. Therefore, performance of SA depends on the cooling schedule.

In a cooling schedule, first an initial value, T_o, should be specified for the temperature parameter. A scheme is then required for reducing T and for deciding how many trials are to be attempted at each value of T. Lastly, the freezing (or final value of the) temperature parameter is specified.

Initial Value of the Temperature Parameter: Its initial value should be high enough to allow nearly all trials to be accepted. This provides complete "melting" at the initial stages of the optimization process. Otherwise, the region will not be thoroughly searched

and thus the algorithm may become trapped in a local minimum. In the physical analogy mentioned earlier, choosing high T_o corresponds to heating up the solid until all particles are randomly arranged in the liquid phase such that atoms may freely arrange themselves.

Length of the Markov Chains: Iterations during which the value of the temperature parameter, T, is kept constant are called Markov chains (or inner loops). Ali et al. (2002) adopted the following equation to decide on the length of a Markov chain (the number of trials (or iterations)) for the kth level of T:

$$L_k = L + L\left(1 - e^{f_\ell - f_h}\right) \tag{43}$$

where

$$L = 10n \tag{44}$$

where n is the dimension of the problem. At high temperatures, the current configurations form a sparse cluster; consequently f_h - f_ℓ is large and Markov chain length is close to $2L$. On the other hand, when they form a dense cluster at low temperatures, it approaches to L. During the execution of kth Markov chain with length L_k, if a configuration is generated having a cost less than f_ℓ, the best value in A, the current chain is stopped, and a new Markov chain is started. If a configuration better than the best configuration in A is not found, the complete chain of length L_k is executed.

The Scheme for Decreasing the Temperature Parameter: After the initial value of the temperature parameter, T_o, is determined, a decrement rule must be established to find the subsequent values of the temperature parameter. The probability of reaching the global optimum solution depends on how fast the value of the temperature parameter is lowered. If the cooling rate is fast, the optimization process will probably end up with one of the higher-cost local minima. If the cooling rate is slow, the reliability of finding the global optimum solution will be high, but, the optimization process will take excessively long

time. Therefore, the choice of the cooling schedule determines the effectiveness of the algorithm.

In DSA, a temperature scale factor, (α_{k+1}), is specified to calculate the value of the temperature parameter in the next Markov chain, T_{k+1}.

$$T_{k+1} = \alpha_{k+1} T_k \tag{45}$$

where T_k is the value of the current temperature. A value for $\alpha_{k+1} \in [\alpha_{\min}, \alpha_{\max}]$ is calculated using the following equation [123]:

$$\alpha_{k+1} = \begin{cases} \alpha_{\max} & \text{if} \quad L_k > L'_k \\ \alpha_k - (\alpha_k - \alpha_{\min})(1 - L'_{k-1}/L_k) & \text{else if} \quad L_k > L'_{k-1} \\ \alpha_{\max} - (\alpha_{\max} - \alpha_k)(L_k / L'_{k-1}) & \text{else} \quad L_k \le L'_{k-1} \end{cases} \tag{46}$$

where L'_k is the actual number of trials executed in the kth Markov chain. If no configuration is found in the kth Markov chain (inner loop) that is better than the best current configuration L'_k is set to the value of L_k. If a configuration which is better than all is found, the inner loop is terminated, and L'_k is set to the number of iterations actually executed in this loop. In this study, $\alpha_{\max} = 0.999$ and $\alpha_{\min} = 0.99$ were chosen as appropriate values, which provided a compromise between the two effectiveness criteria, i.e. short computational time and high probability of locating global minimum. Initial value of α is taken as the average of $\alpha_{\max}$ and $\alpha_{\min}$.

Because, a new configuration is generated by giving perturbations to a configuration selected randomly among a large number of current configurations, and once accepted the new configuration replaces only the worst one, cooling rate has less importance in DSA in comparison to conventional SA. The worst configuration seldom plays a role in the generation process. Again, it is important to start with a temperature high enough to accept almost all generated configurations.

Stopping Criterion: The optimization process is terminated when no further appreciable improvement can be achieved. This occurs when two conditions are satisfied. Firstly, the current temperature parameter should be small, in other words it should be close to the "freezing temperature" (zero), i.e. no further worse designs may be accepted. Secondly, the current configurations, *A*, should form a dense cluster; thus all alternatives were eliminated and optimization process converged to a single configuration. Accordingly, the stopping criterion can be expressed as

$$\begin{aligned} f_h - f_\ell &< \varepsilon_1 \quad \text{and} \\ T_k &< \varepsilon_2 \quad \text{and} \end{aligned} \tag{47}$$

where ε_i are small numbers. For the optimization problems that were considered, it was more than sufficient to take $\varepsilon_1 = \varepsilon_2 = 0.0001$.

3.6. Optimization Methodology

It may be presumed that a general fatigue assessment model exist accounting all the factors affecting fatigue life, geometry, orientation angle, thickness, loading condition, constituent properties, etc.; but this was not possible to develop such a model until now because of the complexity of the failure behavior of composite materials. Hence many investigators restricted their models to specific conditions, e.g. special geometry, lay-up, boundary condition, etc. In this study, a parametric fatigue life prediction model, Fawaz-Ellyin model, was adopted to predict fatigue life of a laminate configuration generated during the optimization process. The optimization procedure was applied to laminates in plane-stress condition. Fatigue life of a lamina was assumed to be the same as a unidirectional or bidirectional laminate having the same thickness and orientation angle under the same stress state. This assumption is conservative considering that neighboring laminae have a constraining effect on the crack development in a laminae.

3.6.1. Formulation of the Objective Function

Failure of any ply signals inception of failure of the whole structure, even though its ultimate load bearing capacity may not be exceeded. For this reason, this is considered as a design limit. Accordingly, the first-ply failure approach is adopted in the design optimization. Because search algorithm is constructed to minimize the objective function it is chosen as the inverse of the fatigue life of the laminate. Using Equations (38), (39), and (40), the objective function is expressed as:

$$f_{\cos t} = \frac{1}{N_f}$$
$$\textit{where} \tag{48}$$
$$S_1 = f(a)T(\theta)\left[89.2 - 10.2\log\left(N_f\right)\right]$$

where N_f is the fatigue life of the composite laminate; S_1 is the lamina's first principal stress value. With this objective function, the fatigue life and as a result the strength of the composite structure is maximized with an effective use of fiber orientation.

3.6.2. Optimization Algorithm

In this study, a variant of simulated annealing (SA) algorithm called "direct search simulated annealing" (DSA) was used to maximize the fatigue life of the composite structures subject to biaxial in-plane loading.

In DSA, shown in Figure 3.4, unlike ordinary SA, a set of current configurations rather than a single current configuration is maintained during the optimization process. Accordingly, unlike the standard SA algorithm where only the neighborhood of a single point is searched, DSA searches the neighborhood of all the current points in the set. At the start of the optimization process, the number of initial configurations, *N*, are randomly created within the design domain by randomly selecting values for the design variables. The number of initial configuration, *N*, is equal to 7(*n* + 1), where *n* is the number of design variables as mentioned before. The design variable is the orientation angle of the

fibers in the plies, θ_k. An angle value number among (-90, -90 + ϕ,…,-2ϕ, -ϕ, 0, ϕ, 2ϕ,…, 90-ϕ, 90) for θ_k. is randomly chosen. The optimization procedure was repeated for different interval values between consecutive angles, ϕ, e.g. 5°, 10°, 30°, and 45°. With these different interval values, the effect of the variation was also examined. After the initial laminate configurations are randomly chosen, their objective functions are calculated. DSA like SA requires random generation of a new configuration in each iteration. A configuration in the neighborhood of one of the current configurations is randomly generated as follows: First, one of the current configurations is randomly chosen. Then, random differences are introduced to the fiber orientation angles.

$$\theta_k' = \theta_k + r\Delta\theta_{\max} \tag{49}$$

where θ_k is the fiber orientation angle in the kth layer of the randomly chosen current configuration; θ_k' is the fiber orientation angle of the newly generated configuration; r_i are randomly chosen real numbers within [-1, 1]; $\Delta\theta_{\max}$ is the maximum variation that may be introduced to θ_k to generate a new lay-up configuration. The lower and upper limits for θ_k' are -90° and 90°, respectively. If a number greater than 90 is generated for θ_k', 180 is subtracted from this number. If it is less than -90, the value of 180 is added. Acceptability of a newly generated trial configuration, A_t, depends on the value of its cost, f_t, which is calculated by Equation (42).

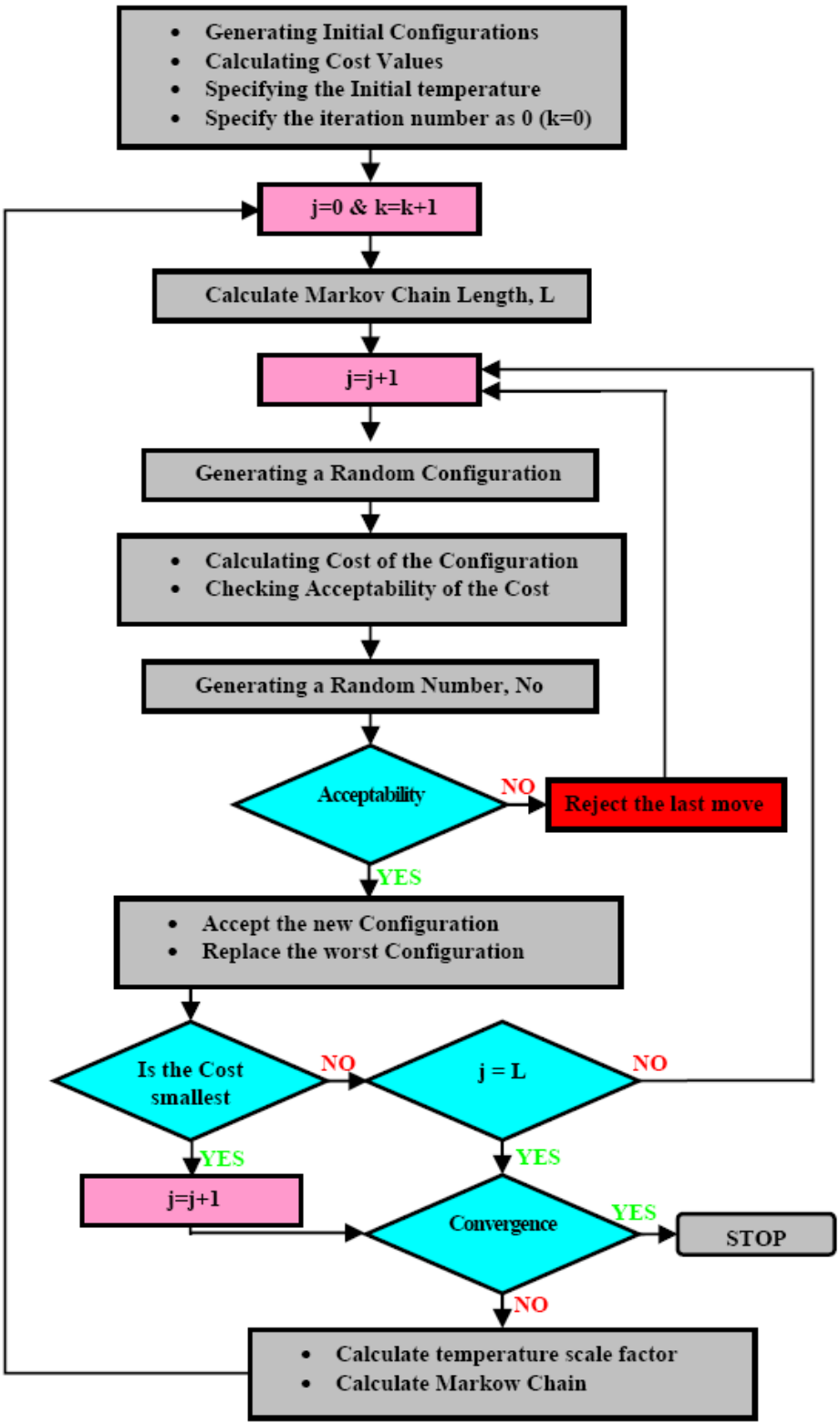

Figure 3.4. The optimization procedure.

Our experience has shown that in order to search the global optimum within a large domain, instead of giving small perturbations to the current configuration to obtain a new configuration in its near neighborhood, we should allow a large variance in the current configurations. For this reason, the magnitude of $\Delta\theta_{\max}$ was taken as 50. This means that the neighborhood of a current configuration, where a new configuration is generated, is initially quite large. This can also be considered as a logical consequence of simulating the physical annealing process, where mobility of atoms is large at high temperatures, and thus the probability that atoms may form a quite different configuration is high. Also, as in the physical process, where mobility of atoms decreases as the temperature is lowered, variation in θ_k is also reduced as the temperature parameter is decreased; but the reduction scheme does not directly depend on temperature. The configuration that is worse than all current configurations except the worst one is defined as the worse configuration, and if no improvement is obtained in the worse configuration during a Markov Chain, $\Delta\theta_{\max}$ is reduced.

3.6.3. Validity of the Optimization Algorithm

Before using the developed code in our problem, it is needed to check the reliability and feasibility of the optimization algorithm with the existing results. So, the developed code has been checked with the known results. It was used a square plate under only one type in plane loading, N_{xx}. Normally the orientation must be through the applied load direction, that is through x direction. As expected the code was correctly predicted that the laminate is strongest for $\theta = 0^\circ$, in which fibers are oriented along the loading direction. This procedure gives the same expected results for different loading conditions and lay-up values. As a result, the reliability and feasibility of the developed optimization algorithm was demonstrated.

Secondly, the Tsai-Wu failure criterion, one of the most reliable static failure criteria, was calculated for different loading conditions and lay-up values for again the square plate under only one type in plane loading, N_{xx}. Using obtained Tsai-Wu value, the safety value, which equal to inverse of the Tsai-Wu, was obtained and compared with the data in literature. As seen in Table 3.1 and Figure 3.5, the results show that the model could

predict the static failure criteria fairly well. The small difference occur because of the nature of the problem. For example, Akbulut et al. (2008) used CLT in their studies, however in our case, it was used a 3-D parametric finite element model (FEM) via ANSYS FE. Hence in the new model, in addition to plane stress values, the values of the third direction were also taken into accounted. This shows us that the new model is more reliable than the old one.

Table 3.1. The comparison of the optimal designs data obtained with the Tsai-Wu failure criteria for the loading N_{xx} = 100 MPa m, $N_{yy} = N_{xy} = 0$ MPa·m, and for two distinct fiber angles ($0 \le j \le 51$).

The criteria used to check feasibility	Optimal lay-up	Half laminate thickness	The value of Tsai-Wu	Safety factor for Tsai-Wu
Akbulut et al (2008)	$[-9_{25}/10_{22}]_s$	47	0.9993	1.0007
The data obtained by FEA	$[-8_{20}/10_{25}]_s$	45	0.9927	1.0070

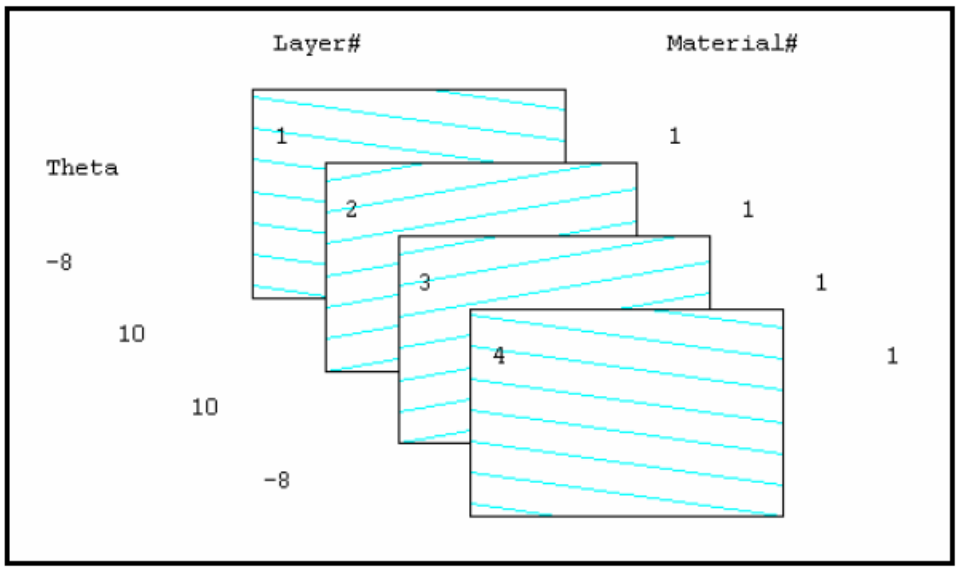

Figure 3.5. Layer Stacking of the composite structure under distributed in plane load, N_{xx}.

3.6.4. Finite Element Model

In order to perform stress analysis of the laminate, a 3-dimensional (3-D) parametric finite element model (FEM) was created by using the ANSYS FE code. The eight-node 3-D tetrahedral layered solid element, SOLID46 (Figure 3.6), with three displacement DOFs per node was used. This element is defined by layer thicknesses, layer material direction angles and orthotropic material properties. SOLID46 has plasticity, stress stiffening, large deflection, and large strain capabilities [46]. Three-dimensional (3-D) mesh was generated to optimize computational time for solution convergence. Moreover, to achieve high accuracy in the calculated stresses, minimize the effect of singularities and capture the high shear and inter-laminar shear and normal stress effects, a convergence analysis was also performed. A dense mesh of the laminate (approximately 8500 elements) was adopted. Because high stress concentration occurs in the vicinities of the hole, much smaller elements were used around the hole in comparison to that of the whole composite structure. Figure 3.7 shows the finite element model of the laminate.

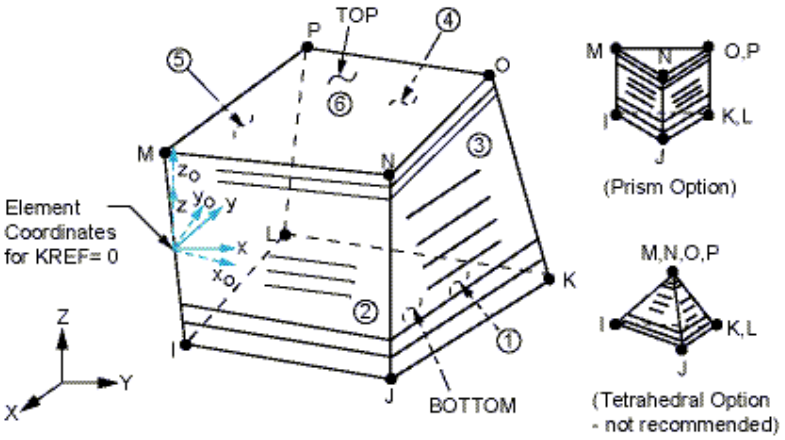

Figure 3.6. General geometry of SOLID 46 element [46].

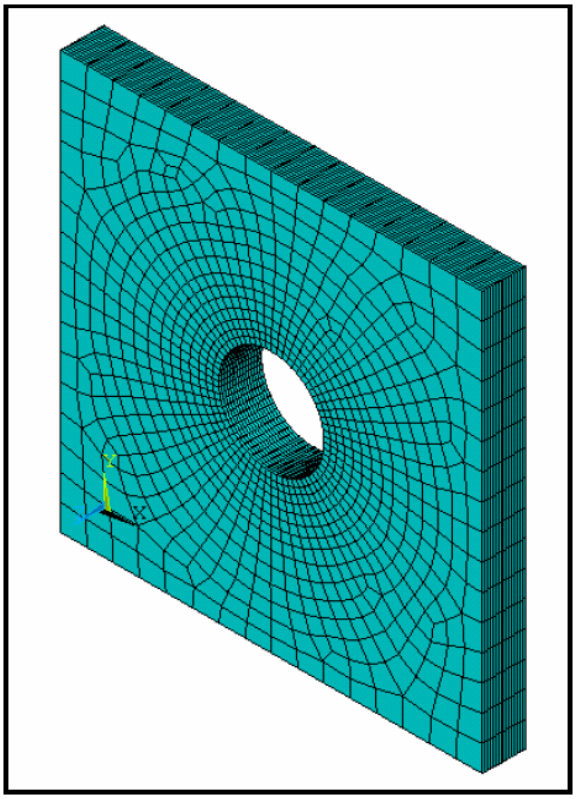

Figure 3.7. Finite element model of the laminate

The boundary conditions in the FEA model are shown in Figure 3.8. Displacements and rotations in all degrees of freedom are fixed at one end; the other end is subject to uniformly distributed in plane load, N_{xx}. Also, a uniformly distributed in plane load, N_{yy}, is applied.

3.6.5. Geometry

The structure to be optimized is a symmetric 3-D multilayered structure reinforced by continuous fibers to in-plane normal loading as shown in Figure 3.8. Two different lay-up, $[\alpha_8, \beta_8]_s$ and $[\alpha_4, \beta_4, \gamma_4, \phi_4]_s$, where α, β, γ, and ϕ are the lamina orientation angles, were examined. Total number of ply is 32 for all lay-ups. The ply thickness is 0.117 mm. The geometrical properties, e.g. length and width of the composite plate, were shown in Figure 3.8. The objective is to find the optimum fiber orientation of the laminate to attain the maximum fatigue life.

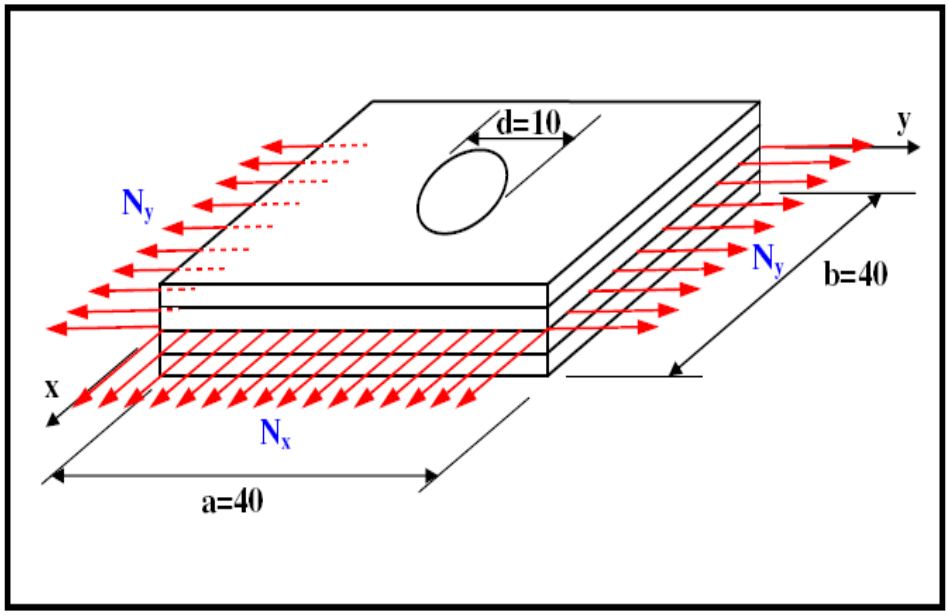

Figure 3.8. A symmetric laminate under distributed in plane loads, N_{xx} and N_{yy}.

3.7. Analysis of a Laminated Composite Plate

SOLID 46 was used as the element type for the composite structure. SOLID 46 is commonly used for 3-D solid-structural modeling. SOLID 46 is a layered version of the 8-node structural solid designed to model layered thick shells or solids. The element allows up to 250 different material layers. The element has three degrees of freedom at each node: translations in the nodal x, y, and z directions. The element has plasticity, creep, swelling, stress-stiffening, large-deflection, and large-strain capabilities. The element input data includes eight nodes and the orthotropic material properties. The default element coordinate system is along global directions. Pressures may be input as surface loads on the element faces in Figure 3.6. Positive pressures act into the element.

The mesh was generated using the eight-node quadrilateral option. The mesh generated was based on the geometry of the composite structure by individual mesh-refining using the smart sizing option. The finite element mesh was checked for individual element connectivity and for other general mesh quality requirements, such as aspect ratio and internal angles. Convergence analysis for both element size and substeps was also

done. An example of a typical mesh used in this analysis and its corresponding three dimensional (3-D) axisymmetric expansion is shown in Figure 3.7. It should be noted that a very fine mesh was used to effectively capture the stress development in the composite at the loading stage.

3.8. Numerical Results and Discussions

In the finite element model of the program, since the necessary constants used in the model were known, a woven E glass fiber-reinforced isophtholic polyester material was chosen. The related material properties are [64] $E_{11} = 17.7 \ \ GPa$, $E_{22} = 17.7 \ \ GPa$, $E_{33} = 3.1 \ \ GPa$, $G_{12} = 2.85 \ \ GPa$, $G_{23} = 2.1 \ \ GPa$, $G_{13} = 2.1 \ \ GPa$, $\upsilon_{12} = 0.156$, $\upsilon_{23} = 0.005$, $\upsilon_{13} = 0.005$, $X_t = 247.7 \ \ MPa$, $X_c = -247.7 \ \ MPa$, $Y_t = 247.7 \ \ MPa$, $Y_c = -247.7 \ \ MPa$, $Z_t = 20 \ \ MPa$, $Z_c = -20 \ \ MPa$, and $S = 143 \ \ MPa$.

In each iteration, a random laminate configuration is generated by introducing random changes to fiber angles. Then, FE analysis of the laminate is carried out to determine the stress state generated due to the maximum load. Since, the structure is assumed to be linear, the stresses corresponding to the minimum load are obtained by reducing the calculated stresses by the minimum-to-maximum-load ratio. Using the stress states at the nodes where the equivalent stress is high, the fatigue lives at all critical locations are estimated using Fawaz-Ellyin model. In order to apply the model, first principal stresses and principal directions are found at each node, and the angle between fiber orientation angle and principal direction is found. Then, the minimum value is chosen as the fatigue life of the laminate. The newly generated configuration is accepted or rejected according to the acceptance criteria of DSA algorithm. Iterations are continued until convergence is obtained.

Figures 3.9-3.12 show the deformation of the optimum composite structure, maximum equivalent stress distribution (in MPa), tensile stress in the x direction (in MPa), and), tensile stress in the y direction (in MPa) under the so called loading condition for four different lay-up configuration and for the possible fiber orientation angles of 0°, 30°, 60°, and 90°,after optimization scheme, respectively.

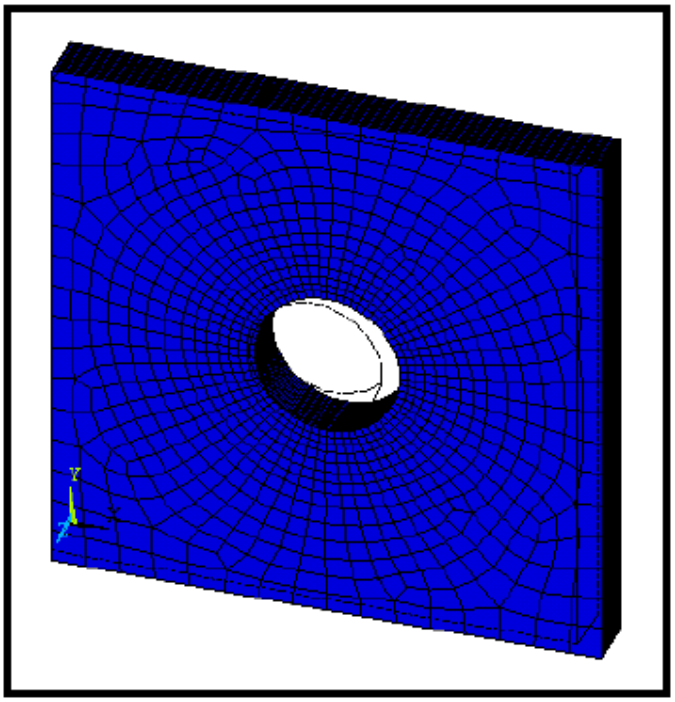

Figure 3.9. Deformation in the optimum laminate.

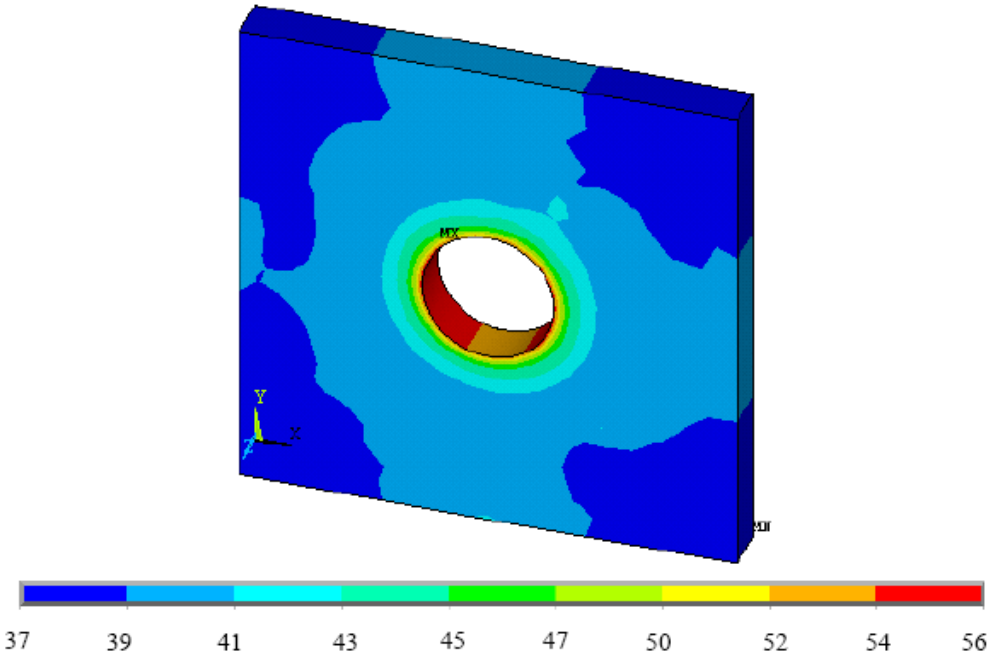

Figure 3.10. Equivalent stress distribution in the optimal laminate.

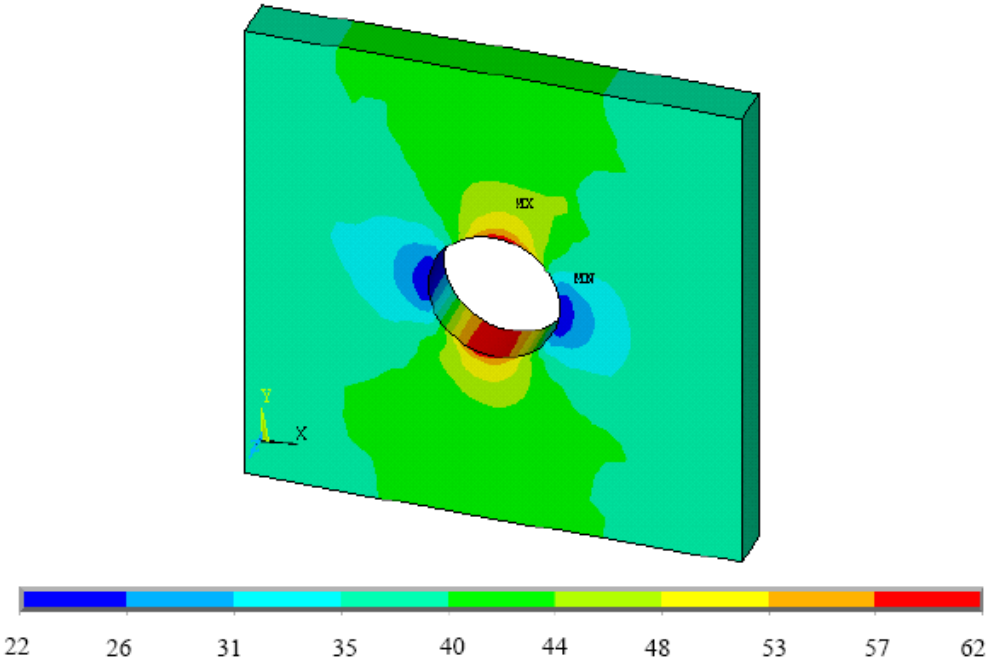

Figure 3.11. Tensile stress distribution, S_{xx}, in the optimal laminate.

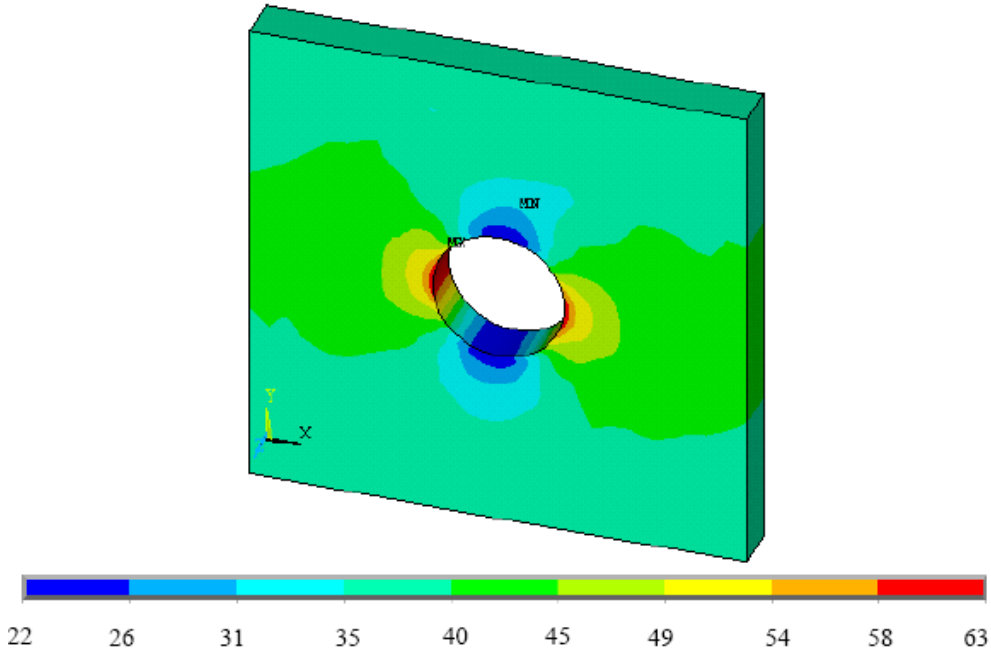

Figure 3.12. Tensile stress distribution, S_{yy}, in the optimal laminate.

Figure 3.13 shows the optimized fiber orientation angles on every lay-up of the composite structure under distributed in-plane load, N_{xx} and N_{yy}, and for the possible fiber orientation angles of 0°, 30°, 60°, 90°. Tables 3.2 and 3.3 show the optimum lay-ups and fatigue life values for the distributed in plane loading, $N_{xx} = N_{yy}$ = 1.5 MPa m which are maximum values of the loading (minimum in-plane loads are equal to 0.75 MPa m), and for different possible fiber orientation angles for 4 and 2 different number of distinct fiber angles, respectively. Half laminate thickness equals to 16.

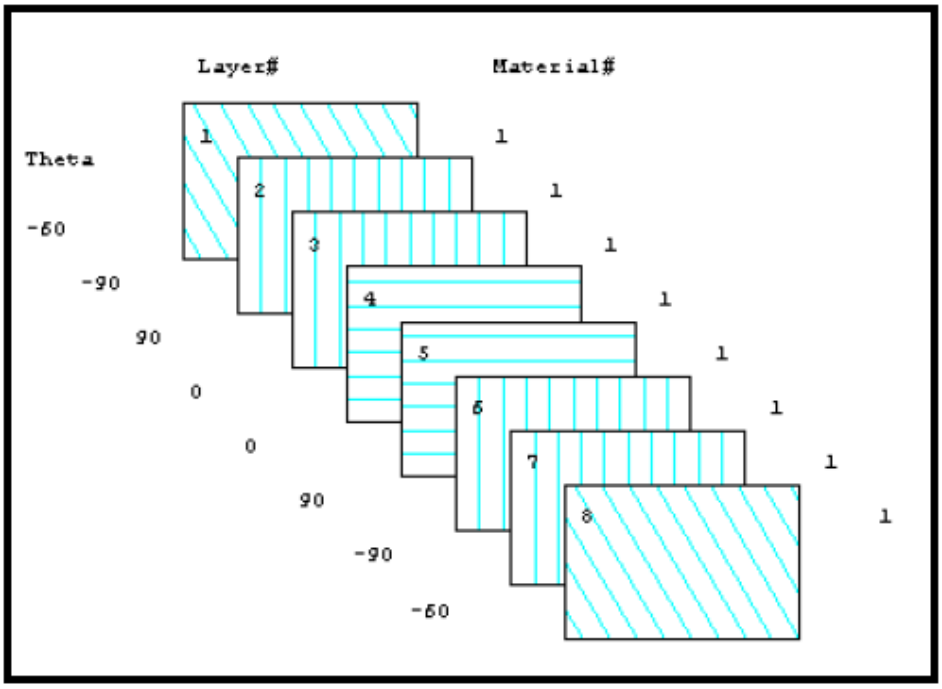

Figure 3.13. Optimized layer stacking of the composite structure under distributed in plane load, N_{xx} and N_{yy}, and for the possible fiber orientation angles of 0°, 30°, 60°, 90°.

Table 3.2. The optimum lay-ups and corresponding fatigue life values for the distributed in plane loading, N_{xx} and N_{yy}, for 4 different number of distinct fiber angles and for different possible fiber orientation angles

Possible fiber angles	Optimum lay-up sequences	Fatigue life (cycle)
±0°, ±45°, ±90°	$[45_4/0_4/0_4/0_4]_s$ $[45_4/\pm90_4/\pm90_4/\pm90_4]_s$	679610
±0°, ±30°, ±60°, ±90°	$[-60_4/\pm90_4/\pm90_4/0_4]_s$	461220
±0°, ±15°, ±30°, ±45°, … ±90°	$[0_4/\pm90_4/\pm90_4/0_4]_s$	679610
±0°, ±5°, ±10°, ±15°, ±20°, … ±90°	$[-45_4/-5_4/0_4/-5_4]_s$	680050

Table 3.3. The optimum lay-ups and corresponding fatigue life values for the distributed in plane loading, N_{xx} and N_{yy}, for 2 different number of distinct fiber angles and for different possible fiber orientation angles

Possible fiber angles	Optimum lay-up sequences	Fatigue life (cycle)
±0°, ±45°, ±90°	$[-45_8/0_8]_s$, $[45_8/0_8]_s$, $[-45_8/-90_8]_s$	470630
±0°, ±30°, ±60°, ±90°	$[30_8/90_8]_s$, $[30_8/0_8]_s$, $[-60_8/0_8]_s$, $[-60_8/-90_8]_s$	339930
±0°, ±15°, ±30°, ±45°, … ±90°	$[\pm90_8/0_8]_s$	473690
±0°, ±5°, ±10°, ±15°, ±20°, … ±90°	$[40_8/0_8]_s$	470690

4. CONCLUSIONS

In the first part of the study, the fatigue failure behavior of modified tensile shear specimens was investigated numerically and compared with experimental results done previously.

FE analyses were carried out taking into account nonlinear constitutive relations, plastic deformation, and residual stresses to determine the stress and strain states in the specimens under cyclic loading. High stresses were found to develop close to the spots on the inner surfaces of the plates, which conformed to the fatigue crack initiation sites observed in the experiments.

The fatigue lives of the specimens were also estimated using the available general purpose fatigue failure models. Because the stress state in the spot weld specimens was multiaxial and the fatigue models were structured for uniaxially stressed parts, equivalent stress or strain approaches were adopted. Among them, Von Mises stress and maximum principal strain (or octahedral shear strain) were found to better reflect the effect of multiaxial strain and stress states. Both stress and strain-based approaches were used to estimate the number of cycles to failure. The fatigue life predictions of stress-based approaches were overly conservative. Among the strain-based approaches, Coffin - Manson and Morrow's mean stress models yielded the best correlations. These models can reliably be used in designing spot weld joints.

Fatigue life of a spot welded joint highly depends on the joint type, applied load amplitude, sheet thickness, and the spot weld diameter. The resistance of TS to fatigue failure is slightly lower in comparison to MTS for small nugget diameters and thicknesses. For larger diameters and thicknesses, TS and MTS have about the same fatigue resistance. Larger flexural rigidity of MTS specimens does not conduce to great improvement in fatigue life because of a higher stress concentration. For this reason, one should not expect to improve fatigue strength by introducing flanges to plates fastened by spot welds except for better deformation behavior. This will only increase material and manufacturing cost, and weight. Fatigue strength of CP joints is much lower in comparison to MCP, TS, and MTS. Hence, one should avoid using CP joints under tensile fluctuating loads.

The fatigue lives of TS, MTS, CP, and MCP type spot weld joints were estimated for various spot weld diameters and sheet thicknesses using Morrow mean stress and Modified Coffin-Manson Models.

Larger diameters and thicknesses resulted in longer fatigue lives within the chosen range of values for these parameters. However, after a certain limit, increase in thickness does not improve fatigue strength. For this reason, one should find the optimum thickness through fatigue analyses in a design process for effective use of material. Moreover, using a large number of small spot welds proved to be more effective in increasing fatigue strength in comparison to large spots having the same cross-sectional area.

In the second part of the study, a methodology is proposed to find the optimum locations of spot welds and the optimum overlapping length of the joined plates for maximum fatigue life. Minimum weld-to-weld and weld-to-edge distances recommended by the industry were considered as side constraints. This procedure was applied to a number of problems in order to check the effectiveness of the algorithm. Because a local search algorithm, Nelder & Mead, was used to determine the optimal positions of spots and optimal overlapping length, the optimization process was repeated many times starting from different configurations and the optimal design with the highest fatigue life was presumed to be the globally optimum design. Since the results show that a limited number of local minima exist, use of a local search algorithm is more appropriate instead of a computationally expensive global optimization algorithm.

In the optimization procedure, penalty functions were introduced to prevent the spots getting close to each other and the boundaries of the plates and to avoid the overlapping length becoming too large. In this way, any interference of spot welds is avoided and the length, and thus material use, is minimized without an adverse effect on fatigue life. With the increased number of spot welds the complexity of the optimization problem increases as well as the possibility of improvement. Significant differences in fatigue life may exist between optimal and non-optimal designs.

Fatigue life of spot welded joints, which depends on the stress and strain states around the spot welds, is a very complex function of the spot-weld positions, even in the case of two spots. Even an experienced designer may not guess the optimal design in many cases. This means that simple rules of thumb for optimal designs are not viable.

In the last part of the study, an optimization procedure to find globally optimum designs of composite laminates subjected to given in-plane biaxial loads for optimum fatigue response. For this purpose, an improved version of simulated annealing algorithm, direct simulated annealing (DSA), was used. Fiber orientation angle in each layer was taken as a design variable. A computer code was developed in ANSYS parametric language, and results were obtained for different number of distinct fiber angles and for different possible fiber orientation angles.

The proposed algorithm can reliably find the global design or a near global design in every run even with a large number of optimization variables. Moreover, because the DSA algorithm uses N number of current configurations, it may find many multiple global or near global optimum designs in a single run.

With the increased number of distinct fiber angles the complexity of the optimization problem increases as well as the possibility of improvement. As seen in the tables presenting the results, significant improvements can be obtained when the number of distinct fiber angles is increased from two to four. Hence, choosing a high number of distinct fiber angles is necessary to obtain the best possible design.

APPENDIX A: THE SIMPLEX METHOD

The Nelder-Mead or the sequential simplex method was originally proposed by Hext, Himsworth and Spendly. Then, the so-called method was improved by Nelder and Mead, so that the simplex method is also known as the Nelder-Mead method.

The Nelder-Mead (Sequential Simplex) method is a robust and at the same time a zero-order deterministic algorithm. Because the Nelder-Mead method is a zero-order search algorithm, it does not need any numerical derivatives of the objective function. Hence, the so called method is easy to use in analysis. However, because the Nelder-Mead method is a deterministic search algorithm, it does not necessarily converge to the global optimum. Hence, a deterministic algorithm should be employed many times starting from different points within the feasible region of design parameters. Then, the lowest value is chosen as the global minimum of the objective function.

The Nelder-Mead search algorithm begins with a regular geometric figure called simplex requiring $n+1$ initial sets (vertices) of the design variables in an n-dimensional space, where n represents the number of the design variables. These vertices can be defined by the origin and by points along each of the n coordinate directions. The following equations are suggested for the calculation of the positions of the vertices of a regular simplex of size "a" in the n-dimensional design space.

$$
\begin{aligned}
&x_j = x_0 + pe_j + \sum_{\substack{k=1 \\ k\neq j}}^{N} qe_k, \qquad j = 1,2,.....n, \\
&\textit{where} \\
&p = \frac{a}{n\sqrt{2}}(\sqrt{n+1}+n-1) \quad \textit{and} \\
&q = \frac{a}{n\sqrt{2}}(\sqrt{n+1}-1),
\end{aligned}
\tag{A.1}
$$

where e_k is the unit base vector along the kth coordinate direction and x_0 is the initial base point. For one variable (that is for one design variable), the initial location number will be

two, hence the simplex will be a line segment. For two variables (that is for two different design variables), the initial location number will be three, hence the simplex leads to an equilateral triangle of side a. For three variables (that is for three different design variables), the initial location number will be four, hence the simplex leads to an coplanar equilateral tetrahedron of side a. Once the simplex method is defined, the objective function is evaluated at each of the $n+1$ vertices, $x_0, x_1, x_2, x_3, ...x_n$. Let x_l and x_h denote the vertices where the objective function assumes its minimum and maximum values, respectively, and x_s is the vertex where it assumes the second highest value. The simplex method discards the highest value and replaces it by a point where objective function has a lower value doing of the following operations, namely "reflection", "contraction", and "expansion". The reflection operation creates a new point x_r along the line joining x_h to the centroid $\bar{x}$ of the remaining point defined as [53]

$$\bar{x} = \frac{1}{n}\sum_{i=1}^{n} x_i, \qquad i \neq h, \tag{A.2}$$

The vertex at the end of the reflection operation is calculated by

$$x_r = \bar{x} + (\bar{x} - x_h), \tag{A.3}$$

If the value of the objective function at this new point satisfies the condition, that is, $f_l \langle f_r \leq f_s$, *where* $f_l = f(x_l)$ then x_h is replaced by x_r and the process is repeated with this new simplex value. If, in contrast, the value of the function at the end of the reflection is less than the lowest value of the function, then, there is a possibility that it can be further decreased to the function by going further along the same direction. It is searched as an improved point x_e by the expansion technique using the relation

$$x_e = \bar{x} + 2(x_r - \bar{x}), \tag{A.4}$$

If the value for this function is smaller than the value at the end of the reflection step, then x_h is replaced by x_e and the process is repeated with the new simplex value. However, if the expansion leads to a function value equal to or larger than the function value of reflection point, then the new simplex is formed by replacing x_h by x_r and continued.

Finally, if the process of the reflection operation leads to a point x_r such that the function value of reflection is smaller than of the maximum, contraction is performed without any replacement using

$$x_c = \bar{x} + 0.5(x_h - \bar{x}), \tag{50}$$

If the function value of this point is greater than that for maximum value, then all the points are replaced by a new set of points

$$x_i = x_i + 0.5(x_l - x_i), \qquad i = 0,\ 1,\ 2,\ .....,n, \tag{51}$$

and the program restarts the process with this new simplex. The operation in the last equation causes the distance between the points of the old simplex and the point with the lowest function value to be halved and is therefore referred to as the “shrinkage” operation

APPENDIX B: DIRECT SIMULATED ANNEALING

The origin of the Simulated Annealing (SA) algorithm is in statistical mechanics. The idea of using the annealing method in optimization problems is due to Kirkpatrick et al. (1983). Since then, SA and its variants are applied to numerous combinatorial and continuous optimization problems. The common fact behind SA type algorithms is the principle of ***annealing***, where the magnitudes of random perturbations are reduced–annealed in a control manner. These random perturbations are injected in a Monte Carlo fashion. Hence, the annealing is designed to enhance the likelihood of avoiding local minima en route to a global minimum of a given a cost function, $C(x)$. The selected initial data or injected randomness helps prevent premature convergence to a local minimum by providing a greater jumpiness to the algorithm [85, 93, 124].

SA is basically a local search method inspired by a criterion for occasionally accepting higher cost configurations. The term ***annealing*** comes from analogies to the cooling of a liquid or solid. Hence, SA is based on thermodynamic considerations, with annealing interpreted as an optimization procedure. From an initial solution, SA repeatedly generates a neighbor of the current solution and transfers to it according to some strategy with the aim of improving the objective function value. During SA process, it is possible that to visit worse neighbors in order to escape from a local minimum. Specifically, a parameter, called temperature, T, is used to control the possibility of moving to a worse neighbor solution. The central issue in statistical mechanics is analyzing the behavior of substances as they cool. Hence, the algorithm, starting from a high temperature, repeatedly decreases the temperature in a strategic manner, which is called as cooling schedule, until the temperature is low enough or some other stopping criteria is satisfied. At high temperatures, molecules naturally have much mobility, but as the temperature decreases, this mobility will begin to lost and the molecules may tend to align themselves in a crystalline structure. In each iteration, the algorithm accepts all “good” moves and some of the “bad” moves according to the Metropolis probability, defined by Equation (B.1) [93, 125, 126].

The aligned structure is the so called minimum energy state for the system. Here, temperature alone does not govern whether the substance has reached a minimum energy

state. To achieve this state, the cooling must occur at a sufficiently slow rate. If the substance is cooled at too rapid a rate, an amorphous or polycrystalline state may be reached which means not a minimum energy state of the substances to reach the minimum energy state [93, 125].

In optimization done by using SA algorithm, the analogy to a minimum energy state for a system is minimizing value of the loss function. The technique of SA attempts to mathematically capture the process of controlled cooling associated with physical processes, which the aim is to reach the lowest value of the loss function in the face of possible local minima. As with the physical cooling process, whereby temporary higher-energy states may be reached as the molecules go through their alignment process, SA also attempts temporary increases in the loss function as the learning process captures the information necessary to reach the global minimum. So it is clear that the critical component of a SA algorithm is the mathematical analogue of the rate of cooling in physical processes [93]. Given a cost function, $C(x)$, which is analogy to energy, and an initial solution state, x_0, the iterative improvement approach seeks to improve the current solution by randomly changing x_0. The main algorithm was used for acceptance or rejection of the new state, x' at a given temperature, T, i.e. Then using the current state, x, and randomly perturbed one, x', corresponding change in cost or objective function, δC is calculated, $\delta C = x' - x$. Then this corresponding change in cost is compared with zero. If $\delta C \langle 0$, the situation is accepted. Otherwise, $\delta C \rangle 0$, the state is accepted with probability of:

$$P(\delta C) = \exp(-\delta C / T) \tag{B.1}$$

Equation (B.1) represents the acceptance-rejection of the SA algorithm. The acceptance criterion is implemented by generating a random number, ρ , which changes between 0 and 1, $\rho \in [0,1]$, and comparing it to $P(\delta C)$; if $\rho \langle P(\delta C)$, then the new state is accepted. The other loop of the algorithm, on the other hand, is referred to as the cooling schedule, and specifies the equation by which the temperature is decreased. The algorithm

terminates when the cost function remains approximately un-chanced, i.e., for n_{no} consecutive outer loop iterations [127].

DSA unlike ordinary SA starts with a set of N configurations, A, rather than starting with only one configuration. For the shape optimization problem, the initial set of N different shapes is selected randomly within the search domain, S, without any regard to cost, but connectivity is observed. Their costs are calculated and stored. The highest and lowest cost function values are denoted as f_h and f_ℓ. The number of these configurations depends on the dimension of the problem.

$$N = 7(n+1) \tag{B.2}$$

where n is the dimension of the problem, i.e. the number of design variables.

In each iteration, first, a configuration is randomly selected from the set of current configurations, and then random fiber orientations are given to the laminate, resulting in a new configuration. Acceptability of a new configuration depends on the value of its cost function, f_t; its acceptability, A_t, is calculated by

$$A_t = \begin{cases} 1 \text{.....if} & f_t \le f_h \\ \exp((f_h - f_t)/T_k) \text{.....if} & f_t > f_h \end{cases} \tag{B.3}$$

here f_h is the highest cost function value in A. This means every new design having a cost lower than the cost of the worst design is accepted. But, if the cost is higher, the trial configuration may be accepted depending on the value of A_t. If it is greater than a number randomly generated between 0 and 1, the trial configuration is accepted, otherwise rejected.

If the trial function is accepted, it replaces the worst configuration. The best configuration, thus, always remains in A. In each iteration, f_h and f_ℓ are updated. At high temperatures it is unlikely that A will form a dense cluster. At low temperatures, because

the likelihood of accepting a worse configuration is low, A will shrink to form a dense cluster.

The simulated annealing process consists of first "melting" the system being optimized at a high "temperature", T, then lowering the temperature slowly until the system "freezes" and no further changes occur. Here, temperature, T, has no physical meaning; it is just a control parameter. Melting corresponds to the initial stage at which configurations are generated within the solution domain, S, without much regard to the cost. At high temperatures, (high values of T) the probability of acceptance is high as Equation (42) implies. Accordingly, configurations that have even very high cost values may be accepted, just as in the physical annealing process the atoms in the melting state may form configurations having very high energy. At low values of temperature parameter, acceptability becomes low and acceptance of worse configurations is then unlikely, just as the atoms become stable, and do not tend to change their arrangements at low temperatures. The cooling schedule in SA controls the convergence of the algorithm to the global minimum just as the cooling scheme in the physical annealing process controls the final microstructure. Therefore, performance of SA depends on the cooling schedule.

In a cooling schedule, first an initial value, T_o, should be specified for the temperature parameter. A scheme is then required for reducing T and for deciding how many trials are to be attempted at each value of T. Lastly, the freezing (or final value of the) temperature parameter is specified.

Initial Value of the Temperature Parameter: Its initial value should be high enough to allow nearly all trials to be accepted. This provides complete "melting" at the initial stages of the optimization process. Otherwise, the region will not be thoroughly searched and thus the algorithm may become trapped in a local minimum. In the physical analogy mentioned earlier, choosing high T_o corresponds to heating up the solid until all particles are randomly arranged in the liquid phase such that atoms may freely arrange themselves.

Length of the Markov Chains: Iterations during which the value of the temperature parameter, T, is kept constant are called Markov chains (or inner loops). Ali et al. (2002)

adopted the following equation to decide on the length of a Markow chain (the number of trials (or iterations)) for the kth level of T:

$$L_k = L + L\left(1 - e^{f_\ell - f_h}\right) \tag{B.4}$$

where

$$L = 10n \tag{B.5}$$

where n is the dimension of the problem. At high temperatures, the current configurations form a sparse cluster; consequently f_h - f_ℓ is large and Markow chain length is close to $2L$. On the other hand, when they form a dense cluster at low temperatures, it approaches to L. During the execution of kth Markow chain with length L_k, if a configuration is generated having a cost less than f_ℓ, the best value in A, the current chain is stopped, and a new Markow chain is started. If a configuration better than the best configuration in A is not found, the complete chain of length L_k is executed.

The Scheme for Decreasing the Temperature Parameter: After the initial value of the temperature parameter, T_o, is determined, a decrement rule must be established to find the subsequent values of the temperature parameter. The probability of reaching the global optimum solution depends on how fast the value of the temperature parameter is lowered. If the cooling rate is fast, the optimization process will probably end up with one of the higher-cost local minima. If the cooling rate is slow, the reliability of finding the global optimum solution will be high, but, the optimization process will take excessively long time. Therefore, the choice of the cooling schedule determines the effectiveness of the algorithm.

In DSA, a temperature scale factor, (α_{k+1}), is specified to calculate the value of the temperature parameter in the next Markow chain, T_{k+1}.

$$T_{k+1} = \alpha_{k+1} T_k \tag{B.6}$$

where T_k is the value of the current temperature. A value for $\alpha_{k+1} \in [\alpha_{\min}, \alpha_{\max}]$ is calculated using the following equation [123]:

$$\alpha_{k+1} = \begin{cases} \alpha_{\max} & \text{if} \quad L_k > L'_k \\ \alpha_k - (\alpha_k - \alpha_{\min})(1 - L'_{k-1}/L_k) & \text{else if} \quad L_k > L'_{k-1} \\ \alpha_{\max} - (\alpha_{\max} - \alpha_k)(L_k / L'_{k-1}) & \text{else} \quad L_k \le L'_{k-1} \end{cases} \tag{B.7}$$

where L'_k is the actual number of trials executed in the kth Markow chain. If no configuration is found in the kth Markow chain (inner loop) that is better than the best current configuration L'_k is set to the value of L_k. If a configuration which is better than all is found, the inner loop is terminated, and L'_k is set to the number of iterations actually executed in this loop. Initial value of α is taken as the average of $\alpha_{\max}$ and $\alpha_{\min}$.

Because, a new configuration is generated by giving perturbations to a configuration selected randomly among a large number of current configurations, and once accepted the new configuration replaces only the worst one, cooling rate has less importance in DSA in comparison to conventional SA. The worst configuration seldom plays a role in the generation process. Again, it is important to start with a temperature high enough to accept almost all generated configurations.

Stopping Criterion: The optimization process is terminated when no further appreciable improvement can be achieved. This occurs when two conditions are satisfied. Firstly, the current temperature parameter should be small, in other words it should be close to the "freezing temperature" (zero), i.e. no further worse designs may be accepted. Secondly, the current configurations, *A*, should form a dense cluster; thus all alternatives were eliminated and optimization process converged to a single configuration. Accordingly, the stopping criterion can be expressed as

$$\begin{aligned} f_h - f_\ell &< \varepsilon_1 \quad \text{and} \\ T_k &< \varepsilon_2 \quad \text{and} \end{aligned} \tag{B.8}$$

where ε_i are small numbers. For the optimization problems that were considered, it was more than sufficient to take $\varepsilon_1 = \varepsilon_2 = 0.0001$ for a good estimate of the global minimum.

APPENDIX C: FATIGUE LIFE PREDICTION MODELS FOR COMPOSITE MATERIALS

C.1. Fatigue Degradation Approach

The simplest degradation model which used for fatigue of composite structures is based on the assumption that all material properties may be assumed to diminish linearly on a logarithmic scale based on the number of cycles endured [128, 129].

$$\frac{P}{P_o} = 1 - \beta \log N \tag{C.1}$$

where P is the current value of a property, P_o is the original value of the same property, β is the logarithmic degradation coefficient, and N is the so called number of load cycles. The log-linear degradation model, Equation (C.1), is fairly effective in describing the cyclic fatigue response of a composite or metallic material that is loaded under a constant type of loading and uniform hydrothermal environment.

A more general degradation model can be constructed in order to take into account temperature, state of stress, and other environmental effects via a Multi-Factor-Interaction Model (MFIM). The importance of MFIM is that material behavior constitutes an n-dimensional space that is called Material Behavior Space (MBS) where each point represents a specific aspect of material behavior. In this approach, MBS is assumed to be defined by the following MFIM [128, 129]:

$$\frac{M_P}{M_{P_O}} = \prod_{i=1}^{N} A_i^{mi} \qquad \text{(C.2)}$$

$$\text{where } A_i = \left(1 - \frac{B}{B_O}\right)_i$$

where M_P is the property affected to be evaluated. M_{P_O} corresponds to the initial or reference material state or condition. A_i represents the *i*th factor that influences material behavior, and m_i is an exponent. B, on the other hand, represents a specific cause factor for behavior (for example, temperature), and B_O is the corresponding final value of the so called cause factor.

C.2. Residual Strength Degradation Approach

Residual strength of notched and unnotched laminates is determined by using a series of two-stage tests. In the first stage, a cyclic test is done in order to produce a desired condition in the test specimen. The condition could be exposure to a specific number of load cycles, a selected change in a stiffness component, a prescribed state or damage, or some condition related to a specific service application. The cyclic loading can be either uniform or non-uniform loading, but at the same time should be repeatable and well characterized for other tests which use in the residual strength series. At the end of the first-stage test, non-descriptive inspection of the specimen should be made in order to determine the damage in the material before the actual strength measurement [88].

The second stage in the procedure, on the other hand, is a monotonic load test, which can be tension or compression, to fracture the test specimen. In order to determine initial strength properties of the material the test is conducted in the same manner as monotonic

tests. Both stages, which are the initial strength tests and the residual strength tests, should be run at the loading rate used in the cyclic loading tests because of the load rate sensitivity of the properties of the composite [88].

Early models for residual strength were written in terms of initial strength, S_u, applied stress level, cycles, and various other parameters. The first model proposed in the literature was the so called wear-out model and takes the general from as the following [88]:

$$S_r^m = S_0^m - Af\left(\sigma^a\right)\left(n - n_0\right) \tag{C.3}$$

where S_r is the remaining strength, S_0 is the initial strength, f is a function of the applied cyclic stress, A and m are material constants, n is the total number of cycles of loading and n_0 is the initial number of cycles.

This model assumes that fatigue behavior of composites is controlled by a dominant crack, as in metal fatigue. However, a more applicable formulation of the wear-out approach for composites assumes that residual strength decreases with applied load cycles until the residual strength equals to the maximum applied stress and the composite material fractures. This new approach, a residual strength degradation model, can be written as the following [88]:

$$R^{\nu}(n_2) = R^{\nu}(n_1) - \frac{R^{\nu}(0) - \sigma^{\nu}}{R^{c}(0) - \sigma^{c}}(n_2 - n_1)KS^{b} \tag{C.4}$$

where $R(n_i)$ is the normalized strength (with respect to initial strength) of the composite at n_i cycles, σ is the normalized maximum cyclic stress, and S is the normalized cyclic stress range. In each case, the normalization factor is the characteristic value (B) of the two-parameter Weibull static ultimate strength distribution which has shape parameter, α. K and b are parameters in the power law representation of the cyclic stress-fatigue life curve. $KS^{b}\tilde{N} = 1$, where $\tilde{N}$ is the characteristic life of the three-parameter Weibull fatigue life distribution with shape parameter, α_f. The ratio of α/α_f is defined as c, and ν is a parameter which influences the rate of residual strength degradation for a given material.

With appropriate approximations and assumptions, Equation (C.4), can be reduced and can be written as the following [88]:

$$R^{c}(n_2) = R^{c}(n_1) - (n_2 - n_1)KS^{b} \tag{C.5}$$

C.3. Fracture Mechanics Approach

The crack-stopping ability of composites, which results from their inhomogeneity nature on a fine scale (the fibre/matrix interface) and on a gross scale (laminated structure) makes it difficult in many cases to apply a fracture mechanics approach to fatigue testing and design. The difficulty, on the other hand, is more prominent with unidirectional composites or laminates pressed from preimpregnated sheets of continuous and non-woven

fibres. Stress concentrating effects of holes and notches may be almost completely eliminated by large-scale splitting in the 0° and 45° plies and by delaminations between the plies, the net result often being disintegration of the composite. Owen et al. (2003) have shown that it is possible to use a fracture-mechanics approach, based on the Paris-Erdogan power law which is related to the crack growth rate, da/dN, to the range of stress intensity factor, ΔK, for some glass-reinforced plastic (GRP) laminates [65, 88]:

$$\frac{da}{dN} = A(\Delta K)^P \tag{C.6}$$

In order to overcome the problem of accurately defining crack length, a compliance calibration was used to determine an equivalent crack length, a procedure somewhat similar to that of using a plastic-or process-zone size correction when applying fracture mechanics to other materials. Underwood and Kendall [65] have also used a fracture-mechanics approach to study the growth of a damage zone during the fatigue of notched GRP laminates and Vancon et al. [65] have shown that fracture mechanics methods and the Paris power law are straightforwardly applicable for the very much simpler case of propogation of delamination cracks in multi-ply laminates. However, the number of situations where such an approach can be applied is very limited [65]

C.4. Damage Accumulation Approach

Studies which have been done on damage accumulation during cyclic loading attempted to obtain useful working relationships of the Miner's rule type, that might be used in design. According to these studies, although debonding did not itself cause reductions in strength, it did serve to initiate resin cracks which weakened the material. For resin cracking during fatigue, a non-linear damage law which is independent of stress level was proposed which gives the damage, Δ, as [92];

$$\Delta = \sum \left[A\left(\frac{n}{N}\right) + B\left(\frac{n}{N}\right)^2 \right] \tag{C.7}$$

where n is the number of cycles sustained by the composite at a stress level which would normally cause failure after N cycles, A and B are constants. Δ is equal to unity at failure.

Fong [92], on the other hand, proposed as alternative single-parameter stress-independent damage model in which the damage factor, Δ, was given by [92];

$$\Delta = \frac{\left(e^{kx} - 1\right)}{\left(e^{k} - 1\right)} \tag{C.8}$$

here for $k \approx 0$ and $0 \langle x \langle 1$, where k and x are constants which are determined from experimental data. This model implies that the rate of accumulation of damage, in other words, matrix cracking, $d\Delta/dt$, depends linearly on the non-logarithmic cycle ratio, t or n/N, as a first approximation. For different values of k this function generates a family of exponential curves.

C.5. A Finite Element Model Approach

There are very little Finite Element (FE) modeling for composite structures in the literature. This approach, on the other hand, is related to the Fracture Mechanics Approach. In other words, the basis of the method is first to use a fracture mechanics approach to obtain experimentally the relationship between the maximum strain energy release rate

experienced during a fatigue cycle and the rate of growth of the damage. For the beam, for instance, the latter was mainly matrix cracking, as determined by observations during a series of fatigue tests. The structure is then analyzed using FE analysis, the local stresses and strains around the critical region determined, the energy release rate calculated and then combined with the fracture mechanics data to give the lifetime of the structure, which is compared with experimental results [92].

The model as mentioned before is based on a combination of FE stress analysis and fracture mechanics. The FE analysis is used in order to get a detailed stress distribution in the structure when the structure subjected to a static load equal to the maximum load applied in the fatigue cycle. Then, the output is interrogated in order to indentify strains which are above a designated threshold, for matrix cracking for instance, and the elements and plies within the so called element in which these strains occur. The elastic properties in the damaged plies are then reduced and the analysis repeated. Then damage is identified and the process continued until final failure is indicated. Because in the experimental work, fibre fracture was identified as being the ultimate cause of failure, in the model fibre strains are monitored and when the ultimate fibre failure strain is reached, at any location, the analysis is lasted. At each iteration of the analysis the strain energy release rate, G, in the structure is calculated. Hence, at the conclusion of the analysis a relationship between G and damage area, A, is available. This information is then combined with fracture mechanics in the form of the Paris Law, and from this the lifetime is calculated [92].

For the beam, the lifetime can be written easily using an initial model based on the simple Paris-Erdogan law, ($dA/dN = DG_{\max}^{n}$), which has link with damage area, A,

number of cycles, N, and maximum strain energy release rate in a cycle, $G_{\max}$, via materials parameters, D and n as the following [88, 92]:

$$N_f = \int_0^{A_f} \frac{dA}{D[G(A)]^n} \tag{C.9}$$

where the final damage area, A_f, corresponds to fibre fracture.

In order to overcome the sensitivity of the initial model to values of n and D, a modified form was used [92]:

$$\frac{dA}{dN} = DG_{\max}^n \frac{\left[1-\left(\frac{G_{th}}{G_{\max}}\right)^{n_1}\right]}{\left[1-\left(\frac{G_{\max}}{G_c}\right)^{n_2}\right]} \tag{C.10}$$

where G_{th} is a threshold value of $G_{\max}$, below which no cracking occurs, and G_c is the critical value above which abrupt failure occurs. The terms n_1 and n_2 are additional materials parameters. The integration in order to get life time was performed numerically.

C.6. A Matrix Damage Model (Secant Modulus) Approach

The model which is a simple analysis developed to predict the decrease in laminate secant modulus caused by matrix damage starts with the matrix cycling plastically. The effective modulus is reduced for the portion of the matrix cycle that is in tension as cracks

develop due to plastic cycling. Hence, the model presents simple equations to approximate the effective matrix modulus due to cracking at an assumed cyclic strain range [88].

Assuming an ideally elastic-plastic matrix laminate, for the illustration of the model and simplicity, and a constant cyclic stress range or shakedown stress limit, ΔS, the axial stress in the matrix material in the loading direction at the shakedown stress limit, σ_{Sh}^{m}, can be written easily in terms of the shakedown stress range, ΔS_{Sh}, the shakedown strain range, δ_{Sh}^{m}, the undamaged laminate's elastic modules, E_0, and the matrix tensile elastic modulus, E_m, as the following [88]:

$$\sigma_{Sh}^{m} = \delta_{Sh}^{m} E_m = \left(\frac{\Delta S_{Sh}}{2E_0} \right) E_m \tag{C.11}$$

The overall laminate stress range, ΔS, can be calculated as follows [88]:

$$\Delta S = \left(\Delta \varepsilon_{comp}^{m} \right) E_0 + \left(\Delta \varepsilon - \Delta \varepsilon_{comp}^{m} \right) E_{SDS} \tag{C.12}$$

or

$$\begin{aligned} &\Delta S = E_{SDS} \Delta \varepsilon + \frac{1}{2} \Delta S_{Sh} \left(1 - \frac{E_{SDS}}{E_0} \right) && for\ \Delta S \rangle \Delta S_{Sh} \\ &\Delta S = E_0 \Delta \varepsilon && for\ \Delta S \langle \Delta S_{Sh} \end{aligned} \tag{C.13}$$

where

$$\Delta\varepsilon_{comp}^{m} = \frac{\Delta S_{Sh}}{2E_0} \tag{C.14}$$

$$E_{eff}^{m} = \frac{\sigma_{Sh}^{m}}{\Delta\varepsilon - \Delta\varepsilon_{comp}^{m}} \tag{C.15}$$

where $\Delta\varepsilon$ represents cyclic strain range, E_{eff}^{m} is effective tensile modulus of the matrix material, $\Delta\varepsilon_{comp}^{m}$ is the compressive strain range of the matrix, E_{SDS} is the so called modulus of elasticity of the laminate.

By selecting a number of different strain-range values, $\Delta\varepsilon$, the corresponding laminate stress range, ΔS, can be calculated and plotted versus $\Delta\varepsilon$. The laminate secant modulus, which is used the fatigue damage of the composite structure, is represented by the following equation [88]:

$$E_S = \Delta S / \Delta\varepsilon \tag{C.16}$$

C.7. Statistical Distribution Model Approach

In engineering applications, the static strength and fatigue life of composite laminates are important property parameters, which are usually statistical values and obtained from a mass of experiments. In order to reduce experiment time and costs, the relationship between static strength distribution and fatigue life distribution of composite materials has been studied [78].

Under cyclic load, the non-inverse structural changes will occur in the micro local field or macro structure of materials. These changes as a result produce the generalized monotonic decreasing characteristics of material $S-N$ curve, as shown in Figure (C.1). The failure probability of the specimen being subjected to N fatigue cycles for a given fatigue strength $\sigma^*_{\max}$ and the failure probability of the specimen being subjected to fatigue strength $\sigma_{\max}$ for a given fatigue life N^* are found as the same with the same confidence level. The failure probabilities for different assigned fatigue lives are also the same, because the $S-N$ curves of materials are derived from the test results with the same survival. In other words, the analytical and experimental investigations have shown that angle ply static failure coincides with first lamina fatigue failure of a laminate under cyclic loading [78, 130]. Because the difference between the first and last ply failure of a composite structure, in a fatigue sense, is of less importance, the failure probabilities of the static strength and the fatigue life for different fatigue load of composite structure can be accepted as the same [58, 78, 130].

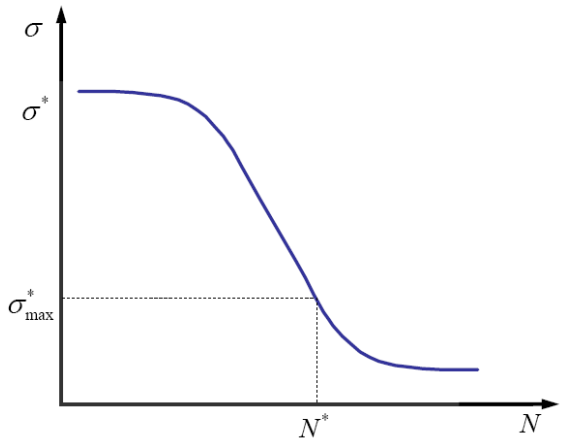

Figure C.1. Fatigue Life Curve [78].

The failure probabilities of the static strength σ^* and any fatigue life value N^* corresponding a given fatigue load $\sigma^*_{\max}$ are the same for the uniform confidence level and the same survival rate $S-N$ curve of composite laminates [78, 130]. A two-parameter Weibull distribution can be applied both to the statistical distribution of the static strength σ_{ult} [78] and to the experimental fatigue life data available in [72]. But it is reasonable to use directly the static strength of the composite laminates because of the lower cost.

A two-parameter Weibull statistical distribution of the static strength σ_{ult} can be expressed as [78];

$$F_{\sigma_{ult}}(X)=P\{\sigma_{ult}\le X\}=1-\left(-\left(\frac{X}{\beta}\right)^{\alpha}\right) \tag{C.17}$$

where $F_{\sigma_{ult}}(X)$ represents the failure probability when the specimen is subjected to a static load X; σ_{ult}, α, and β are the so called static strength, shape parameter, and scale parameter, respectively. The shape parameter, α, describes the failure mechanism of laminates. The scale parameter, β, also depends on the material concerned.

Fugiang et al. (2008) has mentioned a $S-N$ curve model of composite laminates as the following;

$$\frac{\sigma_{\max}}{\sigma_{ult}}=1+m\left(\exp\left(-\left(\frac{\log N}{b}\right)^{a}\right)-1\right) \tag{C.18}$$

In this expression, $\sigma_{\max}$ represents the maximum equaling stress and a, b, and m are constants defined by experiments. As a result, the failure probability of fatigue life of composite laminate can be expressed as [78];

$$F_N(n) = P\{N \le n\} = P\{\sigma_{ult} \le X\} \tag{C.19}$$

where $F_N(n)$ denotes the so called failure probability of the specimen being subject to n fatigue cycles. Combining Equations (C.18) and (C.19) together with Equation (C.17) yields;

$$F_N(n) = 1 - \exp\left(- \left(\frac{\sigma_{\max}}{\beta\left(1 + m\left(\exp\left(-\left(\frac{\log N}{b}\right)^{a}\right) - 1\right)\right)} \right)^{\alpha} \right) \tag{C.20}$$

Equation (C.20) represents the relationship between the static strength distribution and fatigue life distribution. Using this equation together with maximum stress value which can be obtained from FEA results, one can calculate roughly the probability of failure of a composite structure for a given fatigue life value. From the calculated results of three kinds of laminates experimental data, done by Fugiang et al. (2008), it has been concluded that the two-parameter Weibull function can be used to describe the statistical distribution and further to predict the distribution of fatigue life of composite laminates for different fatigue loading by the aid of Equation (C.20) [78, 130].

In Equation (C.20), as mentioned before, there are some parameters, e.g. a, b, m, α, and β, obtained experimentally. α, and β represent statistical distribution values of static strength. The values of α and β change between 25.099 - 43.357 and 14.441 – 88.787, respectively. The values of a, b, and m, on the other hand, represent $S-N$ curve values of laminates which again change between 1.212 - 2.216, 5.539 – 8.097, and 0.54 – 1.0, respectively [78]. The probabilistic fatigue failure of a composite structure can be done for the fatigue life value of 10^3 and 10^6 cycle, not more. Because the fatigue behavior of composite material structures is of a quite different nature than of metallic components for which the giga cycle fatigue regime is totally unknown [68].

APPENDIX D: FATIGUE LIFE PREDICTION MODELS FOR MONOLITHIC MATERIALS: SPOT WELD JOINTS

Over the past thirty years, many fatigue life prediction methods have been proposed. Several of most commonly referenced methods are briefly summarized in this section.

D.1. Local Strain-Based Approach

In local strain-based method, only first stage, that is crack initiation stage, is considered and after initiation of specimen, it is accepted that the specimen is deformed. Hence the first stage is important and considered in this method. In this method, the first stage is typically analyzed by a strain based approach and because of this the method is called as "Local Strain-Based Approach" [6].

Some experimental studies has been conducted using strain gages on the outer faces of specimens and relating that strains to the strains at the notches [2, 19]. The remote stress is related to the local stress and local strain found at the notch by [7, 20, 21].

$$\Delta\sigma.\Delta\varepsilon = \frac{\left(K_f\,\Delta S\right)^2}{E} \tag{D.1}$$

where E is modulus of elasticity, ΔS is remote applied stress, $\Delta\sigma$ is local stress at the notch, $\Delta\varepsilon$ is local strain at the notch, K_f is fatigue notch factor appropriate for the notch geometry.

Fatigue notch factor appropriate for the notch geometry is usually estimated using Peterson's equation;

$$K_f = 1 + \frac{K_t - 1}{1 + \frac{a}{r}} \tag{D.2}$$

where r is notch radius, $\underline{a}$ is material constant and K_t is elastic stress concentration factor.

In Equation (D.2), elastic stress concentration factor can be obtained by a finite element scheme. For tensile-shear spot-weld geometry, it is given by;

$$K_t = 1+\alpha \left(\frac{t}{r}\right)^{1/2} \tag{D.3}$$

where t is metal sheet thickness and α is a material constant.

The actual notch radius of a spot-weld connection is not very well defined. It is assumed that the radius has no specific value, so the worst possible value for a notch radius is used. Extreme for K_f can be found by finding where its derivative with respect to notch radius, *r*, goes to zero. This is a maximum and is given as $K_f^{\max}$ [20];

$$K_f^{\max} = 1+\frac{\alpha}{2} \left(\frac{t}{\underline{a}}\right)^{1/2} \tag{D.4}$$

The initiation life is estimated by modifying the empirical Basquin relationship with the Morrow mean stress correction, which is given as follows [1];

$$\sigma_a = \left(\sigma_f^{'} - \sigma_m\right)\left[2N_I\right]^b \tag{D.5}$$

where N_I is the number of cycles to crack initiation, σ_a is local stress amplitude, σ_m is mean stress, $\sigma_f^{'}$ is fatigue strength constant and b is fatigue strength exponent.

The Basquin relationship is modified by expressing the stress amplitude in terms of applied stress and the fatigue notch factor. Hence the modified Basquin relationship is; [1].

$$\frac{\Delta S}{2} K_f = \left(\sigma_f^{'} - \sigma_m\right)\left[2N_I\right]^b \tag{D.6}$$

As a result, the life of a specimen can be written as;

$$N_I = \frac{1}{2}\sqrt[b]{\frac{\Delta S.K_f}{2\left(\sigma_f^{'} - \sigma_m\right)}} \tag{D.7}$$

Choosing the constants for this empirical equation may be troublesome. Some effort should be made to obtain the constants for the heat affected zone (HAZ), which is where cracks are found. Furthermore, Peterson's equation, Equation (D.3), may not be valid for an arbitrarily small notch radius [22]. Peterson himself warned that his equation was only intended for machined notches with a finite radius whose depth was not much greater that the notch radius [23]. As a notch becomes smaller, the fatigue notch factor, K_f, should increase because the notch is approaching the geometry of a sharp crack. It seems unreasonable to expect a vanishingly small notch radius to produce a longer life than a larger notch radius for the same loading conditions [7].

D.2. Linear Fracture Mechanics Approach

In 1985, Cooper and Smith developed a direct current electric potential difference (PD) method to measure crack growth. They monitored the crack growth in mild steel spot welded joints and concluded that the predominant fatigue mechanism in spot welds is crack propagation [10]. Because of this, this method is sometimes named as "Fatigue Crack Growth Approach".

The linear fracture mechanics approach, that was introduced firstly by Pook in 1975 and then used by Cooper and Smith in 1986, assumes that the notch root is a sharp crack,

and the crack propagation process starts immediately from the existing crack. Most scientists that try to quantify crack extension use a form of the Paris power law to estimate the fatigue life of spot welds, which is of the following form [17, 28-33].

$$\frac{da}{dN} = C\left(\Delta K\right)^n \tag{D.8}$$

where a is crack length, N is the so called fatigue life of the specimen in terms of number of cycle, ΔK is range of stress intensity factor, C is a material constant which depend also on the load ratio of R and n is another material constant.

The stress intensity factors, which is approximate opening mode, K_I , and edge sliding mode, K_{II}, stress intensity factors of point near to the notch cracks for tensile shear (TS) specimens, for example, were given by Pook (1975) [17]. Pook conducted a study using the configurations and at the end of his studies, he proposed the following formulas [17].

For a single spot welded Tensile Shear (TS) specimen with the ratio of spot weld radius to metal sheet thickness ($r/t \le 10$);

$$\begin{aligned} K_I &= \left[\frac{P}{r^{3/2}}\right]\left[0.341\ \left(\frac{r}{t}\right)^{0.397}\right] \\ K_{II} &= \left[\frac{P}{r^{3/2}}\right]\left[0.282 + 0.162\left(\frac{r}{t}\right)^{0.710}\right] \end{aligned} \tag{D.9}$$

For two spot welds in line with centers at least three spot diameter apart and ($1.92 \le r/t \le 10$);

$$K_I = \left[\frac{P}{r^{3/2}}\right]\left[0.282\left(\frac{r}{t}\right)^{0.397} + 0.846\left(\frac{t}{r}\right)\right]$$
$$K_{II} = \left[\frac{P}{r^{3/2}}\right]\left[0.282 + 0.162\left(\frac{r}{t}\right)^{0.710}\right] \quad \text{(D.10)}$$

where K_I and K_{II} are Mode I (opening) and Mode II (sliding) types stress intensity factors, respectively, P is the applied load per spot weld, r and t are the spot weld radius and metal sheet thickness, respectively.

The edge of a spot weld must be at least one spot diameter apart from a plate edge [24].

It is assumed that a crack in a spot-weld, at the failure location, can be modeled as a planar crack. This approximation becomes valid as the ratio t/r is decreased [33]. For the typical welds, cracks grow from the interface of the two steel sheets at the edge of the weld, in a shape similar to a semi-ellipse, but curved slightly out of plane to give it a "thumbnail shape" [33]. If the weld radius is large compared to the sheet thickness, this thumbnail cracks is nearly planar. Although not truly two-dimensional, this crack can be described by a single degree of freedom. Thus Equation (D.9) is used for this single-degree-of-freedom model for a single spot weld, for example [33].

Now that this spot-weld model has been reduced to a single degree of freedom, fatigue life is modeled as starting from a two-dimensional crack, which exists initially under both Mode-I and Mode-II loading. If we assume that the crack propagates perpendicular to the direction of the maximum normal stress at the crack tip, it will initially grow at an angle, θ_0 This angle satisfies Equation (D.11), where K_I and K_{II} are the stress intensity factors initially acting to a point near the spot weld before crack growth occurs [33]. This equation is obtained by combining well-known crack-tip singularity stress field equations for Mode-I and Mode-II stress intensity factors, and finding the principal stress directions. Note that Equation (D.11) is valid only in the case where tearing mode stress intensity factor, K_{III}, is zero [33].

$$K_I \sin\theta_0 = K_{II}\left(3\cos\theta_0 - 1\right) \tag{D.11}$$

where θ_0 is angle of crack growth.

It has been noted in the literature that the crack growth rate in spot-welds remains nearly constant as the test proceeds for constant amplitude loading and for a small ratio of t/r [10]. This suggests that the stress intensity factor also remains nearly constant. On the other hand, these assumptions are not valid for thick sheets and for small welds [34, 36].

Since the stress intensity factor is assumed to be constant according to Newman and Dowling, crack growth angle, θ_0 also remains constant through the test [33]. After solving for θ_0, an effective Mode-I stress intensity factor needs to be calculated in order to calculate fatigue life of desired specimen. This was obtained using equations for stress around large two-dimensional cracks subject to Mode-I and Mode-II loading with an infinitesimally small kinked crack growing from the original crack tip at an angle [7, 35]. The infinitesimal kink is assumed not to disturb the original stress field. The small kink grows in principal stress directions, so no local Mode-II loading exists at the kinked crack tip. The local Mode-I stress intensity factor, acting on the infinitesimal kinked crack, is given in Equation (D.12), and is obtained by examining the principal normal stresses acting on this new kinked crack tip. This is the formulation for effective Mode-I stress intensity factor used for tensile shear (TS) specimen, for example.

$$\Delta K = \frac{\Delta K_I}{4}\left[3\cos\frac{\theta_0}{2} + \cos\frac{3\theta_0}{2}\right] - \frac{\Delta K_{II}}{4}\left[3\sin\frac{\theta_0}{2} + 3\sin\frac{3\theta_0}{2}\right] \tag{D.12}$$

where ΔK is range of stress intensity factors in general, ΔK_I and ΔK_{II} are ranges of opening and sliding modes stress intensity factors, respectively.

In addition to this formula, a Paris-Erdogan crack growth relation, with an adjustment for the R-ratio effect as suggested by Walker (2003), is assumed to describe

crack growth, as in Equation (D.13). Hence, this so called equation is intended only for pure Mode-I loading.

$$\frac{da}{dN} = C\left[\frac{\Delta K}{(1-R)^{(1-\gamma)}}\right]^m \tag{D.13}$$

where C, m and γ are material constants, R is load or stress ratio and also used for stress intensity ratio.

Because both Mode-II and Mode-III loading is not present at the small kinked crack of length *a*, Equation (D.14) can be used in tensile shear (TS) and modified tensile shear (MTS) models. The so called crack grows a distance $a_f = t/\sin\theta_0$ before penetrating the outer surface of the plate. If we consider the crack growth as constant, then Equation (D.13) can be integrated to obtain an equation for fatigue life for this model, Equation (D.14) [33]

$$N_f = \frac{t}{C\sin\theta_0}\left[\frac{\Delta K}{(1-R)^{(1-\gamma)}}\right]^{-m} \tag{D.14}$$

where a_f is crack length at failure and N_f is the cyclic fatigue life of specimen to some degree of failure (here to propagate degree).

Finally, using Equations (D.12) and (D.14) together, Newman and Dowling expressed fatigue life explicitly for any known crack growth angle, θ_0. In these formulas, it is not forgotten that the so called crack growth angle must be known. Hence in order to calculate a proper angle, Equation (D.11) must first be solved for θ_0 using Equations (D.9) and (D.10) for calculating opening and sliding stress intensity factors respectively. As a result, the desired single-degree-of-freedom approximation for fatigue life in this method can be given by Equation (D.15) [33].

$$N_f = \frac{t}{C \sin\theta_0} \left[\frac{\Delta K_I \left[3\cos\frac{\theta_0}{2} + \cos\frac{3\theta_0}{2} \right] - \Delta K_{II} \left[3\sin\frac{\theta_0}{2} + 3\sin\frac{3\theta_0}{2} \right]}{4(1-R)^{(1-\gamma)}} \right]^{-m} \quad \text{(D.14)}$$

D.3. Nugget Deformation Approach

Scientists that work in this field focus on a better understanding of spot-weld fatigue behavior because of changes in automotive designs. In other words, the changes in automotive designs make the fatigue behavior of spot welds one of the primary parameters that governs the safety and reliability of automobiles. Fatigue behavior of spot welds under both constant amplitude load and variable-amplitude load fluctuations is essential to the development of accurate prediction methods of fatigue lives for automobile components [37].

Some scientists have used “Nugget Deformation Method” in order to find the fatigue lives of spot welded specimens. According to Davidson, Imhof, and Barsom , the life of spot weld connections depend on the stiffness of the spot-welded joint [37], in addition to the load level which are applied to the sheets, the metal thicknesses that are used manufacturing steel sheets, the nugget type and diameter, etc. Hence it can be said that the stiffer joints exhibit longer fatigue lives according to these investigators. In “Nugget Deformation Method”, using with simple relations in a design environment, load level or sheet metal thickness for a required fatigue life of specimen can also be found in addition to fatigue life of specimen for a required load level or sheet metal thickness. The less separation (angular rotation, $\Delta\theta_S$) that occurs between the overlapped portions of spot-welded sheets during tensile-shear loading (due to eccentric loading) is dependent on the stiffness of the joint. The angular-rotation parameter, $\Delta\theta_S$, shown in Figure D.1, describes the fatigue life of specimens that loaded tensely, regardless of joint characteristics, because the angular-rotation parameter, $\Delta\theta_S$, is related to the stress-intensity range, ΔK, a fracture-mechanics parameter that is used to describe fatigue crack-growth as shown in Figure D.1.

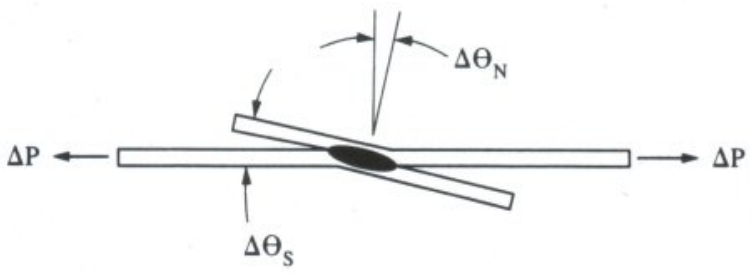

Figure D.1. Side view of a spot-weld connection under tensile-shear loading [38]

The angular rotation, $\Delta\theta_S$ which occurs during fatigue loading of spot-welded connections, is related to the crack-tip opening displacement (CTOD) at the edge of the spot weld. Naturally for a spot-welded specimen and known elastic modulus, the CTOD dependent mostly on the angular rotation, $\Delta\theta_S$ [38]. However, measuring displacement near the edge of the spot weld in order to calculate the angular rotation is extremely difficult. Because of this difficulty, instead of the angular rotation, the nugget rotation, $\Delta\theta_N$, shown in Figure D.1, is measured and used because the nugget rotation is a more convenient variable to measure. The nugget rotation can be used using with finite element analysis [28, 38].After this step, using the nugget rotation, the angular rotation can be found easily because there is a relation between these two variables [38].

In 1985, Barsom and Imhof demonstrated that the driving force for fatigue crack growth of spot-welded sheet is given as the following type [28].

$$\Delta E = \frac{\Delta P \ \ \Delta\theta_N^{1/2}}{t} \tag{D.15}$$

where; ΔE is the driving force for fatigue crack growth, ΔP is fatigue load range, θ_N is the nugget rotation of spot welded specimen, t is metal sheet thickness.

In this formula, the driving force for fatigue crack growth of as-welded sheet, ΔE, is a measure of the cyclic energy and generally this formula is valid for tensile shear (TS) specimens [3]. Finally, it was shown that the fatigue life in cycles to failure can be related

to the driving force for fatigue crack growth, ΔE, by the simple power function as the following type [38].

$$N_f = C\left(\Delta E\right)^m \tag{D.16}$$

where m and C are material constants, spot weld fatigue life exponent and coefficient, respectively, N_f is fatigue life of the specimen in terms of cycles.

D4. Combined Initiation and Propagation Method

In this method, both crack initiation and crack propagation were taken into consideration and related equations were obtained. For example, McMachon and Lawrence proposed a combined initiation and propagation approach that took into consideration the initiation and propagation stages of the fatigue behavior of spot welded specimen together in 1985. Hence, the fatigue life of spot welds was treated as the sum of crack initiation life and propagation life [3].

The first part of the life estimation, which is the crack initiation life estimation, according to "Combined Initiation and Propagation Method" was similar to "Local Notch Strain Method", that is;

$$N_i = N_I = \frac{1}{2}\sqrt[b]{\frac{\Delta S.K_f}{2\left(\sigma_f^{'} - \sigma_m\right)}} \tag{D.17}$$

where N_i is initiation part of the total life, initiation life.

In calculation of fatigue notch factor appropriate for the notch geometry, K_f, we used elastic stress concentration factor, K_t, in "Local Notch Strain Method" and some formulas for both fatigue notch factor and elastic stress concentration factor were proposed in that method, but in 1984, Wang proposed a different elastic stress concentration factor

for simplicity for tensile shear (TS) specimen used in McMahon and Lawrence's work, that is "Combined Initiation and Propagation Method". This stress concentration factor is given as follows;

$$K_t = \frac{W\,t}{(\pi\,r)^{1/2}\,D^{3/2}}\left[1.61\left(\frac{D}{t}\right)^{0.397} + 0.593 + 0.34\left(\frac{D}{t}\right)^{0.710}\right] \tag{D.18}$$

where W is width of the metal sheet, D is diameter of the spot weld.

In addition to Equation (D.17), McMachon and Lawrence by using Basquin's equation derived a different equation for the initiation life of spot-welded tensile shear specimens as follows [3];

$$\int_1^{2N_I}\left[\left(\frac{\sigma'_f}{\frac{\Delta\sigma}{2}}\right)\left(1-\sigma_0\,\frac{(2N)^k}{\sigma'_f}\right)\right]^{1/b} dN = 1 \tag{D.19}$$

where N_I is cycles to crack initiation used in the Basquin relation, portion of life devoted to creating a crack length, a_i; σ'_f is a material constant used in Basquin relation, also called as fatigue strength coefficient; $\Delta\sigma$ is range of stress locally; b is material constant used in the Basquin relation, also called as fatigue strength exponent; k is mean stress relaxation exponent; σ_0 is mean stress.

The second part of the life estimation, that is the crack propagation life estimation, was derived by integration of the well-known Paris-Erdogan law, that is;

$$N_P = \frac{1}{C}\int_{a_i}^{a_f}\Delta K^{-m}\,da \tag{D.20}$$

where a_i and a_f are initial and final crack lengths, respectively; N_P is portion of life devoted to creating a crack length of $a_f - a_i$, the propagation (second part) life of the specimen.

In Equation (D.20), the stress intensity factor is an equivalent parameter given as;

$$K = \sqrt{K_I^2 + \beta K_{II}^2} \tag{D.21}$$

where β is a constant that is determined from tests.

As a result, the fatigue life of spot-welded specimen in this method can be obtained by adding these two steps results to each other, that is;

$$N_f = N_i + N_P \tag{D.22}$$

$$N_f = \frac{1}{2} \sqrt[b]{\frac{\Delta S.K_f}{2\left(\sigma_f^{'} - \sigma_m\right)}} + \frac{1}{C} \int_{a_i}^{a_f} \Delta K^{-m}\, da \tag{D.23}$$

D5. Structural Stress Method

The structural or hot-spot stress approach, sometimes also called geometric stress approach, considers the stress increase due to the structural configuration or in other words, the macro-geometry [39]. In other words, structural stress method proposes that fatigue behavior can be described by the nominal stress in the sheet in the radial direction (with respect to the spot), and then calculated from the overall loadings at the spot itself [8]. For example for a spot welded specimen, because of the geometric complexity and hence difficulty of stress distribution in spot welds, the structural (nominal) stress at a distance of half the diameter of the weld nugget from the center of the weld is taken into consideration and is accepted that the structural stress is related to the fatigue life of the spot welds. As a

result, the stresses (membrane type and bending type) at that point are calculated using some constants and formulas and considered for the life of the specimen

Structural Stress Method was used firstly in the late 1980s and early 1990s [3]. The leading researchers that dealt with this approach are Sheppard, Radaj, Rupp and Henrysson. There are, of course, similarities and differences between the different models of structural stress that proposed by different scientists [3].

D.5.1. Sheppard's Structural Stress Method

According to Sheppard's Structural Stress Approach, for fatigue life estimation the structural stress at a distance of half the diameter of the weld nugget from the center of a weld is related to the fatigue life of spot welds. Hence, the fatigue failure in this method can be defined as crack initiation and growth through the sheet thickness. Sheppard and Strange developed a general equation for structural stress in 1992 as the following type [3];

$$\Delta S_{ij} = \frac{\Delta P_{ij}}{w t_i} + \frac{6\Delta M^*_{ij}}{t_i^2 \beta_s} \quad i, j = 1,2 \tag{D.24}$$

where ΔP_{ij} and ΔM^*_{ij} are membrane load and moment ranges at the edge of the nugget respectively; w is effective width [defined as $\frac{\pi D}{3}$ (based on the work by Wang)]; t_i, D and β_s are thickness, diameter and width of the sheet, respectively; ΔS_{ij} are structural stress components; i and j are subscripts refer to the sheet (first and second) and the side of the nugget edge, respectively.

A refinement of Equation (D.24) was given by Sheppard (1992), in which the effect of a "cupping" deformation mode that results from a transverse load applied to the sheet was included as being following Equation (D.25) [3];

$$\Delta S_{ij} = \frac{\Delta P_{ij}}{wt_i} + \frac{6\Delta M_{ij}^{*}}{t_i^2 \beta_s} + \frac{\Delta P_{Ai}}{t_i^2} \quad i, j = 1,2 \tag{D.25}$$

where ΔP_{Ai} are axial load ranges in the nugget.

The subject of whether or not there is an initiation and early crack growth stage has been debated in the past and remains unsettled. For example, using electrical-potential drop method in order to measure the crack growth, Cooper and Smith showed that fatigue in a spot weld joint is a pure crack propagation process, as we mentioned in Linear Fracture Mechanics Method, which means that there was no crack initiation stage observed at all. In addition to this, Cooper and Smith also observed that the crack propagation rate of the spot weld fatigue crack remains constant during the crack propagation process. Using the same electrical-potential drop method, however, Swellam and Lawrence found that there was a finite amount of fatigue life that was attributed to the crack initiation in 1992 [3].

Nevertheless, Sheppard and Strange argued that the early crack growth period is not described by linear elastic fracture mechanics method (LEFM), because according to Sheppard and Strange, LEFM typically breaks down when the crack is less than 5-10 times the grain size (the average size of a grain in HAZ was 20 μm). As a result, using the structural stress idea, Sheppard and Strange developed a specimen independent model in order to predict the fatigue life of a crack initiation and early crack growth to a crack length of 0.25 mm in resistance spot weld. Sheppard and Strange using Neuber's rule and cyclic Ramberg-Osgood materials law, the maximum local stress, $\sigma_{\max}$, and strain, $\varepsilon_{\max}$, values were defined as the following [3];

$$\frac{\left(K_f \left[\max S_{ij_{peak}}\right] + \sigma_{rs}\right)^2}{E} = \sigma_{\max}\varepsilon_{\max} \tag{D.26}$$

$$\varepsilon_{\max} = \frac{\sigma_{\max}}{E} + 2\left(\frac{\sigma_{\max}}{2K'}\right)^{1/n'} \tag{D.26}$$

where $\max S_{ij_{peak}}$ are maximum structural stress values at the peak load of a loading cycle; $\sigma_{\max}$ and $\varepsilon_{\max}$ are maximum local stress and strain, respectively; K_f is fatigue notch factor; K' is cyclic strength coefficient; n' is cyclic strain hardening exponent and σ_{rs} is residual stress.

Using these formulas, Sheppard and Strange estimated the fatigue life for a crack to initiate and grow to a length of 0.25 mm in HSLA spot weld joints. The equation was given as [3];

$$2N_i = \left(\frac{0.5\Delta\sigma_{\max}}{\sigma'_f - \sigma_m} \right)^{1/s} \tag{D.26}$$

where N_i is fatigue life of crack initiation and early growth; s is fatigue strength exponent determined experimentally; σ_m is stress amplitude defined as ($\sigma_m = \sigma_{\max} - 0.5\Delta\sigma_{\max}$) and σ'_f is another material property which also known as fatigue strength coefficient.

Here the most important point is that the early crack growth considered by Sheppard and Strange represents the crack growth to a length of approximately 0.25 mm.

In addition to this formula, that is the formula of fatigue life of crack initiation and early growth, Sheppard, in 1993, extended the early crack growth work and developed a model to use the structural stress to estimate fatigue life solely in terms of propagation. And the resulting formula was proposed by her as the following type [3];

$$\begin{aligned} &N_p = A_2 \left(\Delta S_T + \Delta S_B \right)^{-s} \\ &\textit{where} \\ &A_2 = \frac{2 \quad a_0^{(-s+2)/2}}{(s-1) C \pi^{s/2}} \end{aligned} \tag{D.27}$$

where a_0 is crack length at which initiation ends and crack propagation begins; N_p is total life spent propagation the crack through the sheet thickness; ΔS_T is nominal membrane stress range and is equal to the $\Delta P / wt$ term; ΔS_B is the bending stress range and is equal to the $6\Delta M / \beta t^2$.

Sheppard further refined the structural stress method for fatigue life prediction in order to include the stress ratio effect as the following type;

$$\frac{N_p}{1-R} = A_2 \left(\Delta S_{\max}\right)^{-s} \tag{D.28}$$

where A_2 is material constant and is the same as defined in Equation (D.27); $\Delta S_{\max}$ is the structural stress range that is defined as $\Delta S_{\max} = \max\left\{\Delta S_{11}, \Delta S_{12}, \Delta S_{21}, \Delta S_{22}\right\}$.

Finally, the total life, N_t, in Sheppard's work defines as the sum of the number of cycles for a crack to initiate, N_i, and grow through the sheet thickness, N_p.

D.5.2. Radaj's Structural Stress Method

In 1989, Radaj defined the meaning of structural stress term. According to him, there are three important parameters at the region around a spot weld nugget and these are structural stress, notch stress and stress intensity factor. Radaj explained these three terms as the following expressions [3].

- Structural stress is the stress linearly distributed over the sheet thickness with the singularity at the spot weld edge being completely suppressed.
- The notch stress is the stress at the slit edge of the spot weld with a fictitious radius of $\rho_f \approx 0.25$ mm. The slit is assumed to be an ideal slit (i.e. there is no gap between the two plates). The notch stress equals the product of the nominal structural stress and a stress concentration factor.

- The third important parameter according to Radaj is stress intensity factor. What is more is that the crack initiation and crack propagation at the weld spot edge are controlled not by the structural stress but by the stress intensity factor at the end of the slit.

Radaj showed that the stress intensity factors at the end of the slit of spot weld edge (not the crack in the through-thickness direction) are related to the structural stress by;

$$\begin{aligned} K_I &= 0.15\left(\sigma_{ti} - \sigma_{to} + \sigma_{bi} - \sigma_{bo}\right)\sqrt{t} \\ K_{II} &= 0.25\left(\sigma_{ti} - \sigma_{bi}\right)\sqrt{t} \\ K_{III} &= 0.71\left(\tau_{ti} - \tau_{bi}\right)\sqrt{t} \end{aligned} \tag{D.29}$$

where σ is nominal structural stress (tensile stress); τ is nominal structural stress (shearing stress); t is the metal sheet thickness; subscripts t and b represent top and bottom plate, respectively; subscripts i and o are represent inner and outer surfaces of the plate, respectively.

Radaj (1990) gave expressions for structural stress in terms of "running-through" tensile force, F', and "running-through" bending moment, M'_b. F' and M'_b are the element forces at the spot weld nodal point of the considered plate. Hence;

- The structural stress for the case with "running-through" tensile force is:

$$\sigma_{ns} = 1.54\frac{F'}{wt} \tag{D.30}$$

where σ_{ns} is nominal structural stress; t and w are metal sheet thickness and width, respectively.

- The structural stress for the case with "running-through" bending moment is:

$$\sigma_{ns} = 9.244\frac{M'}{wt^2} \tag{D.31}$$

The "running through" tensile force, F', and "running through" bending moment, M_b', in Radaj's equations are equivalent to the membrane load at the edge of the nugget, P_{ij}, and bending moment, M_{ij}, in Sheppard's work.

In conclusion, the major differences between the Radaj's and Sheppard's approaches can be summarized as follows:

- Sheppard assumed that the crack is the through-thickness crack while Radaj assumed that the crack is the edge slit.
- Although the conceptual definitions of structural stress in these two different approaches are the same, the mathematical representations between the various loads are different, as shown in Equations (D.20) and (D.31) respectively.

D.5.3. Rupp's Structural Stress Method

In 1995, Rupp and Grubisic also proposed a structural stress formula that is similar to Equation (D.20). In Rupp's equations, an empirical stress correction factor, $K = 0.6\sqrt{t}$, is multiplied by the bending and tension terms. Hence, Rupp's structural stress equations are:

$$\begin{aligned}
\sigma_{r,\max} &= \frac{F_{x,y}}{\pi \quad D \quad t_j} \\
\sigma_r &= K \quad 1.744\frac{F_z}{t^2} \\
\sigma_{r,\max} &= K \quad 1.872\frac{M_{x,y}}{D \quad t^2}
\end{aligned} \tag{D.32}$$

where $F_{x,y}, F_z, M_{x,y}$ are force and moments terms.

D.5.4. Henrysson's Structural Stress Method

Henrysson and Akerson, in 1996, used Rupp's structure stress formula in order to predict the fatigue life of spot welds specifically for H-shape and tensile shear specimens. At the end of his studies, Henrysson showed that Rupp's equations need to be modified by a set of modification factors:

$$\begin{aligned}
\sigma_{\max}\left(V_i\right) &= \frac{V_i}{\pi \quad D \quad t_j} Factor_V \\
\sigma\left(F_z\right) &= K_j \quad 1.744 \frac{F_z}{t^2} Factor_F \\
\sigma\left(M_{ij}\right) &= K_j \quad 1.872 \frac{M_{ij}}{D \quad t^2} Factor_M
\end{aligned} \tag{D.33}$$

where $Factor_V, Factor_F, Factor_M$ are corrections factors and K_j is empirical stress correction factor.

The correction factors $Factor_V$=2, $Factor_F$=0.5 and $Factor_M$=1 were obtained from fatigue tests. In addition to these values, the definition of V_i in Henrysson's work is the same as $F_{x,y}$ in Rupp's equation. Here, there is an interesting point that the stress results for the H-shape specimens and tensile shear specimens from Equation (D.33) that was proposed by Henrsson and Akerson are similar to those obtained by using Equation (D.20) that was proposed by Sheppard et al (1992).

REFERENCES

1. Thornton, P. H., A. R. Krause and R. G. Davies, "The Aluminum spot weld", *Welding Journal*, Vol. 75, No. 3, pp. 101s-108s, 1996.

2. Pollard, B., "Fatigue strength of spot welds in Titanium-bearing HSLA steels", SAE International Congress and Exposition, Michigan, 1982.

3. Barkey, M. E., H. Kang, and Y. L. Lee, "Failure modes of single resistance spot welded joints subjected to combined fatigue loading", *International Journal of Materials and Product Technology*, Vol. 16, No. 6/7, pp. 510-527, 2001.

4. Rathbun, R. W., D. K. Matlock, and J. G. Speer, "Fatigue behavior of spot-welded high-strength sheet steels", *Welding Journal*, Vol. 82, No. 8, pp. 207s-218s, 2003.

5. Chao, Y. J., "Failure mode of spot welds: interfacial versus pullout", *Science and Technology of Welding and Joining*, Vol. 8, No. 2, pp. 133-137, 2003.

6. Deng, X., W. Chen, and G. Shi., "Three-dimensional finite element analysis of the mechanical behavior of spot welds", *Finite Elements in Analysis and Design*, Vol. 35, No. 1, pp. 17-39, 2000.

7. Nam, H. W., W. Hwang and K. S. Han, "Stacking sequence design of fiber-metal laminate for maximum strength", *Journal of Composite Materials*, Vol. 35, No. 18, pp. 1654-1683, 2001.

8. Kang, J. H. and C. G. Kim, "Minimum-weight design of compressively loaded composite plates and stiffened panels for post buckling strength by genetic algorithm", *Composite Structures*, Vol. 69, pp. 239-246, 2005.

9. Chao, Y. J., "Ultimate strength and failure mechanism of resistance spot weld subjected to tensile, shear, or combined tensile/shear loads", *Journal of Engineering Materials and Technology*, Vol. 125, No. 2, pp. 125-132, 2003.

10. Linder, J., and A. Melander, "Fatigue strength of spot welded stainless sheet steels exposed to 3 % NaCl solution", *International Journal of Fatigue*, Vol. 20, No. 5, pp. 383-388, 1998.

11. Henrysson, H. F., "Fatigue life prediction of spot welds using coarse FE meshes", *Fatigue & Fracture of Engineering Materials & Structures*, Vol. 23, No. 9, pp. 737-746, 2000.

12. Di Fant-Jaeckels, H. and A. Galtier, "Fatigue lifetime prediction model for spot welded structures", *La Revue de Metallurgie-CIT*. pp. 83-95, 2000.

13. Xu, S. and X. Deng, "An evaluation of simplified finite element models for spot welded joints", *Finite Elements in Analysis and Design*, Vol. 40, No. 9-10, 2004.

14. Wonseok, J., D. Bae and I. Sohn, "Fatigue design of various type spot welded lap joints using the maximum stress", *KSME International Journal*, Vol. 18, No. 1, pp. 106-113, 2004.

15. Sheppard, S. D. and M. Strange, "Fatigue life estimation in resistance spot welds: initiation and early growth phase", *Fatigue & Fracture of Engineering Material & Structures*, Vol. 15, No. 6, pp. 531-549, 1992.

16. Radaj, D., "Theory of forces and stresses in spot welded overlap joints", *Archive of Applied Mechanics*, Vol. 67, pp. 22-34, 1996.

17. Pook, L. P., "Fracture mechanics analysis of the fatigue behavior of spot welds", *International Journal of Fracture*, Vol. 2, pp. 173-176, 1975.

18. Sadagopan, D. and R. Pitchumani, "Application of genetic algorithms to optimal tailoring of composite materials", *Composite Science and Technology*, Vol. 58, pp. 571-589, 1998.

19. Pan N., "Fatigue life study of spot welds", PhD. Thesis, Stanford University, 2000.

20. Kan, Y. R., "Fatigue resistance of spot welds - an analytical study", *Metals Engineering Quarterly*, pp. 26-36, 1976.

21. Gero, B. M., "Acousto-ultrasonic evaluation of cyclic fatigue of spot welded structures", M.Sc. Thesis, Virginia Polytechnic Institute and State University, 1997.

22. Ertaş, A. H., "Fatigue behavior of spot welds", M. Sc. Thesis, Boğaziçi University, 2004.

23. El-Sayed, M. E. M. and E. H. Lund, "Structural optimization with fatigue life constraints", *Engineering Fracture Mechanics*, Vol. 37, No. 6, pp. 1149-1156, 1990.

24. Davidson, J. A., "A review of the fatigue properties of spot-welded sheet steels", *SAE International Congress and Exposition*, Michigan, 1982.

25. Puchner, K., H. Dannbauer and M. Meise, "Spot weld optimization regarding stiffness and fatigue using standard software", *SAE Technical paper*, No. 1247, 2006.

26. Adib, H., J. Gilbert and G. Pluvinage, "Fatigue life duration prediction for welded spots by volumetric method, *International Journal of Fatigue*, Vol. 26, pp.81-94, 2004.

27. Hou, Z., Y. Wang, C. Li and C. Chen, "An analysis of resistance spot welding, *Welding Journal*, Vol. 85, No. 3, pp. 36-40, 2006.

28. Socie, D. F., "Fatigue-life prediction using local stress-strain concepts, *Engineering Mechanics*, Vol. 17, No. 2, pp. 50-56, 1977.

29. Zhang, Y., and D. Taylor, "Optimization of spot-welded structures", *Finite Elements in Analysis and Design*, Vol. 37, pp. 1013-1022, 2001.

30. Peeker, E., and E. Niemi, "Fatigue crack propagation model based on a local strain approach", *Journal of Constructional Steel Research*, Vol. 49, pp. 139-155, 1999.

31. Roessle, M. L., and A. Fatemi, "Strain-controlled fatigue properties of steels and some simple approximations", *International Journal of Fatigue*, Vol. 22, pp. 495-511, 2000.

32. Roessle, M. L., A. Fatemi and A. K. Khosrovaneh, "Variation in cyclic deformation and strain-controlled fatigue properties using different curve fitting and measurement techniques", *SAE International Congress and Exposition*, Michigan, 1999.

33. Cooper, J. F. and R. A. Smith, "The measurement of fatigue cracks at spot welds", *International Journal of Fatigue*, Vol. 3, pp. 137-140, 1985.

34. Davidson, J. A. and E. J. Imhof, "A fracture mechanics and system-stiffness approach to fatigue performance of spot-welded sheet steels, *SAE International Congress and Exposition*, Michigan, 1983.

35. Newman, J. A. and N. E. Dowling. "A crack growth approach to life prediction of spot-welded lap joints", *Fatigue & Fracture of Engineering Materials & Structures*, Vol. 21, pp. 1123-1132, 1998.

36. Stephens, R. I., A. Fatemi, R. R. Stephens and H. O. Fuchs, *Metal Fatigue in Engineering*, John Wiley & Sons, ISBN 0-471-51059-9, 2000.

37. Suresh, S., *Fatigue of Materials*, Cambridge: Cambridge University Press, 2004.

38. Cui, W., "A state of the art review on fatigue life prediction methods for metal structure", *Journal of Marine Science and Technology*, Vol. 17, pp. 43-56, 2002.

39. Schijve, J., *Fatigue of Structures and Materials*, John Wiley & Sons, ISBN 0-471-51059-9, 2001.

40. Ertas, A. H., O. Vardar, F. O. Sonmez, and Z. Solim, "Measurement and assessment of fatigue life of spot weld joints", *Journal of Engineering Materials and Technology-Transactions of the ASME*, Vol. 131, No. 1, Art. No. 011011, 2009.

41. Zhou, M., S. J. Hu and H. Zhang, "Critical specimen sizes for tensile-shear testing of steel sheets", *Welding Journal*, Vol. 78, pp. 305s-313s, 1999.

42. Achintya, H. and M. Sankaran, *Probability, Reliability and Statistical Methods in Engineering Design*, John Wiley & Sons , ISBN 0-471-33119-8, 2000.

43. Tryon, R. G. and T. A. Cruse, "A reliability-based model to predict scatter in fatigue crack nucleation life", *Fatigue & Fracture of Engineering Material & Structures*, Vol. 21, 257-267, 1998.

44. Achintya, H. and M. Sankaran, *Probability, Reliability and Statistical Methods in Engineering Design*, John Wiley & Sons , ISBN 0-471-33119-8, 2000

45. Salvini, P., F. Vivio, and V. Vullo, "A spot weld finite element for structural modeling, *International Journal of Fatigue*, Vol. 22, No. 8, pp. 645-656, 2000.

46. ANSYS Documentation, ANSYS v.10, 2007.

47. N., Pan, "Fatigue Life Study of Spot Welds", Ph.D. Thesis, Stanford University, 2000.

48. Sheppard, S. D. and M. Strange, "Fatigue life estimation in resistance spot welds: initiation and early growth phase, *Fatigue & Fracture of Engineering Materials & Structures*, Vol. 15, No. 6, pp. 531-549, 1992.

49. Chae, S. W., K. Y. Kwon and T. S. Lee, "An optimal design system for spot welding locations, *Finite Elements in Analysis and Design*, Vol. 38, pp. 277-294, 2002.

50. Rui, Y., R. J. Yang and C. J. Chen, "Fatigue optimization of spot welds", Body Des Eng. IBEC 96. Berlin, 1996.

51. Liangsheng, W., K. B. Prodyot and J. P. Leiva, "Design optimization of automobile welds", *International Journal of Vehicle Design*, Vol. 31, No. 4, pp. 377-391, 2003.

52. Ertas, A. H. and F. O. Sonmez, "A parametric study on fatigue strength of spot weld joints", *Fatigue & Fracture of Engineering Materials & Structures*, Vol. 31, No. 9, pp. 766-776, 2008.

53. Haftka, R. T. and Z. Gurdal, *Elements of Structural Optimization*, Kluwer Academic, ISBN 0-7923-0608-2, 1992.

54. Rao, S. S., *Engineering Optimization: Theory and Practice*, Wiley New York, ISBN 13-9780471550341, 1996.

55. Fatemi, A. and D. F. Socie, "A critical plane approach to multiaxial fatigue damage including out-of-phase loading", *Fatigue & Fracture of Engineering Materials & Structures*, Vol. 11, No. 3, pp. 149-165, 1988.

56. Hahn, H. T. and R. Y. Kim, "Fatigue behavior of composite laminate", *Journal of Composite Materials*, Vol. 10, pp. 56-180, 1976.

57. Noda, J., M. Nakada and Y. Miyano, "Fatigue life prediction under variable cyclic loading based on statistical linear cumulative damage rule for CFRP laminates", *Journal of Reinforced Plastics and Composites*, Vol. 26, No. 7, pp. 665-680, 2007.

58. Nyman, T., "Composite fatigue design methodology: a simplified approach", *Composite Structures*, Vol. 35, pp. 183-194, 1996.

59. Shokrieh, M. and L. B. Lessard, "Progressive fatigue damage modeling of composite materials, part I: modeling", *Journal of Composite Materials*, Vol. 34, No. 13, pp. 1056-1080, 2000.

60. Shokrieh, M. and L. B. Lessard, "Progressive fatigue damage modeling of composite materials, part II: material characterization and model verification", *Journal of Composite Materials*, Vol. 34, No. 13, pp. 1081-1115, 2000.

61. Shokrieh, M. and L. B. Lessard, "Multiaxial fatigue behavior of unidirectional plies based on uniaxial fatigue experiments-I. modeling", *International Journal of Fatigue*, Vol. 19, No. 3, pp. 201-207, 1997.

62. Sihn, S. and J. W. Park, "An integrated design tool for failure and life prediction of Composites", *Journal of Composite Materials*, Vol. 42, No. 11, pp. 1-22, 2008.

63. Sims, D. F. and V. H. Brogdon, "Fatigue behavior of composites under different loading modes", *ASTM Special Technical Publication*, No: 636 (185-205), 1977.

64. Smith, E. W., "Cyclic biaxial deformation and failure of a glass fibre-reinforced composites", Ph.D. Thesis, Cambridge University, 1976.

65. Harris, B., *Fatigue in Composites: Science and Technology of the Fatigue Response of Fibre-Reinforced Plastics*, Woodhead Publishing, Cambridge, 2003.

66. Adali, S., "Optimization of fibre reinforced composite laminates subject to fatigue loading", *Composite Structures*. Vol. 3, pp. 43-55, 1985.

67. Akbulut, M. and F. O. Sonmez, "Optimum design of composite laminates for minimum thickness", *Computers & Structures*, Vol. 86, pp. 1974-1982, 2008.

68. Bathias, C., "An engineering point of view about fatigue of polymer matrix composite materials", *International Journal of Fatigue*, Vol. 28, pp. 1094-1099, 2006.

69. Bennett, J. A. and M. E. Botkin, "Structural shape optimization with geometric description and adaptive mesh refinement", *Journal of American Institute of Aeronautics and Astronautics*, Vol. 23, pp. 458-464, 1985.

70. Braibant, V. and C. Fleury, "Shape optimal design using B-spline", *Computer Methods in Applied Mechanics and Engineering*, Vol. 44, pp. 247-267, 1984.

71. Callahan, K. J. and G. E. Weeks, "Optimum design of composite laminates using genetic algorithms", *Composites Engineering*, Vol. 2, No. 3, pp. 149-160, 1992.

72. Caprino, G., "Predicting fatigue life of composite laminates subjected to tension-tension fatigue", *Journal of Composite Materials*, Vol. 34, pp. 1334-1355, 2000.

73. Ding, Y., "Shape optimization of structures: A literature survey", *Computers & Structures*, Vol. 24, No. 6, pp. 985-1004, 1986.

74. Ellyin, F., and H. El-Kadi, "A fatigue failure criterion for fiber reinforced composite laminae", *Composite Structures*, Vol. 15, pp. 61-74, 1990.

75. Epaarachchi J. A. and P. D. Clausen, "An empirical model for fatigue behavior prediction of glass fibre-reinforced plastic composites for various stress ratios and test frequencies", *Composites Part A: Applied Science and Manufacturing*, Vol. 34, pp. 313-326, 2003.

76. Fawaz Z. and F. Ellyin, "A new methodology for the prediction of fatigue failure in multidirectional fiber-reinforced laminates", *Composite Science and Technology*, Vol. 53, pp. 47-55, 1995.

77. Fawaz Z. and F. Ellyin, "Fatigue failure model for fibre-reinforced materials under general loading conditions", *Journal of Composite Materials*, Vol. 28, No. 15, pp. 1432-1451, 1994.

78. Fuqiang W. and Y. Weixing, "A model of the fatigue life distribution of composite laminates based on their static strength distribution", *Chinese Journal of Aeronautics*, Vol. 21, pp. 241-246, 2008.

79. Hashin, Z., "Failure criteria for unidirectional fiber composites", *Journal of Applied Mechanics-Transactions of the ASME*, Vol. 47, pp. 329-335, 1980.

80. Hashin, Z. and A. Rotem, "A fatigue failure criterion for fiber reinforced materials", *Journal of Composite Materials*, Vol. 7, pp. 448-464, 1973.

81. Huang Z. M., "Micromechanical life prediction for composite laminates", *Mechanics of Materials*, Vol. 33, pp. 185-199, 2001.

82. Hwang W. and K. S. Han, "Fatigue of composites-fatigue modulus concept and life prediction", *Journal of Composite Materials*, Vol. 20, pp. 154-165, 1986.

83. Kassapoglou, C., "Fatigue life prediction of composite structures under constant amplitude loading", *Journal of Composite Materials*, Vol. 41, No. 22, pp. 2737-2754, 2007.

84. Kere, P., M. Lyly and J. Koski, "Using multicriterion optimization for strength design of composite laminates", *Composite Structures*, Vol. 62, pp. 329-333, 2003.

85. Kirkpatrick, S., C. D. Gelatt, and M. P. Vecchi, "Optimization by simulated annealing, *Science*, Vol. 220, pp. 671-680, 1983.

86. Liu, Y. and S. Mahadevan, "Probabilistic fatigue life prediction of multidirectional composite materials", *Composite Structures*, Vol. 69, pp. 11-19, 2005.

87. Mouritz, A. P., "A simple fatigue life model for three-dimensional fiber-polymer composites", *Journal of Composite Materials*, Vol. 40, No. 5, pp. 455-469, 2006.

88. Reifsnider, K. L., *Fatigue of Composite Materials*, Elsevier Science, ISBN 0-948749-76-8, 1991.

89. Ochoa, O. O. and J. N. Reddy, *Finite Element Analysis of Composite Laminates*, Kluwer Academic, ISBN 0792311256, 1992.

90. Shokrieh, M. and D. Rezaei, "Analysis and optimization of a composite leaf spring", *Composite Structures*, Vol. 60, pp. 317-325, 2003.

91. Mao, H. and S. Mahadevan, "Fatigue damage modeling of composite materials", *Composite Structures*, Vol. 58, pp. 405-410, 2002.

92. Matthews, F. L., G. A. O. Davies, D. Hitchings, C. Soutis, *Finite Element Modeling of Composite Materials and Structures*, Woodhead Publishing, ISBN 1 85573 422 2, 2000.

93. Spall, J. C., *Introduction to Stochastic Search and Optimization*, Wiley-Interscience Publication, ISBN 0-471-33052-3, 2003.

94. Sonmez, F. O., *Structural optimization using Simulated Annealing*, in *Simulated Annealing*, In-Tech Publishing, ISBN 978-853-7619-07-7, 2008.

95. Wu, W. F., L. J. Lee and S. T. Choi, "A study of fatigue damage and fatigue life of composite laminates", *Journal of Composite Materials*, Vol. 30, No. 1, pp. 123-137, 1996.

96. Soares, C. M. M., V. F. Correia, H. Mateus and J. A. Herskovits "Discrete model for the optimal design of thin composite plate – shell type structures using a two – level approach", *Composite Structures*, Vol. 30, pp. 147-157, 1995.

97. Le-Riche, R. and R. T. Haftka, "Improved genetic algorithm for minimum thickness composite laminate design", *Composites Engineering*, Vol. 5, No. 2, pp. 143-161, 1995.

98. Jayatheertha, C., J. P. H. Webber and S. K. Morton, "Application of artificial neural networks for the optimum design of a laminated plate", *Computers & Structures*, Vol. 59, No. 5, pp. 831-845, 1996.

99. Kim, C. W., W. Hwang, H. C. Park and K. S. Han, "Stacking sequence optimization of laminated plates, *Composite Structures*, Vol. 39, No. 3-4, pp. :283-288, 1997.

100. Miki, M., Y. Murotsu, T. Tanaka and S. Shao "Reliability- based optimization of fibrous laminated composites", *Reliability Engineering and System Safety*, Vol. 56, pp. 285-290, 1997.

101. Mateus, H. C., C. M. M. Soares and C. A. M. Soares, "Buckling sensitivity analysis and optimal design of thin laminated structures", *Computers & Structures*, Vol. 64, pp. 461-472, 1997.

102. Lombardi, M. and R. T. Haftka, "Anti-optimization technique for structural design under load uncertainties", *Computer Methods in Applied Mechanics and Engineering*, Vol. 157, pp. 19-31, 1998.

103. Le-Riche, R. and J. Gaudin, "Design of dimensionally stable composites by evolutionary optimization", *Composite Structures*, Vol. 41, pp. 97-111, 1998.

104. Walker, M., "A method for optimally designing laminated plates subject to fatigue loads for minimum weight using a cumulative damage constraint", *Composite Structures*, Vol. 48, pp. 213-218, 2000.

105. Adali, S. and V. E. Verijenko, "Optimum stacking sequence design of symmetric hybrid laminates undergoing free vibrations", *Composite Structures*, Vol. 54, pp. 131-138, 2001.

106. Soremekun, G., Z. Gurdal, R. T. Haftka and L. T. Watson, "Composite laminate design optimization by genetic algorithm with generalized elitist selection", *Computers & Structures*, Vol. 79, pp. 131-143, 2001.

107. Walker, M. and R. E. Smith, "A technique for the multiobjective optimization of laminated composite structures using genetic algorithms and finite element analysis", *Composite Structures*, Vol. 62, pp. 123-128, 2003.

108. Sciuva, M. D., M. Gherlone and D. Lomario, "Multiconstrained optimization of laminated and sandwich plates using evolutionary algorithms and higher-order plate theories, *Composite Structures*, Vol. 59, pp. 149-154, 2003.

109. Adali, S., F. Lene, G. Duvaut and V. Chiaruttuni, "Optimization of laminated composites subject to uncertain buckling loads", *Composites Structures*, Vol. 62, pp. 261-269, 2003.

110. Park, C. H., W. I. Lee, W. S. Han and A. Vautrin, "Weight minimization of composite laminated plates with multiple constraints", *Composite Science and Technology*, Vol. 63, pp. 1015-1026, 2003.

111. Erdal, O. and F. O. Sonmez, "Optimum design of composite laminates for maximum buckling load capacity using simulated annealing", *Composite Structures*, Vol. 71, pp. 45-52, 2005.

112. Rahul, S. G, D. Chakraborty and A. Dutta, "Multi-objective optimization of hybrid laminates subjected to transverse impact", *Composite Structures*, Vol. 73, pp. 360-369, 2006.

113. Rotem, A., "Fatigue failure of multidirectional laminate", *Journal of American Institute of Aeronautics and Astronautics*, Vol. 17, No. 3, pp. 271-277, 1979.

114. Rotem, A. and Z. Hashin, "Fatigue failure of angle ply laminates", *Journal of American Institute of Aeronautics and Astronautics*, Vol. 14, No. 7, pp. 868-872, 1976.

115. Nijssen, R. P. L., "Fatigue life prediction and strength degradation of wind turbine rotor blade composites", PhD. Thesis, Technical University Delft, 2006.

116. Graesser, D. L., Z. B. Zabinsky, M. E. Tuttle and G. I. Kim, "Optimal design of a composite structure", *Composite Structures*, Vol. 24, pp.273-281, 1993.

117. Krikanov, A. A., "Composite pressure vessels with higher stiffness", *Composite Structures*, Vol. 48, pp. 119-127, 2000.

118. Soares, C. M. M., C. A. M. Soares and H. C. Mateus, "A model for the optimum design of thin laminated plate - shell structures for static, dynamic and buckling behavior", *Composite Structures*, Vol. 32, pp. 69-79, 1995.

119. Correia, V. M. F. and C. M. M. Soares, "Buckling optimization of composite laminated adaptive structures", *Composite Structures*, Vol. 62, pp. 315-321, 2003.

120. Moses, F. and D. E. Kinser, "Optimum structural design with failure probability constraints, *Journal of American Institute of Aeronautics and Astronautics*, Vol. 5, pp. 1152-1158, 1967.

121. Vassilopoulos, A. P., and R. Bedi, "Adaptive neuro-fuzzy inference system in modeling fatigue life of multidirectional composite laminates", *Computational Materials Science*, Vol. 43, pp. 1086-1093, 2008.

122. Harik V. M. and T. A. Bogetti, "Low cycle fatigue of composite laminates: a damage-mode-sensitive model", *Journal of Composite Materials*, Vol. 37, No. 7, pp. 597-610, 2003.

123. Ali, M. M. A., A. Torn and S. Viitanen, "A direct search variant of the simulated annealing algorithm for optimization involving continuous variables", *Computer Operation Research*, Vol. 29, pp. 87-102, 2002.

124. Doerner, K. F., M. Gendreau, P. Greistorfer, W. J. Gutjahr, R. F. Hartl and M. Reimann, *Metaheuristics: Progress in Complex Systems Optimization*, Springer Science & Business Media Publisher, ISBN 978-3-902613-09-7, 2007.

125. Steeb, W. H., Y. Hardy and R. Stoop, *The Nonlinear Workbook*, World Scientific Publishing, ISBN 981-256-112-9, 2005.

126. Ibaraki, T., K. Nonobe and M. Yagiura, *Metaheuristics: Progress as Real Problem Solvers*, Springer Science & Business Media Publisher, ISBN 0-387-25382-3, 2005.

127. Siarry, P. and Z. Michalewicz, *Advances in Metaheuristics for Hard Optimization*, Springer-Verlag Publisher, ISBN 978-3-540-72959-4, 2008.

128. Minnetyan, L., *Computational Stimulation of Composite Structural Fatigue*., NAG3-2609 NASA Project: 375-556, 2005.

129. Lee, M. C. H. and F. Abdi, "A GENOA-math-based methodology for the prediction of mechanical fatigue longevity of 3D woven fiberglass reinforced vinyl-ester composites", *SAE Technical Paper*, No. 2006-01-0001, 2006.

130. Rotem A. and Z. Hashin, "Failure modes of angle-ply laminates", *Journal of Composite Materials*, Vol. 9, pp. 191-206, 1975.